INFORMATION TO USERS

This manuscript has been reproduced from the microfilm master. UMI films the text directly from the original or copy submitted. Thus, some thesis and dissertation copies are in typewriter face, while others may be from any type of computer printer.

The quality of this reproduction is dependent upon the quality of the copy submitted. Broken or indistinct print, colored or poor quality illustrations and photographs, print bleedthrough, substandard margins, and improper alignment can adversely affect reproduction.

In the unlikely event that the author did not send UMI a complete manuscript and there are missing pages, these will be noted. Also, if unauthorized copyright material had to be removed, a note will indicate the deletion.

Oversize materials (e.g., maps, drawings, charts) are reproduced by sectioning the original, beginning at the upper left-hand corner and continuing from left to right in equal sections with small overlaps. Each original is also photographed in one exposure and is included in reduced form at the back of the book.

Photographs included in the original manuscript have been reproduced xerographically in this copy. Higher quality 6" x 9" black and white photographic prints are available for any photographs or illustrations appearing in this copy for an additional charge. Contact UMI directly to order.

University of Alberta

Development of Equivalent Uniform Dose Models
for Normal Tissue Irradiation

by

Isabelle Marie Gagné ©

A thesis submitted to the Faculty of Graduate Studies and Research in partial
fulfillment of the requirements for the degree of Master of Science

in

Medical Physics

Department of Physics

Edmonton, Alberta
Spring 1999

Canada

University of Alberta

Library Release Form

Name of Author: Isabelle Marie Gagné

Title of Thesis: Development of Equivalent Uniform Dose Models for Normal Tissue Irradiation

Degree: Master of Science

Year this Degree Granted: 1999

Permission is hereby granted to the University of Alberta Library to reproduce single copies of this thesis and to lend or sell such copies for private, scholarly, or scientific research purposes only.

The author reserves all other publication and other rights in association with the copyright in the thesis, and except as hereinbefore provided, neither the thesis nor any substantial portion thereof may be printed or otherwise reproduced in any material form whatever without the author's written permission.

Isabelle Gagné

10739-125 Street
Edmonton, Alberta
T5M 0L3
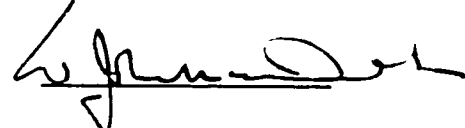
08 april 99

University of Alberta
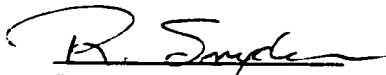
Faculty of Graduate Studies and Research

The undersigned certify that they have read, and recommended to the Faculty of Graduate Studies and Research for acceptance, a thesis entitled **Development of Equivalent Uniform Dose Models for Normal Tissue Irradiation** submitted by **Isabelle Marie Gagné** in partial fulfillment of the requirements for the degree of **Master of Science in Medical Physics.**

Dr. DM Robinson

Dr. WJ McDonald

Dr. WHY Roa

Dr. RE Snyder

Mr. C Field

03/03/99

to

my parents and friends

Abstract

Modern treatment planning systems are able to conform more adequately to tumors, but the large volume of data that needs to be processed in 3-dimensonal conformal radiotherapy renders the precise reporting and analysis of doses actually delivered to irradiated organs and volumes of interest very difficult. A new method of summarizing and reporting non-uniform dose distributions, better known as the *EUD* method, is described in this work. The *EUD* concept assumes that any two dose distributions are equivalent if they cause the same radiobiological effect. In this thesis, the *EUD* concept is applied to normal tissues, as they are rarely avoided during irradiation. Since normal tissues, unlike tumors, vary from one another in their architecture and therefore behave differently to radiation, only the most fundamental normal tissue architectures, serial and parallel, are considered in this work. Extensions of the idealized *EUD* concept to include nonuniform density of clonogens, dose per fraction effects, absolute volumes, intra-patient inhomogeneity, and inhomogeneity of patient population are also presented in this work. The application of the basic *EUD* concept for tumors, and serial and parallel architecture organs is demonstrated with a number of simple dose-volume histograms and relevant clinical dose distributions.

Acknowledgments

I would like to take this opportunity to acknowledge and thank all the generous people who have helped make the completion of this thesis possible. Firstly, I would like to thank my supervisor, Dr. Don Robinson for his constant support, guidance and many reviews of the thesis throughout the last $2^{\frac{1}{2}}$ years. I would also like to thank the reviewing committee for their insightful comments and encouragement.

Many thanks to the members of the Medical Physics department at the Cross Cancer Institute for their support, advice and many coffee break invitations. I would especially like to thank Claire McCartney and Ernie Mah for solving the many computer and computer programs problems that surfaced in the last leg of my work.

My friend Marek Malac deserves my appreciation and acknowledgment for his support, encouragement and many Power Plant invitations over the last two years.

I would like to acknowledge my colleagues, Parmider Basran, HJ Kim, Marc Mackenzie and Geetha Menon for their advice, assistance and motivation.

I would also like to thank my many sport colleagues and friends for their incredible moral support, encouragement and many social invites.

Finally, I would like to thank my family for believing in me and being there for me in times of needs. MERCI!

TABLE OF CONTENTS

LIST OF TABLES

LIST OF FIGURES

LIST OF ABBREVIATIONS

3-D CRT	3-Dimensional Conformal Radiation Therapy
AMU	Atomic Mass Unit
CDVH	Cumulative Dose-Volume Histogram
CTV	Clinical Target Volume
DDVH	Differential Dose-Volume Histogram
DNA	Deoxyribonucleic acid
DVH	Dose-Volume Histogram
EUD	Equivalent Uniform Dose
FSU	Functional Sub-Unit
GTV	Gross Tumor Volume
ICRU 50	International Commission on Radiation Units and Measurement
LET	Linear Energy Transfer
LET_∞	Total Linear Energy Transfer
LET_Δ	Restricted Linear Energy Transfer
NTCP	Normal Tissue Complication Probability
PTV	Planning Target Volume
SF	Survival Fraction
TCP	Tumor Control Probability
VOI	Volume of Interest

1. INTRODUCTION

1.1 Cancer Management

Cancer is the second leading cause of death due to diseases in Alberta, the first being heart disease. According to studies conducted by the Alberta Cancer Board, one in three Albertans will develop cancer during their lifetime.[1] Conventional therapies such as surgery, chemotherapy and radiation therapy are considered the primary treatments for cancer. Of the three conventional therapies mentioned above, radiation therapy and surgery are considered the most effective treatments for cancer. In the majority of localized cancers, surgery is the primary form of treatment. However, surgery used in conjunction with radiation therapy usually yields improved result. For other kinds of cancer, such as inoperable localized cancers or Hodgkin's disease, radiation is the predominant form of treatment. Radiation therapy can also be used to control the disease rather than cure it. This is known as palliative treatment, and it is used primarily to decrease symptoms such as pain when the cancer metastasizes.

1.2 Three Dimensional - Conformal Radiation Therapy Planning

1.2.1 Volume Assessment

Ideally, one would like to deliver a prescribed dose to the planning target volume and spare all normal tissues. However, because of the characteristics of radiation beams, limitations associated with radiotherapy equipment and uncertainties in patient setup and true spatial extent of the disease, a certain amount of normal tissue irradiation is unavoidable. Delineation of target volumes and critical structures are therefore important steps in treatment planning. The 50th International Commission on Radiation Unit and Measurement report[2] or ICRU 50 recommends that certain volumes, such as the gross tumor volume, clinical target volume, planning target volume, organs at risk, treated volume and irradiated volume be defined prior, during and as a result of treatment planning (see **Figure 1.1**). The volume which denotes the gross tumor volume or GTV plus any marginal spread of the disease is defined in ICRU 50 as the clinical target

volume or CTV. In order to achieve cure, the clinical target volume has to be treated adequately. The planning target volume or PTV consists of a volume that includes the gross tumor, any microscopic spread of the disease and a margin to account for the following factors:[2]

> 1) movements of the tissues which contain the CTV,
>
> 2) patient movement during irradiation,
>
> 3) size and shape variations of the tissues which contain the CTV,
>
> 4) variations in the characteristics of the beam.

Proper delineation of the planning target volume is crucial to the proper treatment of the clinical target volume.
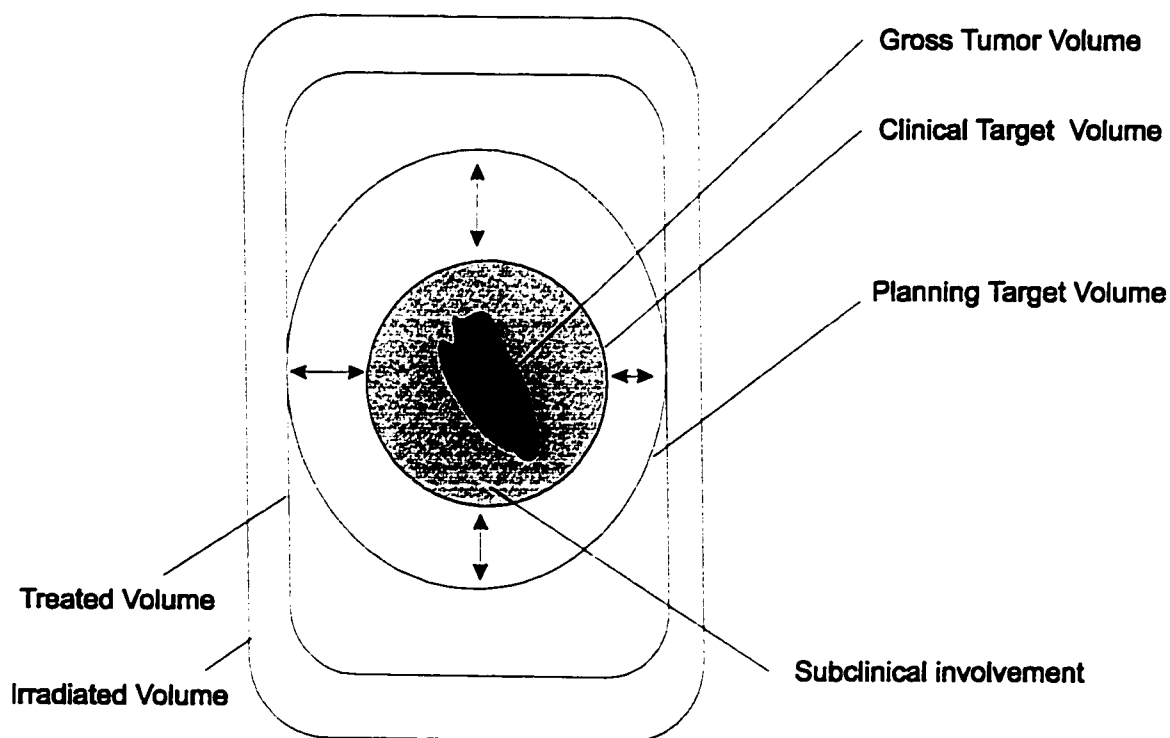
Figure 1.1: Volume delineation for treatment planning as recommended by ICRU 50.

After delineation of the PTV, the treated volume is specified. The treated volume is defined, in ICRU 50, as the volume enclosed within a specified isodose envelope that

adequately covers the PTV. This isodose value represents the minimum required target dose to achieve tumor eradication. The treated volume is usually larger than the PTV because of the differences in treatment technique and equipment. Reduction between the treatment volume and the PTV has been made possible in the past few decades with the advent of three-dimensional conformal radiation therapy or 3-D CRT. 3-D treatment planning allows one to direct and shape radiation fields so as to achieve greater conformation to the PTV.

Next in importance to the delineation of the planning target volume is the localization of the critical structures. This is an important initial step in the treatment planning process as critical structure radiosensitivities can limit delivery of the prescribed dose to the tumor. As with planning target volume delineation, margins must be imposed to account for patient and organ movements during treatment as well as uncertainties in the set up and limitations of the radiotherapy equipment. The overall volume of tissue which receives a dose that is considered meaningful with regards to normal tissue tolerance is defined as the irradiated volume.

1.2.2 Treatment Plan Evaluation

Treatment plans have traditionally been evaluated by reviewing simple dose distributions for a few cross sections (often one) of the patient's anatomy and a limited amount of quantitative information, such as minimum tumor dose and maximum dose to normal organs. Comparison between rival plans was guided by tradition and clinical experience. This conventional approach to treatment plan evaluation is being eclipsed by modern practice as the amount of data available for evaluation in 3-D conformal radiotherapy is considerably greater and the dose distributions generated may be considerably different and more complex than those of the traditional methodology and are therefore more difficult to evaluate. To aid in the evaluation of 3-D treatment plans, new quantitative tools, such as dose-volume histograms and biological indices have been developed. These new quantitative tools are being used more and more in modern radiation therapy to evaluate treatment plans along with dose statistics and other qualitative tools, such as beam's eye view and color wash dose distribution technique.[3]

Despite the fact that they facilitate the evaluation of complex treatment plans, these new quantitative tools have to be used carefully due to current limitations.

1.2.2.1 Dose-Volume Histograms or DVHs

The dose-volume histogram or DVH is certainly the most popular plan evaluation tool used in treatment planning today. Since the large volume of information in 3-D CRT planning may make it difficult to interpret and assimilate the data, condensing the 3-D dose distribution data into a dose-volume histogram enables one to graphically summarize the radiation distribution throughout one or several volume of interests (VOIs).

There are two types of dose-volume histogram: the differential dose-volume histogram or DDVH and the cumulative dose-volume histogram or CDVH (see **Figure 1.2**). The differential histogram is a plot of the accumulated volume of those elements within the volume of interest receiving dose in a specified dose interval. The cumulative dose-volume histogram is, on the other hand, a plot of the volume receiving a dose less than or equal to a given dose. In most papers and literature, the cumulative dose-volume histogram is simply referred to as a dose-volume histogram or DVH.

DVHs are powerful tools in treatment planning as they reduce the amount of data that a planner has to deal with and they help in the identification of hot spots, cold spots and other dose heterogeneities that would be otherwise difficult to assess rapidly and consistently from a large set of dose distributions. Dose-volume histograms also serve as precursors to certain normal tissue complication probability and tumor control probability models. Finally, DVHs aid the planner in comparing rival plans in order to decide on the best possible one. Unfortunately, when DVHs for rival plans intersect, it becomes difficult to choose the best plan by visual inspection and other means must be taken to complete the task.

Even though DVHs drastically reduce the amount of data in 3-D CRT, they should not be the sole criterion for plan evaluation as they eliminate the spatial information of the dose distribution within a volume of interest and they are solely based on physical dose. Furthermore, DVHs assume that each voxel within a sub-volume is radiobiologically identical. Since the ultimate goal of radiation therapy is to achieve

4

uncomplicated tumor control, quantitative tools that can assess the biological outcome of a radiation scheme must be designed. Biological indices, such as tumor control probability (*TCP*) and normal tissue complication probability (*NTCP*), have been developed in the recent decades to aid in the evaluation of treatment plans, but at the present these biological indices rely on unreliable clinical data and must therefore be used cautiously.
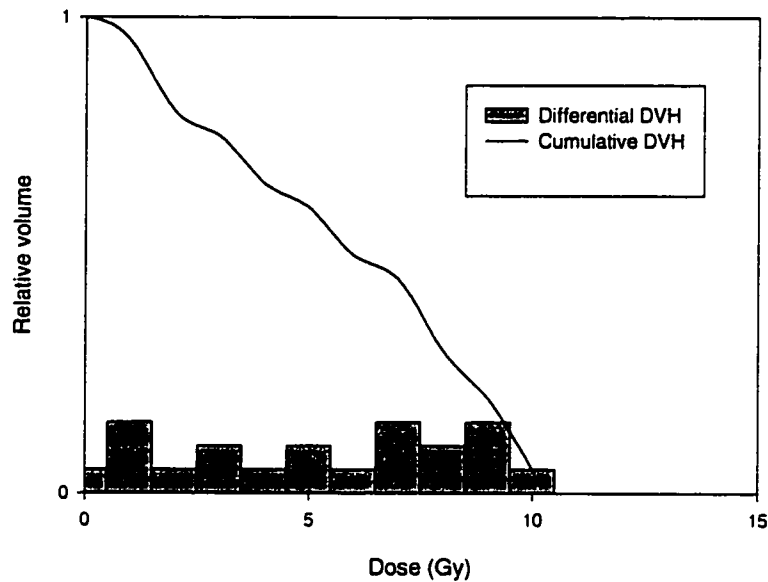
Figure 1.2: Schematic of a cumulative dose-volume histogram and a differential dose-volume histogram.

1.2.2.2 Biological Indices

Unlike DVHs, which are based entirely on the physical dose, biological indices attempt to provide a quantitative biological measure of the effectiveness of a dose distribution. The most popular biological indices used in modern radiation therapy are *TCP* and *NTCP* values. *TCP* predicts the likely biological response of irradiated tumors while *NTCP*s measure the likelihood that a given dose distribution will lead to serious complications in the patient. The probabilities of both tumor control and tissue complication are believed to be sigmoidal functions of dose.

Models of tumor control are generally based on the assumption that a tumor is destroyed only when all viable clonogens within it are killed. Because all clonogens are

assumed to be independent, the probability of eradicating all of them is simply a product of individual probabilities. Thus,

$$TCP = \prod_{i=1}^{n} \left(1 - SF(D_i)\right)^{k_i} \tag{1.1}$$

where n = number of voxels,

k_i = number of clonogens in the ith voxel,

and $SF(D_i)$ = probability that a single clonogen survives a dose D_i. This simple model of TCP assumes that all voxels are characterized by the same dose-response relationship. It also assumes that the response of individual patients is the same as that of the patient population. Clinical studies have shown that this is not the case and that clonogenic cells both within the same tumor, and among patients, differ in their radiosensitivity.[4] These differences in radiosensitivity are believed to be one of the factors responsible for the flattening of the tumor control probability curve obtained from clinical studies.[5] It is therefore important to allow for factors such as these when modeling tumor control probability.

Numerous models for predicting normal tissue complication probabilities of non-uniformly irradiated tissues and organs have been suggested. Some, such as Lyman's[6,7] four-parameter model, are empirical or phenomenological in nature. Others are statistical and are based on tissue architecture.[8,9]

Lyman's four-parameter model describes the $NTCP$ for uniform dose irradiation through the following error function of dose and volume:

$$NTCP = \frac{1}{\sqrt{2\pi}} \int_{-\infty}^{t} \exp\left(-t^2/2\right) dt \tag{1.2}$$

where $t = \dfrac{\left(D - TD_{50}(v)\right)}{\left(m * TD_{50}(v)\right)},$ \tag{1.3}

$$TD_{50}(1) = TD_{50}(v) * v^{-n}, \tag{1.4}$$

and

$$v = V/V_{ref}. \tag{1.5}$$

$TD_{50}(1)$ is the tolerance dose yielding 50% complications for whole organ irradiation, whereas $TD_{50}(v)$ is the tolerance dose to partial volume v producing a similar complication probability. The arbitrary parameters m and n are empirically obtained from normal tissue tolerance data. The parameter m is the slope of the dose response function at TD_{50} and is thus a measure of the dose sensitivity of the organ. The parameter n is, on the other hand, a measure of the volume effect. When n is near unity (e.g. lungs and kidneys), the volume effect is large, and when it is near zero (e.g. brain and colon), the volume effect is small. As will be seen later in the statistical models, an organ with a large n is a parallel architecture organ, and one with a small n, a serial organ. The most recent determinations of n and m are provided in **Table 1.1**.

Organ	V_{ref}	n	m	TD_{50} (Gy)	Endpoint
Brain	Whole	.25	.15	60	Necrosis/Infarction
Kidneys	Whole	.70	.10	28	Clinical nephritis
Lungs	Whole	.87	.18	24.5	Pneumonitis
Colon	Whole	.17	.11	55	Obstruction/perforation/ ulceration

Table 1.1: Normal tissue complication end points and tolerance parameters.[10]

Extension of this model to inhomogeneous irradiation is accomplished by converting the non-uniform dose-volume histogram into an equivalent uniform histogram, using either the interpolation[11] or the effective volume method.[12] Both these dose-volume histogram reduction schemes attempt to calculate a biologically equivalent dose or volume for each tissue that contains dose heterogeneities.

Empirical models are simple and flexible to use for computing normal tissue complication probabilities for whole or partial organ irradiation, but they have their downfalls. The main drawback is that these models rely on clinical data (e.g. TD_{50}) that, for a vast majority of tissues, is unreliable and poorly documented.[13] Inconsistencies in

dose and volume reporting methods are believed to be responsible for the poor quality of clinical data.[14,15] The issue of consistent dose prescription, specification and reporting in radiation therapy has been addressed in ICRU 50. However, the proposed methodology has not been universally accepted and there continues to be a lack of rigor and compliance worldwide.[16]

Another downfall of these empirical models is that they relate partial volume tolerance doses through a power law in volume as per **equation 1.4**. This implies that there is always a partial volume dose for which a given probability of complication occurs. For organs with a large volume effect, such as lungs and kidneys, this does not apply, as no complication occurs in these organs if less than their functional reserve is irradiated. Lastly, the reduction schemes used to convert the non-uniform dose-volume histogram into an equivalent uniform one are not sufficiently biologically orientated.

In the last few decades, biologically-orientated theoretical models for predicting *NTCP* and *TCP* have been proposed. These more complex models use binomial statistics in combination with the assumption that normal tissues and even tumors are composed of independent functional sub units (FSUs). Since these models attempt to incorporate the underlying architecture of the irradiated structures, they are thought to represent more closely the radiation response (i.e. the volume effect).

Two types of functional organization are modeled statistically: serial and parallel. Serial models assume that certain organs (e.g. spinal cord) are organized like chains, and that damage to one of the links will damage the whole chain. Organs with such an architecture have a small volume effect. Parallel models assume, on the other hand, that certain organs (e.g. lungs) have functional reserves. Thus, a complication does not arise in these organs until a significant fraction of independent functional sub units have been eradicated. Organs of parallel architecture exhibit a large volume effect. A more detailed description of these models is given in **Chapter 3**.

Until recently, relative *TCP* and *NTCP* were thought to be very useful tools for treatment plan ranking. However, a recent study[17] revealed, through several theoretical tests, that plan rankings are not uniquely determined by relative tissue complication probabilities as is widely claimed. The study also revealed that uncertainties in calculated

NTCP values do affect plan ranking when exchanging one complication for another. Thus, one may conclude that proper plan ranking can not be achieved if *TCP* and *NTCP* calculations are based upon relative complication data. The use of *TCP* and *NTCP* functions to arrive at the best possible plan can be rendered more accurate by reducing the errors that exist in calculated *NTCP* and *TCP* values. The large errors in *NTCP* and *TCP* values arise mainly, as stated earlier, from poorly documented clinical data. This is especially true in the case of normal tissue irradiation where the dose distributions are very complex and non-uniform.

1.3 The Concept of *EUD*

In order to reduce these large errors in the *NTCP* and *TCP* values and concurrently improve dose reporting methods, a recent model which eliminates the need to report several doses during documentation has been proposed by Niemierko. The proposed model, better known as the Equivalent Uniform Dose or *EUD* model is a new method of summarizing and reporting non-uniform dose distributions. The main feature of the *EUD* is its uniformity, which allows one to describe an entire dose distribution, within a volume of interest, with a single number. The concept of *EUD* assumes that any two dose distributions are equivalent if they cause the same radiobiological effect.[18] Therefore, any non-uniform dose distribution can be transformed into an equivalent uniform dose.

The concept of equivalent uniform dose proposed by Niemierko can more than facilitate communication between centers and improve the quality of the collected biological data. It can biologically summarize the data and thus reduce the amount of data a planner has to face without losing too much biological information. Furthermore, the *EUD* can serve as a precursor to the *NTCP* and *TCP* models and thus improve the quality of their values. By reducing the errors in the *NTCP* and *TCP* values, the *EUD* can render the clinical application of these biological indices more significant.

1.3.1 Overview of Thesis:

Most of the work on equivalent uniform dose performed by Niemierko has been directed at tumors. The main objective of this thesis is to apply Niemierko's *EUD*

9

concept in order to develop *EUD* models for normal tissue irradiation. In order to carry this through one must attempt to include tissue architecture into the model. However, before attempting such a task, one must take a closer look at Niemierko's *EUD* model and its assumptions. Furthermore, one must be aware of the effects of radiation on biological matter.

This work therefore begins, in **Chapter 2**, with a review of the basic physics of ionizing radiation, with specific focus on the different possible interactions with biological matter. A description of the most important radiation quantities and units is also presented in this chapter. In **Chapter 3**, a description of the chemistry and biology of radiation absorption at the molecular, cellular and tissue levels is given. In **Chapter 4**, the concept of Equivalent Uniform Dose is introduced and *EUD* models for both serial architecture and parallel architecture organs are developed. **Chapter 5** is dedicated to the testing of the simple models presented in the previous chapter. The thesis concludes, in **Chapter 6**, with a brief summary and discussion of the results.

2. THE BASIC PHYSICS OF IONIZING RADIATION

Since their discovery by Roentgen in 1895, x-rays have played a major role in medicine. Their first major application was in diagnostic imaging. However, not too long after this discovery, x-rays became therapeutic tools in cancer therapy. Subsequent studies of the underlying physics of ionizing radiation have lead to major improvements in the treatment of cancer. Because of the importance of radiation physics in the treatment of cancer, this chapter will concentrate on the basic physical interactions of ionizing radiation with biological materials and also the physical quantities frequently used in radiation therapy.

2.1 The time-scale of radiation effects

During and after irradiation of any biological system, several events occur that differ quite widely in their time-scale. For convenience, these processes are generally divided in three phases, namely the physical, chemical and biological phases[19].

The physical stage is characterized by the interactions of radiation with the atoms of the biological system irradiated. The end result of these interactions is either ionization or excitation. The time-scale over which these interactions occur is extremely short (10^{-18} to 10^{-17} sec) and varies with the velocity of the particle, the dimensions of the atom or molecule and the amount of energy transferred in the process.

The chemical stage describes the period in which free-radicals, radical-ions and energetically excited molecules are formed and then engage in a succession of reactions with neighboring cellular components in order to restore the electronic charge equilibrium. Most free-radical reactions are completed within times much less than a millisecond. However, some may take somewhat longer.

The biological stage encompasses all subsequent events such as enzyme reactions, DNA repair processes, and early and late effects. Failure to repair critical DNA lesions eventually leads to cell death and the manifestation of early effects in the days and months following irradiation of normal tissues. These early reactions result from the killing of stem cells and their subsequent loss of progeny.

2.2 Ionizing Radiation

Ionizing radiation can be defined as any radiation capable of ejecting electrons from the atoms or molecules with which they interact. To be considered ionizing, the radiation must carry sufficient kinetic or quantum energy to cause a valence electron to escape an atom. Ionizing radiation can be broadly divided into two categories: particulate, in which the individual energy carriers have rest mass and may be electrically charged, and electromagnetic, where the energy carriers are photons which have neither charge nor rest mass.

2.2.1 Electromagnetic Radiation

Electromagnetic radiation, used in radiation therapy, consists primarily of x-rays and γ-rays. These rays behave identically and differ only in the way in which they are produced. The physical properties of x-ray and γ-ray radiations are best described if these radiations are considered to have a dual nature, in that they sometimes behave as waves and sometimes as particles.

2.2.1.1 Wave nature

Electromagnetic waves can, under the wave model, be represented by spatial variations in the intensity of an electric field ($\vec{E}$) and a magnetic field ($\vec{H}$) as shown in **Figure 2.1**. At any given time the fields are always at right angles to each other.
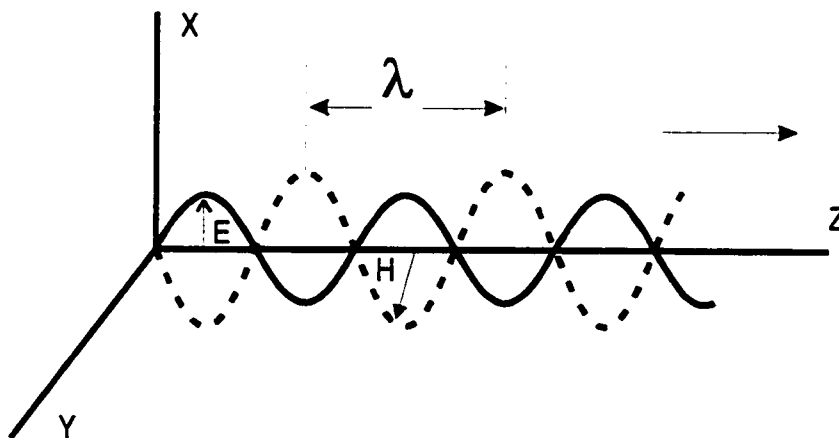
Figure 2.1: Schematic of an electromagnetic wave.

Due to their wave nature, these radiations undergo interference, diffraction, reflection, refraction and polarization. They travel with a velocity c of 3.0×10^8 m/sec in a vacuum. The velocity of an electromagnetic wave can be related to its wavelength λ and frequency υ by the following relation:

$$\upsilon\lambda = c \cong 3 \times 10^8 m / \sec .$$ (2.1)

2.2.1.2 Quantum nature

The quantum nature of electromagnetic radiation is based on the observation that the energy carried by such radiation is absorbed and emitted in the form of discrete bundles called quanta or photons. The amount of energy carried by a quantum or photon depends upon the frequency of the radiation and is given by:

$$E = hv = \frac{hc}{\lambda}$$ (2.2)

where E is the energy in Joules carried by the photon and h is the Plank's constant of 6.62×10^{-34} J-sec. The above equation indicates that as the wavelength of electromagnetic radiation becomes smaller or the frequency becomes larger, the energy of a quantum becomes greater.

2.2.2 Particulate Radiation

Particulate radiations, just as electromagnetic radiations, also exhibit a dual nature and therefore sometimes appear to behave like waves. There are many types of particulate radiation, each varying in mass, charge, and method of production. The most common elementary particles used in radiation physics are listed in **Table 2.1**.

Particle	Symbol	Charge	Mass
Electron	e^-	-1	0.000548 amu
Positron	e^+	+1	0.000548 amu
Proton	p, $_1^1H^+$	+1	1.00727 amu
Neutron	n, $_0^1n$	0	1.00866 amu

Table 2.1: Elementary particles used in radiation therapy.

2.3 Photon Interactions with Biological Materials

The International Commission on Radiation Units and Measurements (ICRU) recommends that photons be classified as indirectly ionizing radiations since their deposition of energy in matter is a two-step process. In order to deliver their energy to matter, photons first transfer, in a few relatively large interactions, their energy to charged particles of the matter through which they pass. The resulting fast charged-particles then, generally, deposit their energy to the matter through many Coulomb-force interactions.

There are five major types of photon interactions by which a photon beam may be attenuated:

1) Photoelectric effect

2) Compton scattering

3) Rayleigh scattering

4) Pair production and triplet production

5) Photo-nuclear disintegration

Each of these processes can be described by a mass attenuation coefficient which is proportional to the fraction of photons removed per unit thickness by the given process. The mass attenuation coefficient of an individual interaction is also numerically equal to the probability of such an event occurring when a single photon passes through this unit thickness. The mass attenuation coefficient has units of cm^2 per g. The total mass attenuation coefficient (μ/ρ), in a given medium, is the sum of all these individual coefficients:

$$\frac{\mu}{\rho} = \frac{\tau}{\rho} + \frac{\sigma}{\rho} + \frac{\pi}{\rho} + \frac{\sigma_{coh}}{\rho} + \frac{\kappa}{\rho} \tag{2.3}$$

where $\tau, \sigma, \sigma_{coh}, \pi$, and κ are the linear attenuation coefficients for the photoelectric effect, Compton scattering, photo-nuclear disintegration, Rayleigh or coherent scattering, and pair production respectively.

At the energies under consideration in conventional radiotherapy, the photoelectric effect, Compton scattering and pair production are the dominant photon interactions in biological materials, as they contribute significantly to the absorbed dose, D. The relative importance of these three processes depends on both the characteristic Z

of the absorbing medium and the photon quantum energy E as depicted in **Figure 2.2**.[20] A brief description of all three dominant photon interactions is presented in the following sections.

2.3.1 Photoelectric Effect

The photoelectric effect is the predominant interaction in biological tissue at low energies. In this process, a photon of energy $E = h\nu$ interacts with an atom and transmits its entire energy to one of the orbital electrons as shown in **Figure 2.3**. This atomic electron or photoelectron is then ejected with a kinetic energy E:

$$E = h\nu - E_b - E_{atom} \tag{2.4}$$

where E_b is the binding energy of the electron and E_{atom} is the negligible kinetic energy given to the atom.
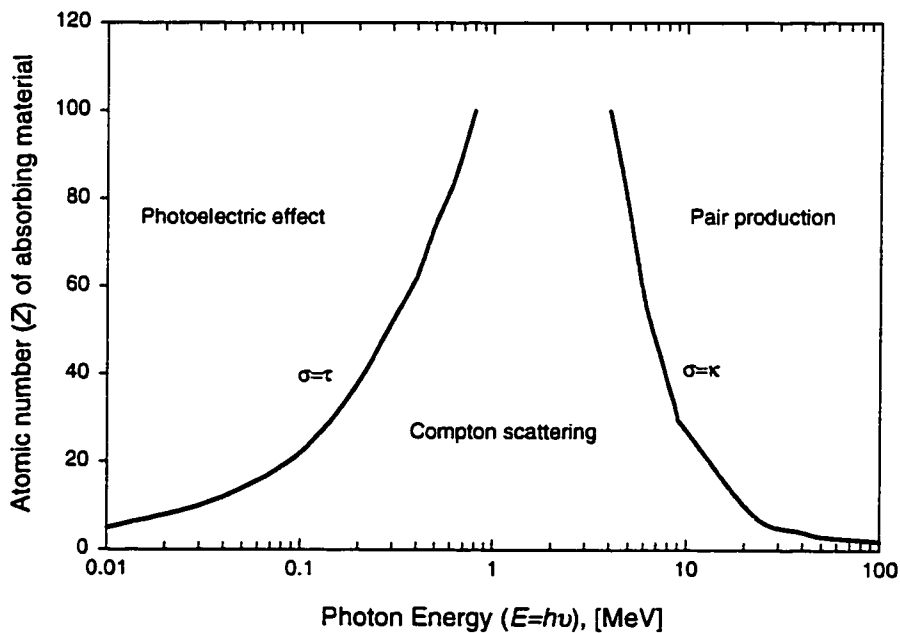
Figure 2.2: Relative importance of photoelectric effect, Compton scattering and pair production.
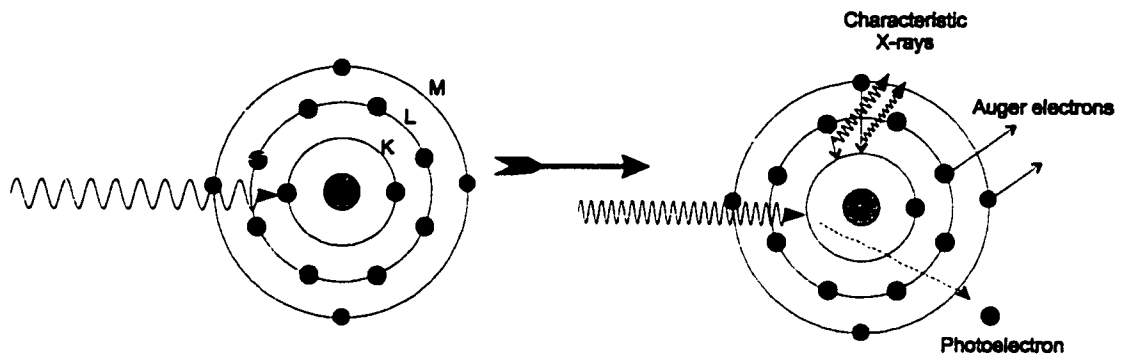
Figure 2.3: Schematic of the photoelectric effect.

When an electron is removed from an inner atomic shell, the vacancy is promptly filled by an outer orbital electron. For any shell vacancy, this transition is either accompanied by the emission of characteristic x-rays or the emission of Auger electrons. The probability of characteristic x-ray emission is called the fluorescence yield, Y, and is dependent upon the atomic number of the absorbing medium. For biological material, the chance of fluorescence x-ray emission during the filling of any vacancy is negligibly small.

Consequently, the Auger effect is the dominant mechanism by which an atom can dispose of the excess energy in biological materials. The Auger effect is the process by which an atom ejects, with sufficient kinetic energy, one or more of its relatively shallow outer shell electrons to account collectively for the excess energy not removed by characteristic x-rays. The total energy carried away by all Auger electrons and/or characteristic x-rays equals the original shell binding energy. One thing to note is that when no characteristic x-rays are emitted, the Auger electrons account collectively for all the original shell binding energy.

The probability of photoelectric absorption depends on both the energy E of the photon and the atomic number, Z, of the absorbing medium. In the energy region $E \leq 0.1$ MeV, where the photoelectric effect becomes important in biological materials, the mass attenuation cross section for this effect is approximately[21]:

$$\frac{\tau}{\rho} \propto \left(\frac{Z}{E}\right)^3 \qquad (2.5)$$

where τ is the sum of the cross section values for the different shells.

16

For energies beyond 0.1 MeV,

$$\frac{\tau}{\rho} \propto \frac{Z^n}{(h\nu)^m}$$ (2.6)

where n gradually rises to ≈ 3.6 at 3 MeV and m gradually decreases to 1 at 5 MeV.

2.3.2 Compton Scattering

Compton scattering is the dominant process in biological materials over the wide range of 50 keV to 20 MeV. In the Compton scattering process, a photon interacts with an atomic electron as though it were a "free" electron. To be considered free, the binding energy of the struck orbital electron must be small compared to the incident photon energy. In this type of elastic interaction, an incident photon transmits some of its energy to an orbital electron and subsequently scatters at an angle ϕ with reduced energy. Having acquired sufficient energy, the recoil electron departs the atom at an angle θ with an energy E_e as shown in **Figure 2.4**.
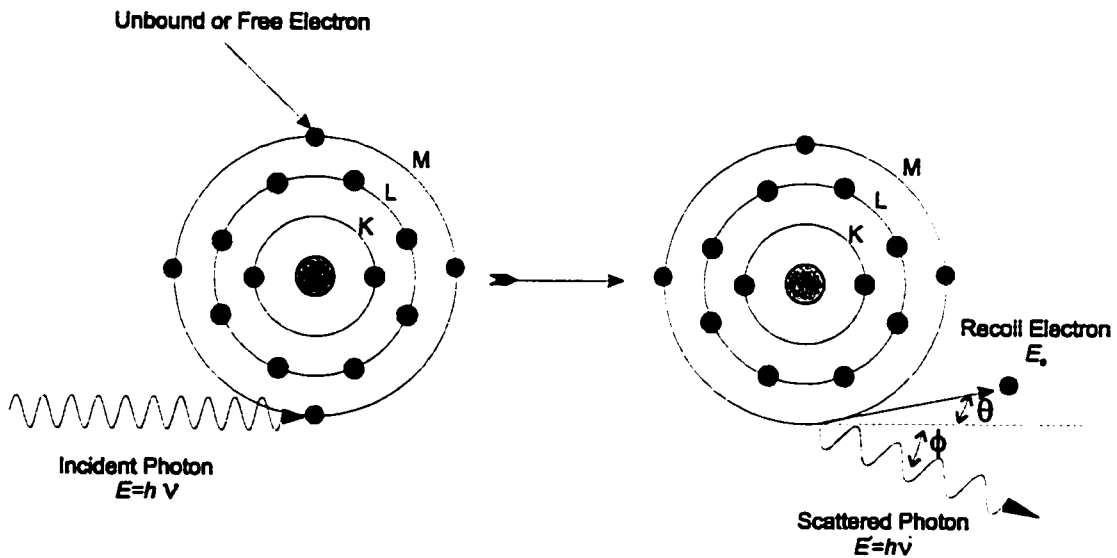
Figure 2.4: Schematic of a Compton scattering interaction.

By applying the laws of conservation of energy and momentum to this elastic collision, one can derive the following equations:

$$E_e = h\nu \cdot \left(\frac{\alpha(1 - \cos\phi)}{1 + \alpha(1 - \cos\phi)} \right),$$ (2.7)

and $hv' = hv \cdot \left(\dfrac{1}{1 + \alpha(1 - \cos\phi)} \right)$. $\qquad$ (2.8)

where hv, hv' and E_e are the quantum and kinetic energies of the incident photon, scattered photon and recoil electron, respectively, and $\alpha = E / m_o c^2$, where $m_o c^2$ is the electron's rest mass energy.

If a photon makes a direct hit on an electron, the electron will travel straight forward ($\phi = 0^o$) and the scattered photon will be backscattered ($\theta = 180^o$). Thus, in this type of collision, maximum energy transfer occurs with

$$E_{max} = hv \cdot \frac{2\alpha}{1 + 2\alpha} \, , \qquad (2.9)$$

and $hv_{min} = hv \cdot \dfrac{1}{1 + 2\alpha}$ $\qquad$ (2.10)

The probability of Compton collision can be described by several differential cross sections[22] derived by Klein-Nishina, one being the differential cross section for photon scattering at angle ϕ, per unit solid angle and per electron:

$$\frac{d_e\sigma}{d\Omega_\phi} = \frac{r_o^2}{2} \cdot \left(\frac{hv'}{hv} \right)^2 \cdot \left(\frac{hv}{hv'} + \frac{hv'}{hv} - \sin^2\phi \right) \qquad (2.11)$$

where r_o is the classical electron radius.

Another useful Klein-Nishina formula, is the differential cross section for electron scattering at angle θ, per unit solid angle and per electron:

$$\frac{d_e\sigma}{d\Omega_\theta} = \frac{e^4}{2m_o^2 c^4} \cdot \left[\frac{1}{1 + \alpha(1 - \cos\theta)} \right]^2 \cdot \left[1 + \cos^2\theta + \frac{\alpha^2(1 - \cos\theta)^2}{1 + \alpha(1 - \cos\theta)} \right]^2 . \qquad (2.12)$$

In order to find the total electron cross section for Compton scattering, **formulas (2.11)** and **(2.12)** must be multiplied by the element of solid angle, and integrated over all angles. One can conclude, without performing this task, that the electron cross section for Compton scattering is independent of the atomic number (Z) of the absorbing material since the electrons involved in the Compton process are assumed to be free and stationary. Therefore all materials will absorb about the same amount of radiation per electron by this process. Since the electron density is almost constant for most material,

the mass attenuation coefficient for Compton scattering (σ/ρ) is nearly the same for all materials, except for hydrogen which has no neutrons.

For low incident photon energies, one must take into account that energy is required to eject orbital electrons. Thus, a multiplicative correction factor, which takes into account the binding of the atomic electrons, must be added to the Klein-Nishina differential cross section formulas. The main effect of this binding correction is to decrease the differential cross section at low incident photon energies as shown in **Figure 2.5**.
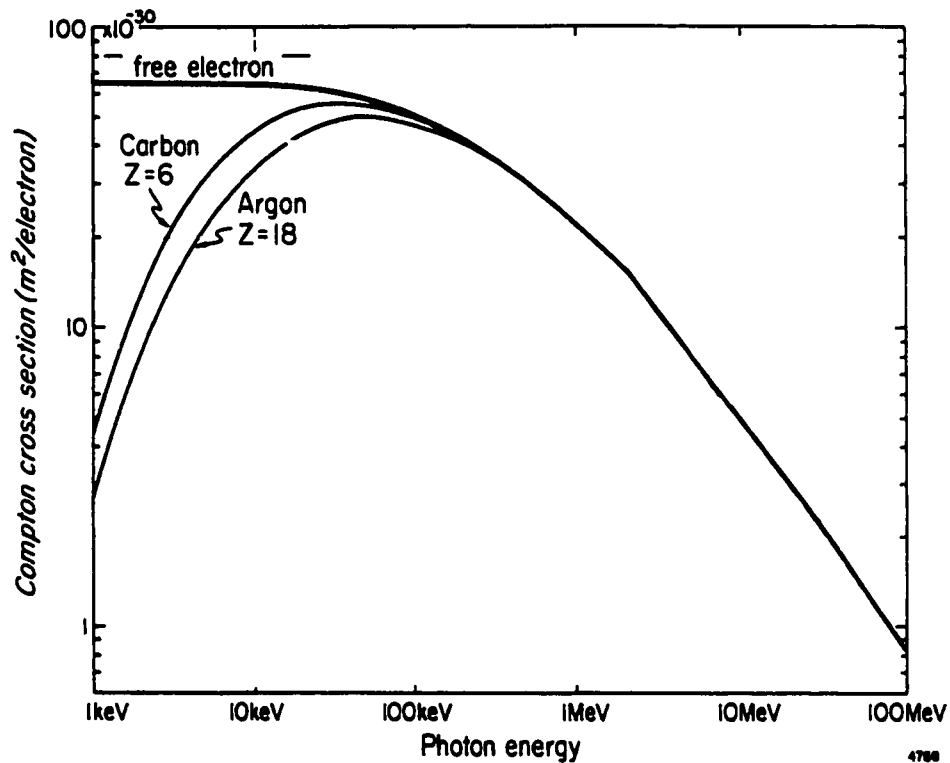
Figure 2.5: The effect of binding energy on the Klein-Nishina differential cross section.

2.3.3 Pair and Triplet Production

Pair production is a process that can occur when a high energy photon passes sufficiently close to the nucleus of an atom. By interacting with the Coulomb-force field of the atomic nucleus, a high-energy photon gives up all its energy, disappears and gives

19

rise to a positron (e⁺) and an electron (e⁻) as shown in **Figure 2.6**. The photon energy threshold for such an interaction is $2m_oc^2$. If the photon has energy in excess of 1.022 *MeV*, the excess energy is shared between the positron and the electron.

If the interaction occurs in the field of an atomic electron rather than in the field of the nucleus, triplet production results. The threshold for such an interaction may be shown to occur at twice the threshold of the pair production, thus $4m_oc^2$. In this process one positron and two electrons, one being the host electron that provided the Coulomb field, are ejected from the site of the interaction (See **Figure 2.6**).
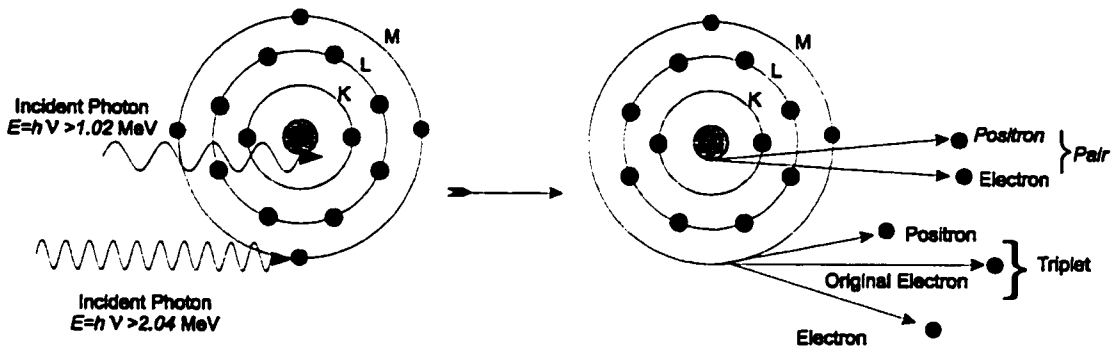
Figure 2.6: Schematic of pair and triplet production processes.

The atomic cross section for pair production increases rapidly with photon energy above the threshold of 1.022 MeV as shown in **Figure 2.7**. Since the probability of triplet production is small compared with pair production, the total cross section for pair and triplet production is approximated by the pair production cross section. The mass attenuation coefficient for pair production increases rapidly with atomic number since the interaction occurs with the electromagnetic field of the nucleus.
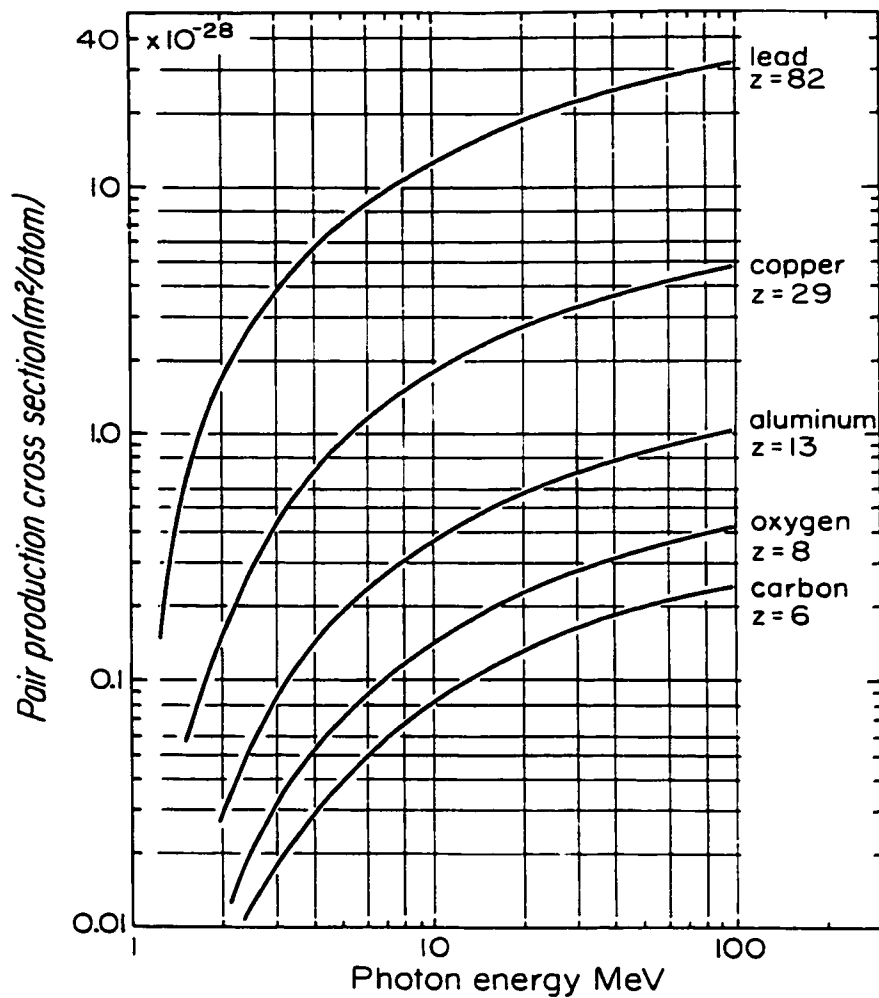
Figure 2.7: Pair production cross section as a function of photon energy.[23]

2.4 Charged Particle Interactions with Matter

Electrons and positrons generated by the photoelectric effect, Compton scattering and pair production loose their energy through either collisional or radiative interactions with the surrounding medium. Collisional interactions are mediated by the Coulomb force between the electric fields of the traveling electron/positron and the electric fields of orbital electrons, whereas, radiative interactions are mediated by the Coulomb force between the electric field of the traveling electron/positron and the electric field of the atomic nuclei. Collisional interactions can be classified as either "soft" or "hard", depending on the relative size of the classical impact parameter, b, and the atomic radius, a, as shown in **Figure 2.8**. Collisions between the traveling charged particle and the

nucleus (i.e. radiative interactions) result in radiative loss of energy better known as bremsstrahlung. Another mode of kinetic energy dissipation, known as in-flight annihilation does exist. However, this mechanism of energy dissipation is only available to positrons.

Undisturbed Trajectory
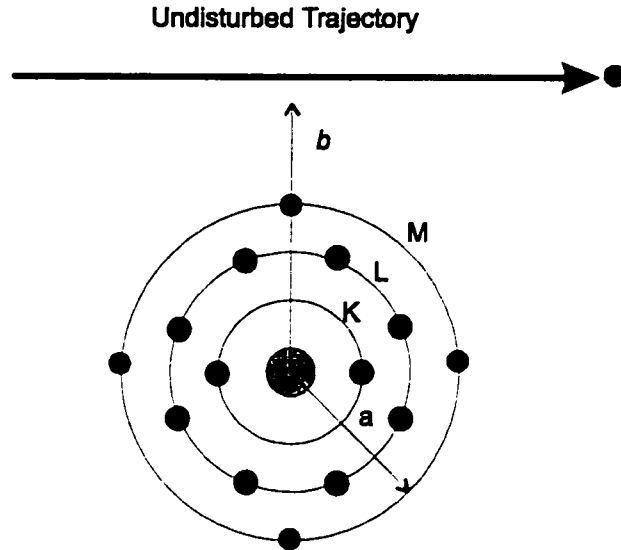
Figure 2.8: Important parameters in charged-particle interactions with atoms: the classical impact parameter, b and the classical atomic radius, a.

The total energy lost (dE), by a charged particle in traversing a path length (dx) in matter of density ρ is known as the total mass stopping power, which has units of MeV cm^2/g. Since collisional and radiative interactions account for the energy imparted to the medium, the total mass stopping power can be divided into a collisional term and a radiative term as follows:

$$\left(\frac{dE}{dx}\right) = \left(\frac{dE}{dx}\right)_c + \left(\frac{dE}{dx}\right)_r \tag{2.13}$$

where $\left(\dfrac{dE}{dx}\right)_c$ = collision stopping power,

and $\left(\dfrac{dE}{dx}\right)_r$ = radiative stopping power.

If one divides the stopping power by the density of the absorbing medium, one gets a quantity called the mass stopping power:

$$\left(\frac{dE}{\rho \cdot dx}\right) \tag{2.14}$$

typically in MeV cm^2/g or J m^2/kg. Mass stopping powers vary with the energy of the particle, the particle type and the atomic number of the medium through which the particle is traveling. Tabulated tables of mass stopping powers can be found in many radiation physics textbooks.

2.4.1 "Soft" Collisions

"Soft" collisions are, by far, the most common type of charged particle interaction. They occur when charged particles interact with atomic electrons from distances that are greater than the atomic radius ($b>>a$). "Soft" collisions are responsible for the transfer of roughly half of the energy deposition even though only minute amounts of energy are transferred to the medium per interaction.

2.4.2 "Hard" Collisions

"Hard" or knock -on collisions are less common than soft collisions, but the energy transferred to the medium by these few collisions is comparable to the energy transferred by the greater number of "soft" collisions. For a knock-on collision to occur, the impact parameter must be in the range of the atomic nucleus ($b\sim a$). When $b\sim a$, a traveling charged particle is more likely to interact with a single atomic electron. In a collision of this type, the struck electron is ejected from the atom with considerable kinetic energy. If the recoil electron has enough energy to produce further ionization or excitation it is usually referred to as a delta ray. As mentioned earlier, the vacancy caused by the ejection of an atomic electron is eventually filled and characteristic x-rays and/or Auger electrons are emitted as a result.

2.4.3 Coulomb-Force Interactions with the External Nuclear Field

This type of interaction is predominant for positrons and electrons. It occurs when the impact parameter is much less than the atomic radius ($b<<a$). The small impact parameter causes the Coulomb-force interaction to take place with the nucleus of the atom. In the majority of these interactions, the electron or positron is elastically

scattered and no energy is transferred to the medium. However, in about 2 or 3 % of the cases, inelastic interactions occur which result in radiative losses or bremsstrahlung radiation.

2.4.4 In-Flight Annihilation

This mode of kinetic energy dissipation is available only to positrons. In this process, the positrons slow down enough to recombine with a free electron before stopping. The extra kinetic energy of the positron at the time of annihilation is given to one or both of the annihilation photons.(See **Figure 2.9**) When the extra kinetic energy is shared equally, the annihilation photons are ejected at angles $\phi = \theta$. However, when the extra kinetic energy is not shared equally, the annihilation photons travel off in directions that enables them to conserve momentum. The amount of kinetic energy given to these photons is comparable to the amount given to bremsstrahlung radiation.

$h\nu \geq 0.511$ MeV

Positron $E > 0.511$ MeV

Electron ϕ

θ

$h\nu \geq 0.511$ MeV
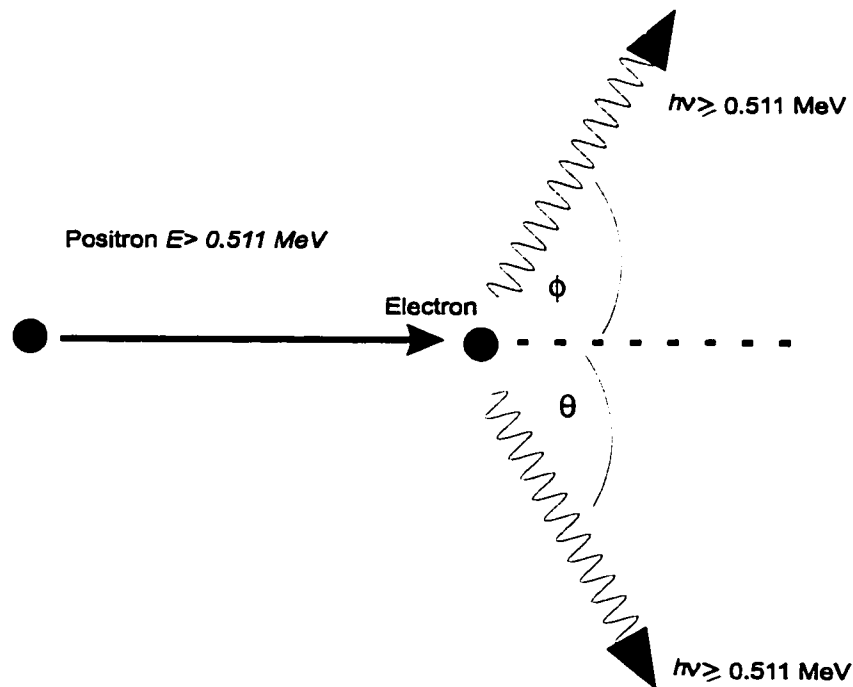
Figure 2.9: Schematic of an in-flight annihilation process.

2.5 Direct and Indirect Action of Radiation

There is strong evidence that biological effects such as cell death, mutation and oncogenesis result mainly from damage to DNA, the genomic material of the cell. Such

damage can be incurred directly or indirectly by radiation as shown in **Figure 2.10**. Since the method of action depends greatly on the linear energy transfer or *LET* of the radiation, a definition of *LET* is in order.
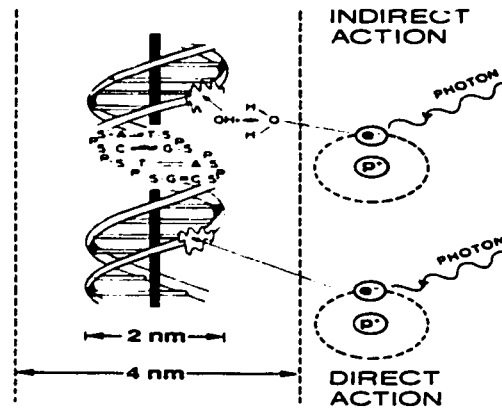
Figure 2.10: Direct and indirect action of radiation[24].

2.5.1 Linear Energy Transfer

In radiation physics, the rate of energy loss per unit path length is referred to as the linear energy transfer or simply *LET* and it is usually measured in $keV / \mu m$.

When the total energy lost by the charged particle includes the energy carried away by energetic secondary electrons or delta-rays, the *LET* is referred to as the total linear energy transfer and is defined as:

$$LET_\infty = \frac{dE}{dx}.$$
(2.15)

When the energy lost by a charged particle in traversing a distance dx includes only those energy losses due to collisions with energy transfers less than some specified delta value, Δ, the linear energy transfer becomes restricted and thus,

$$LET_\Delta = L_\Delta = \left(\frac{dE}{dx}\right)_\Delta$$
(2.16)

where Δ is an arbitrary energy limit below which energy transfers are considered dissipative.

The restricted linear energy transfer is a useful concept in radiation physics as it is used in calculating the absorbed dose or the energy "locally" absorbed per unit mass.

2.5.2 Direct Action

Direct action is the dominant process when the radiations involved have high linear energy transfer, such as neutrons or alpha particles. In such a process, the radiation interacts directly with the DNA molecule, ionizing or exciting its atoms. These ionizations and excitations eventually lead to biological damage.

2.5.3 Indirect Action

Indirect damage to the DNA occurs when radiation interacts with other atoms near the critical target to produce free radicals that are able, by diffusion, to reach and damage the target. A free radical is a free molecule or atom that has an unpaired orbital electron. This unpaired electron causes the free radical to be highly reactive.

2.6 Radiation Quantities and Units

In order to describe a radiation field at a point P, let us associate some nonzero volume (i.e. a sphere centered at P) with the point as shown in **Figure 2.11**. The size of the sphere depends on the physical quantities we wish to measure. If the quantities are stochastic, and therefore not predictable, the sphere must have a small but finite volume. The values of stochastic quantities are random in nature and can only be described by a probability distribution. ICRU defines the expectation value N_e of a stochastic quantity as the mean $\overline{N}$ of its measured values N as the number n of observations approaches ∞. That is,

$$\overline{N} \to N_e \quad \text{as} \quad n \to \infty \ . \tag{2.17}$$
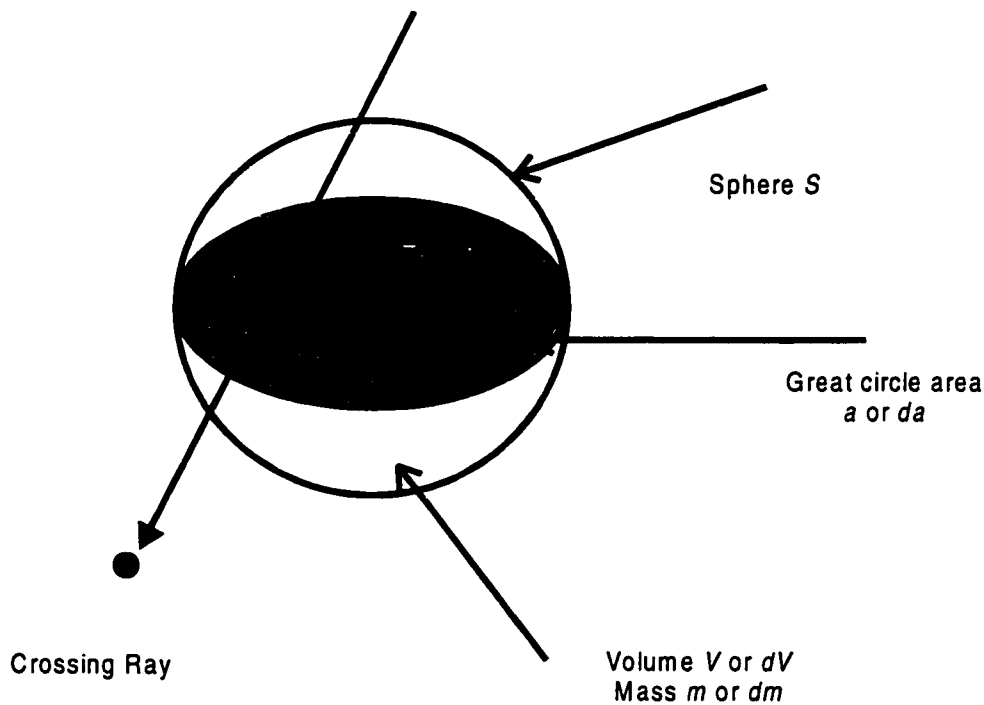
Figure 2.11: Characteristics of the sphere needed to describe a radiation field.

If, on the other hand, the quantities are nonstochastic, then the sphere must be of infinitesimal volume (dV). Nonstochastic quantities are usually point functions, and are therefore differentiable. ICRU states that the values of nonstochastic quantities common in radiation physics are equal to, or based upon, the expectation value of a related stochastic quantity. Since most of the quantities used to describe ionizing radiation fields and their interactions with matter are nonstochastic, we will, in this section, focus mainly on them.

2.6.1 Fluence and Energy Fluence

The fluence Φ of photons or particles is the quotient dN_e by da, where dN_e is the expectation value of the number of rays or particles that enter an imaginary sphere of cross-sectional area da.[25] Thus,

$$\Phi = \frac{dN_e}{da} \tag{2.18}$$

and is usually expressed in m^{-2} or cm^{-2}.

When we take into account the energies of the rays or particles, we usually use the quantity energy fluence to describe a radiation field. The energy fluence Ψ is the quotient dR by da, where dR is the expectation value of the sum of all energies carried by rays or particles that enter the imaginary sphere of cross-sectional area da.[25] Thus,

$$\Psi = \frac{dR}{da}$$
(2.19)

and is expressed in units of J/m^2 or erg/cm^2.

For monoenergetic beams of energy E,

$$\Psi = E\Phi,$$
(2.20)

since

$$R = EN_e.$$
(2.21)

2.6.2 Fluence Rate and Energy Fluence Rate

Fluence rate or flux density ϕ is simply the fluence per unit time and is expressed in units of $m^{-2}s^{-1}$ or $cm^{-2}s^{-1}$.[25] Thus,

$$\phi = \frac{d\Phi}{dt}$$
(2.22)

where dt is the time interval in seconds.

When we consider the energies of the particles or photons, we can define a quantity known as the energy fluence rate or energy flux density. The energy fluence rate or energy flux density ψ is the energy fluence per unit time. It is given by:

$$\psi = \frac{d\Psi}{dt}$$
(2.23)

and is expressed in J/m^2s or erg/cm^2s.

For a monoenergetic beam of energy E, the following relationship between the energy fluence rate and the fluence rate holds:

$$\psi = E\phi.$$
(2.24)

2.6.3 Exposure

The quantity "exposure" is a measure of the ionization of air by photons and it is expressed in roentgens. ICRU defines exposure X as the quotient of dQ by dm, where dQ

is the absolute value of the total charge of the ions of one sign produced in air when all the electrons (electrons and positrons) liberated by photons in air of mass dm are completely stopped in air. Thus,

$$X = \frac{dQ}{dm}.$$

(2.25)

2.6.4 Kerma

Kerma K is a nonstochastic quantity that is principally used to describe the energy transferred to charged particles by indirectly ionizing radiation such as photons and neutrons. The Kerma at a point P is given as the quotient of $d(\varepsilon_{tr})_e$ by dm, where $d(\varepsilon_{tr})_e$ is the expectation value of the energy transferred to charged particles in an infinitesimal volume dV of mass dm, including radiative energy loss, but excluding the kinetic energy passed from one charged particle to another.[25] Thus,

$$K = \frac{d(\varepsilon_{tr})_e}{dm}.$$

(2.26)

The energy transferred ε_{tr} in a volume V is given by:

$$\varepsilon_{tr} = (R_{in})_u - (R_{out})_u^{nonr} + \sum Q$$

(2.27)

where $(R_{in})_u$ =   radiant energy of indirectly ionizing radiations entering V,

$(R_{out})_u^{nonr}$ =   radiant energy of indirectly ionizing radiations leaving V minus radiative energy losses by charged particles while in V,

and $\sum Q$ =   net energy derived from rest mass.

For monoenergetic photons of energy E, the Kerma at P is related to the photon energy fluence by the mass energy-transfer coefficient $\left(\mu_{tr}/\rho\right)_{E.Z}$ as follows:[25]

$$K = \Psi \cdot \left(\frac{\mu_{tr}}{\rho}\right)_{E.Z}.$$

(2.28)

The mass energy-transfer coefficient is dependent upon the energy of the photons and the atomic number of the absorbing medium.

2.6.5 Absorbed Dose

Absorbed dose, D, is one of the most useful nonstochastic quantities used in radiation physics. It is relevant to all types of radiation and is defined, at any point P, as the quotient of $(d\varepsilon)_e$ by dm, where $(d\varepsilon)_e$ is the expectation value of the energy imparted in an infinitesimal volume dV of mass dm.[25] Thus,

$$D = \frac{(d\varepsilon)_e}{dm} \tag{2.29}$$

and its units in the International System (SI) are J/kg, also known as gray (Gy).

The energy imparted ε in a finite volume V of mass m is given by:[25]

$$\varepsilon = \left(R_{in}\right)_u - \left(R_{out}\right)_u + \left(R_{in}\right)_c - \left(R_{out}\right)_c + \sum Q \tag{2.30}$$

where $\left(R_{in}\right)_u$ =   radiant energy of indirectly ionizing radiations entering V,

$\left(R_{out}\right)_u$ =   radiant energy of indirectly ionizing radiations leaving V,

$\left(R_{in}\right)_c$ =   radiant energy of charged particles entering V,

$\left(R_{out}\right)_c$ =   radiant energy of charged particles leaving V,

and $\sum Q$ =   net energy derived from rest mass.

2.6.6 Relative Biological Effectiveness

Relative biological effectiveness or RBE is defined as the ratio of the absorbed dose of a reference radiation (usually x-rays) to the absorbed dose of a test radiation that produce the same biological effect, other conditions being equal.[26] Thus,

$$RBE = \frac{D_{ref}}{D_{test}}. \tag{2.31}$$

To measure the RBE, the biological system used must allow the quantitative scoring of the radiation effects. Biological systems with single endpoints usually facilitate the study of RBE. Relative biological effectiveness is a very complex quantity. It depends on various factors such as the type of radiation, the absorbed dose, the dose per fraction, the number of fractions, the endpoint or effect being measured and the level of effect. **Figure 2.12** illustrates the dependence of RBE on LET_∞ for human kidney cells. It

can be seen that the maximum *RBE* occurs at a LET_∞ of about 100 keV/μm. It can also be seen that the maximum *RBE* depends, as mentioned earlier, on the level of effect.
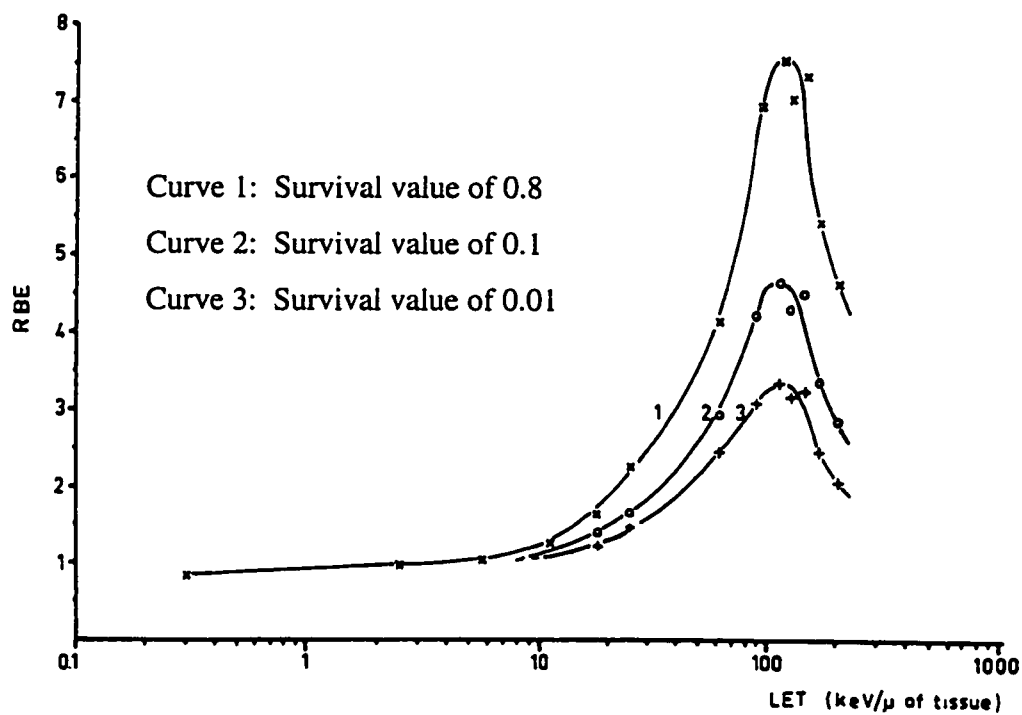
Figure 2.12: The dependence of relative biological effectiveness (*RBE*) on linear energy transfer (*LET*) for human kidney cell.[27]

3. THE CHEMISTRY AND BIOLOGY OF RADIATION ABSORPTION IN BIOLOGICAL MATERIAL

3.1 Radiochemical Events in Biological Systems

3.1.1 General

For the purpose of this present study, living cells can be described as an assembly of water and organic molecules such as proteins and nucleic acids. Irradiation of living cells leads to a large number of ionizations which can directly, or indirectly, damage DNA, the most crucial molecule of the cell. Since cells are composed of more than 70% water, most of the ionizations produced by radiation occur with water molecules. The end result of these ionizations is the production of free radicals which possess unpaired orbital electrons and are therefore highly reactive[28].

3.1.2 Radiochemistry of Water

Ionization of water molecules by radiation leads to the formation of ion radicals and free electrons:

$$H_2O + radiation \rightarrow H_2O^{\bullet+} + e^- . \tag{3.1}$$

The negatively charged free electrons rapidly associate with water molecules which are strongly polarized:

$$e^- + (H_2O)molecules \rightarrow e_{aq}^- . \tag{3.2}$$
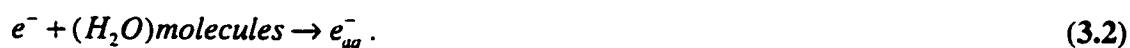
The end result of such associations is the formation of hydrated electrons (e_{aq}^-) which have reduced mobility and lifetimes of a few microseconds.

The ion radicals also associate with water molecules, forming uncharged hydroxyl radicals:

$$H_2O^{\bullet+} + H_2O \rightarrow H_3O^+ + OH^\bullet . \tag{3.3}$$

These hydroxyl radicals ($OH^\bullet$) are regarded as being the most biologically damaging radicals. They are highly reactive and can diffuse short distances to reach critical targets in the cell.

Another free radical that results from the interaction of radiation with water is the $H^\bullet$ free radical. This radical results from the break down of the excited water molecule and, like the hydroxyl radical, is highly reactive:

$$H_2O + radiation \rightarrow H_2O^\bullet \rightarrow OH^\bullet + H^\bullet.$$ (3.4)

The extent of the indirect damage incurred by these 3 main products of radiolysis ($e_{aq}^-, OH^\bullet, H^\bullet$) depends on the amount of radical scavenging reactions that occur during the first few milliseconds after irradiation. The compounds responsible for these scavenging reactions are the ones which contain sulphydryl (-SH) groups. Such compounds have an affinity for free radicals and therefore act to lower the biological damage by reducing the amount of free radicals present near critical targets[28].

3.2 Radiation Damage to DNA

Radiation can damage any molecule and, therefore, any part of the living cell. It is, however, believed that damage to DNA is of primary importance, particularly in relation to cell killing[29]. DNA damage is also believed to be responsible for radiobiological effects such as mutation and carcinogenesis. For these reasons, DNA is considered the principal target for the biological effects of radiation.

3.2.1 Structure of DNA

The DNA molecule is a double-helix structure consisting of 2 complementary chains, which are linked together by hydrogen bonding between the bases (see **Figure 3.1**). The chains forming DNA are composed of a sequence of nucleotides, which are sub-units in which bases are linked through a sugar group to a phosphate group. Bases of opposite strands must always compliment each other for hydrogen bonding to occur. Therefore, a thymine base will always face an adenosine base. Likewise, a cytosine base will always pair up with a guanine base. Bases are of utmost importance in biology because their order along the DNA molecule specifies the genetic code.
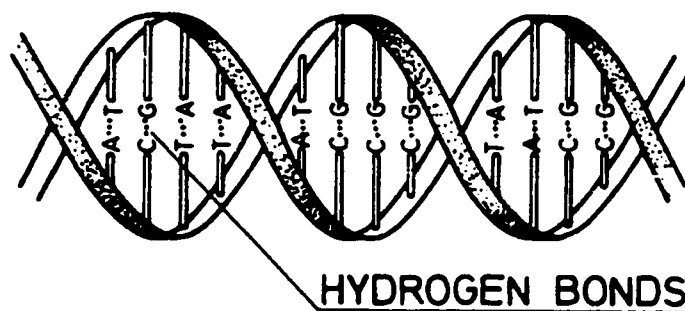
Figure 3.1: Schematic drawing of the structure of a DNA molecule.[30]

3.2.2 DNA Lesions and Damage

There are a variety of types of DNA lesions and radiation induced damaged. The most important is the double-strand break, which is believed to be responsible for cell death. Other types of DNA lesions and damage include single-strand break, formation of cross-links and base damage (see **Figure 3.2**).
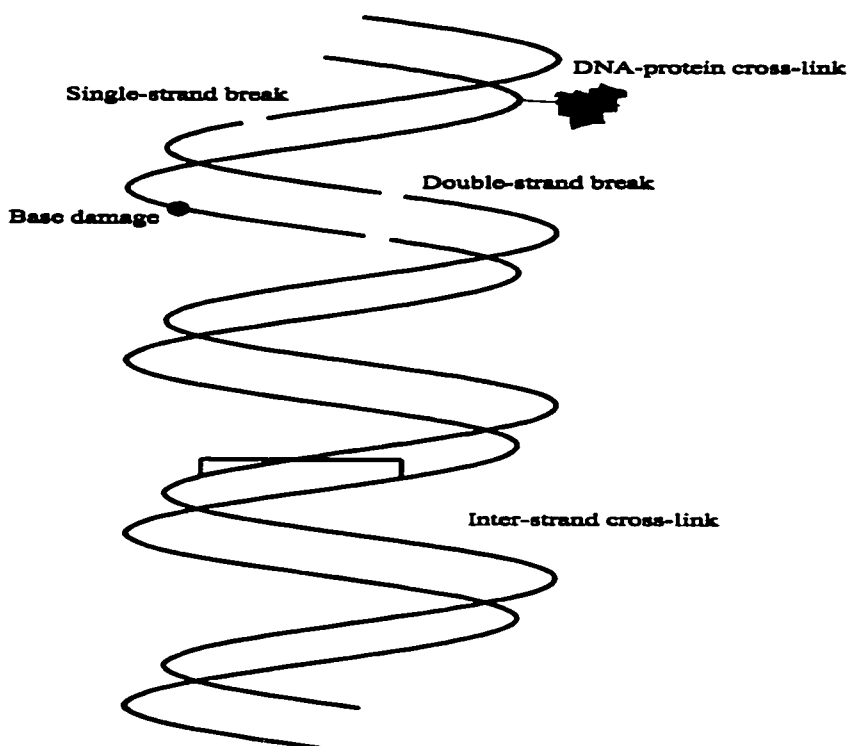
Figure 3.2: Types radiation-induced lesions and damage in DNA.

DNA strand breakage involves a break in the bonds between the sugar and phosphate groups. There are 2 possible categories of DNA strand breaks: single-strand break (SSB), which affects only one strand of the double-helix structure and double-strand break (DSB), which affects both strands. Single-strand breaks are one of the most frequent lesions that occur in DNA. The number of single-strand breaks in oxic mammalian cells per mean lethal dose D_0 has been estimated to be approximately 1000 compared to 40 for double-strand breaks.[31] Double-strand breaks comprise either two opposite single-strand breaks or two single-strand breaks in close proximity. While they are not as frequent as single-strand breaks, they are believed to be the most important group of DNA lesions that cause biological damage.

Cross-links are a type of DNA damage that occur at a low frequency when compared to other DNA lesions. These occur either between the DNA strands, hence the name inter-strand cross-link, or between the DNA and chromosomal proteins. The latter is generally know as DNA-protein cross-link. The most crucial of the two is the inter-strand cross-link since it may be converted to a double-strand break during the repair process.

The last type of damage that can occur in DNA due to irradiation is base damage. Base damage involves chemical alteration of the DNA base without actual strand breakage. However, base damage can eventually lead to strand breaks if the base-damaged sites are cleaved by specific enzymes.

3.2.3 Repair of DNA Damage

Numerous lesions are induced by radiation in DNA, many of which are successfully repaired by the cell. The repair half-time of different types of lesion are found to vary, ranging from 2-5 minutes[32] for single-strand breaks to 1.5-4 hours[33] for double-strand breaks. Base damage repair takes, on average, longer than single-strand break repair. The slower repair is thought to be associated with the induction of a single-strand break after the removal of the damaged base.

3.3 Radiation Damage at the Cellular Level

Radiation induced cell damage can be divided into three categories:

1) Lethal damage

2) Sublethal damage

3) Potentially lethal damage

Lethal damage is defined as any non-repairable damage that leads to the death of a cell or its progeny. Sublethal damage, on the other hand, is defined as non-lethal cellular injury that can be repaired, or accumulated with further dose to become lethal. Potentially lethal damage is defined in 2 ways in the current literature. In some papers, PLD is the equivalent of SLD while in others, it is referred to as the damage that can be repaired when suboptimal growth conditions prevail immediately after irradiation. All three types of damage are simply operational terms, since in, mammalian cells, the mechanisms of repair and radioresistance are not fully understood at the molecular level.[34]

3.3.1 The role of Double-Strand Break

Of all the radiation-induced lesions, double-strand breaks (DSBs) appear to be associated most closely with cell lethality.[35,36] The close association does not, however, show which DSBs are lethal or exclude the possibility that some other lesion (produced in proportion to DSB) is the critical lesion.[37]

Not all double-strand breaks give rise to cell death; only a very small fraction of them do. The reasons for this low frequency conversion are not yet fully known, but it is believed that the majority of DSBs are repaired and the remainder may be misrepaired or left unrepaired during the repair process. In relation to cell killing, double-strand breaks can be thus regarded as potentially lethal lesions.

3.3.2 Chromosomal Aberrations

Double-strand breaks can lead to the formation of chromosomal aberrations. Radiation-induced chromosomal aberrations can be classified as either chromatid or chromosome aberrations. Chromosome aberrations result when a cell is irradiated early in interphase, before the chromosome material has a chance to duplicate, while chromatid aberrations result when a cell is exposed to radiation later in interphase and therefore, after duplication of the DNA material.

Many types of chromosomal aberrations and rearrangements are possible, but only three types (all asymmetrical) are lethal to the cell: the dicentric, the ring and the anaphase bridge (see **Figure 3.3**). The dicentric and the ring are both chromosome aberrations but one results from the interactions of two double-strand breaks from different chromosomes, and the other from within the same chromosome.

Several studies[38,39] suggest that a close correlation exists between failure of cells to proliferate after radiation exposure and chromosomal aberrations (see **Figure 3.4**). Since a correlation exists between lethal chromosomal aberrations and double-strand breaks, these studies further support the idea that double-strand breaks are the most important lesion biologically.
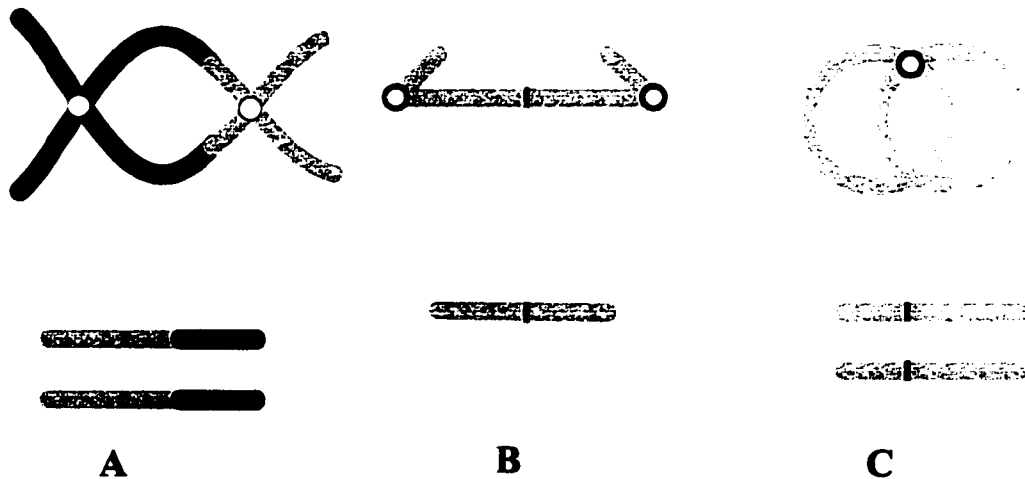
Figure 3.3: Schematic of radiation-induced lethal chromosomal aberrations following duplication. (A) The dicentric chromosome plus acentric fragments. (B) Dicentric chromatid plus acentric chromatid fragment. The anaphase bridge results from the chromatid being stretched between poles at the anaphase. (C) Overlapping rings and acentric fragments.
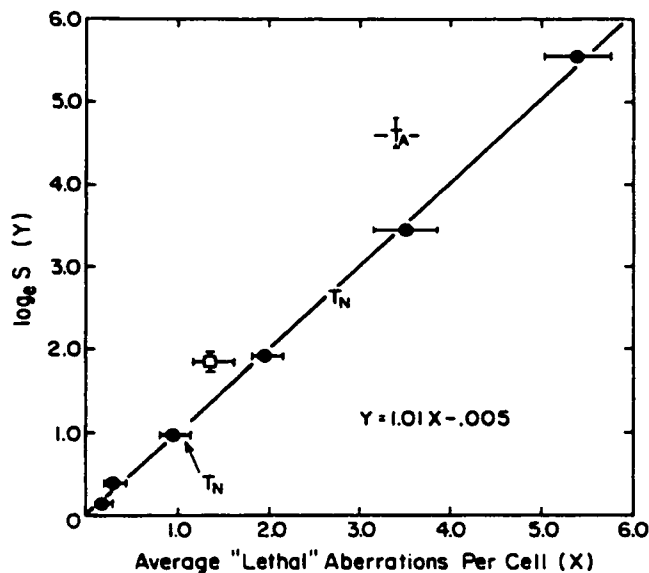
Figure 3.4: Correlation between the average lethal aberrations per cell and ln(S) in 1522 normal human fibroblasts exposed to x-rays.[40]

3.3.3 Survival Curves

3.3.3.1 Concept of Clonogenic Cells

Tumors and renewal tissues contain a small number of stem cells, which have a high capacity for cell proliferation[41]. These stem cells can produce a large family of descendants and can undergo self-renewal to avoid depletion. Since it is not always possible, at the present time, to study colony-forming cells in situ within tumors or renewal tissues, defined environments, such as cell-culture, are used to do so. Cells that, under defined experimental circumstances, have the ability to produce a colony of descendants (usually more than 50) are known as clonogenic cells.[42] Since clonogenic cells are assumed to be similar to stem cells, they are the ones that are studied in radiobiology.

3.3.3.2 Mathematical Models of Cell Survival

Evaluation of the survival of clonogenic cells following irradiation is an important aspect of radiobiology. Curves that plot the surviving fraction of clonogenic cells against absorbed dose are referred to as survival curves. Survival curves are essential tools in

radiobiology because they help predict treatment outcome. The shape of a given survival curve depends on various factors such as the type of radiation, the fractionation scheme, oxygenation, repair processes, etc. Many mathematical models based on assumed mechanisms of cell killing have been proposed to account for the shape of mammalian cell survival curves and for the way they change with various factors, but their validity is still unproved. In addition, the scatter exhibited by the biological survival data makes it even more difficult to discriminate between mathematical models, as illustrated in **Figure 3.5**. These survival curves are characterized by an initial rapidly changing slope (often referred to as the shoulder) in low dose regions followed by a much more gradually changing slope at higher dose levels.
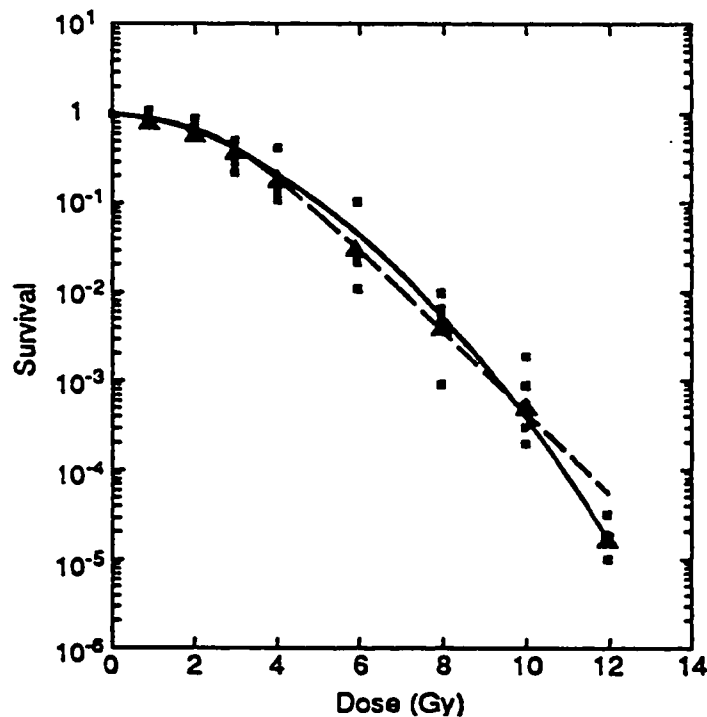
Figure 3.5: Survival data for a murine melanoma cell line treated with low-*LET* radiation. The data from five independent survival experiments are shown as the small squares with the geometric mean value at each dose shown as the large triangles. The survival curves shown are from fitting the data to the two component model (dashed line) or to the linear-quadratic model (solid line).[43]

In general, mammalian cell survival curves, for densely ionizing radiations, have little or no shoulder and are linear on a logarithmic-linear graph (i.e. every radiation damage is lethal) as shown in **Figure 3.6**. Experimental data from high-*LET* radiation are best fitted by:

$$SF = e^{\left(-D_i / D_o\right)}$$
(3.5)

where SF = fraction of cells that survive a given absorbed dose D_i or probability that any individual cell will survive the radiation dose D_i,

and D_o = mean lethal dose

The mean lethal dose, D_o, is defined as the dose required to reduce the fraction of surviving cells to 37% or $1/e$ of its initial value. This is, on average, the dose required to deliver one inactivating event per cell.
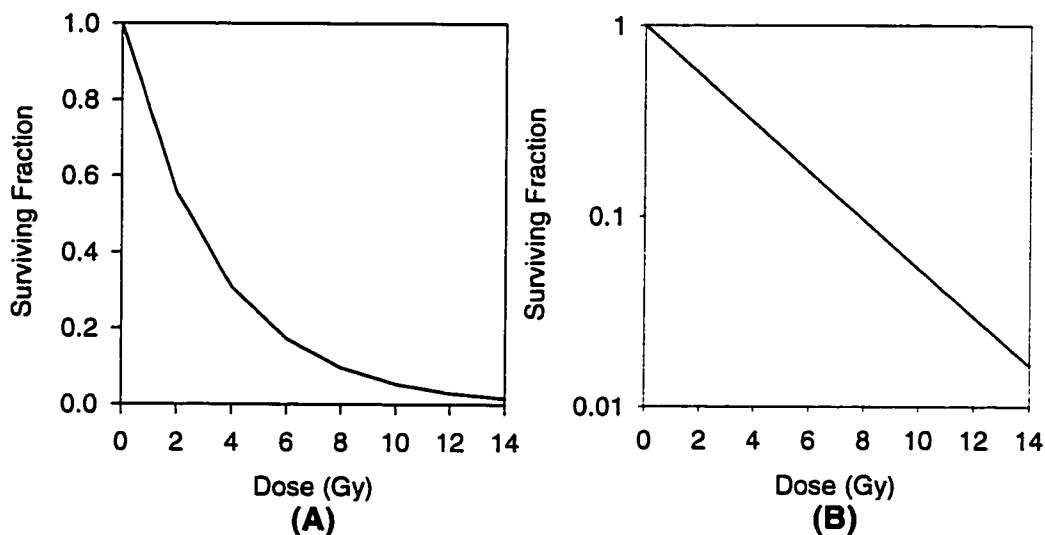
Figure 3.6: A typical exponential cell survival curve for cells irradiated by high-*LET* radiation in tissue culture. (A) data plotted on a linear survival scale. (B) same data plotted on a logarithmic scale.

Mammalian cell survival curves for sparsely ionizing radiation are, on the other hand, characterized by an initial shoulder region followed, generally, by a roughly exponential region at higher dose. Two points of view roughly account for the shoulder of the survival curve. One set of models (target theory models) assumes that the shoulder is primarily due to the interaction of sublethal lesions or the accumulation of sublethal

damage. The second set of models (repair models) assumes that the shoulder is the result of the repair of single lesions produced by single tracks. A brief description of these models and their effects on the survival curve is given in the following sections.

3.3.3.2.1 Target Theory Models

Target theory models assume that there are a fixed number of critical sites in the cell which must each be hit in order to cause cell death. These critical sites or sensitive targets are actually responsible for the reproductive integrity of the cell and their number vary depending on the mathematical model. There exist three survival curve models which originate from target theory. They are the multi-target single-hit, the two component model and the linear-quadratic model.

The multi-target single-hit model or simple multi-target model suggests that there are more than one target in the cell, which must each receive a single hit, in order for the cell to die. Since the probability p of inactivating one target is equal to:

$$p(\text{one target}) = \left(1 - e^{\left(-D/D_o\right)}\right),$$

(3.6)

then the probability of inactivating n targets is:

$$p(n \text{ targets}) = \left(1 - e^{\left(-D/D_o\right)}\right)^n$$

(3.7)

where n is, according to target theory, the number of targets in a cell that have to be inactivated. However, because the parameter n varies greatly with the cell cycle stage, the physiological cell state, and the conditions of irradiation, it is almost impossible to equate n with any specific target structure in the cell.

The probability of survival, or the survival fraction, after a dose D_i is simply given by:

$$SF = 1 - \left(1 - e^{\left(-D/D_o\right)}\right)^n.$$

(3.8)

This gives a survival curve with zero initial slope, a shoulder at low dose and a final exponential region when D_i/D_o is large as shown in **Figure 3.7**.

41
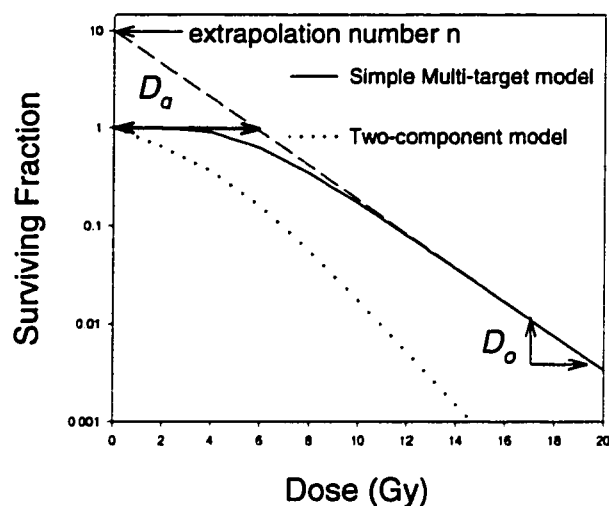
Figure 3.7: Typical survival curves for the simple multi-target and the two-component models.

The size of the shoulder can be described by the quasi-threshold dose D_q, which is related to the parameter n and D_0 by the following relation:

$$D_q = D_o \ln n .$$ (3.9)

The multi-target plus single-hit component or two-component model, is a flexible model that fits most data very well. It combines the simple multi-target model with a single-event component. The probability of survival is given by:

$$SF = e^{\left(-D/D_1\right)}\left[1-\left(1-e^{\left(-D/D_2\right)}\right)^n\right]$$ (3.10)

where D_1 is the initial slope due to single-event killing, and D_2 is the final slope due to multiple-event killing. The effect of the first term is to bend the whole curve down and therefore induce a non-zero initial slope as depicted in **Figure 3.7**.

The main drawback of the above target theory models is that the shoulder on the cell-survival curve varies as a function of cell cycle stage. This variation makes it rather difficult to comprehend how the number of targets could be responsible for this.

The last target theory model, the linear-quadratic model is characterized by a continuously bending survival curve, which has the expected initial slope but which never becomes exponential, even at very high dose as shown in **Figure 3.8**.

The LQ model is represented by the following linear-quadratic equation:

$$SF = e^{-(\alpha D + \beta D^2)}$$

(3.11)

where α and β are the linear and quadratic coefficient, which determine the relative importance of the single radiation track and dual radiation track events.
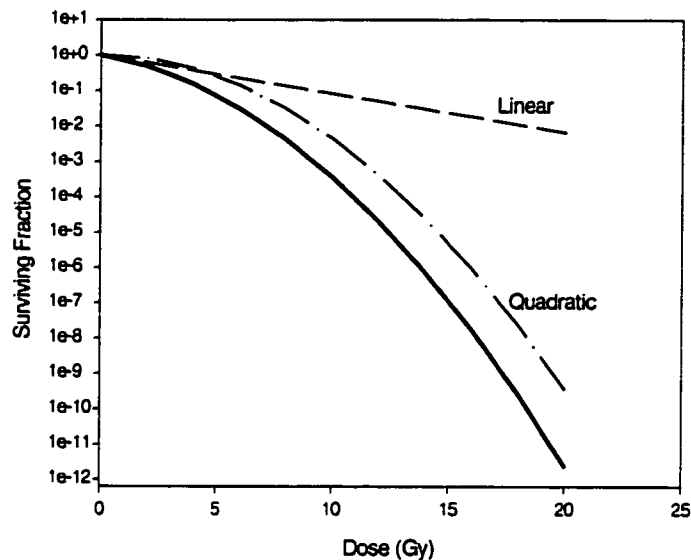
Figure 3.8: The linear-quadratic formula which results from the summation of the linear term and the quadratic term.

The LQ model is currently the most popular cell survival model. Part of the LQ model's widespread use is a result of its mathematical simplicity. Because of its mathematical simplicity the LQ model can easily be generalized to describe fractionated radiation. The main drawback of the model is that, over the range of dose rate considered in radiotherapy, physical or chemical lesions from statistically independent charged-particle tracks do not interact. Therefore, double-strand breaks cannot arise from the interaction of two single-strand breaks as proposed by the model. Furthermore, the cell survival data do not really support the use of the LQ model at high doses, since most clinical survival curves do not fit the LQ equation in that high range. However,

individual daily doses used in fractionated radiotherapy more frequently lie over the low-dose range of survival curves, i.e. shoulder portion, where the LQ model fits the survival data well. Thus, for fractionated regimen, the LQ equation can be used to describe the dose-response relationship.

3.3.3.2.2 Repair Theory Models

A number of cell killing models, based upon processes of radiation repair, have been proposed to account for the shape of mammalian cell survival (e.g. lethal potentially lethal model & repair-saturation models). These models all assume that cell killing is caused by single-hit events. Therefore damage at any DNA site is unlikely to be due to interaction between radiation tracks. The main drawback of repair theory models is that the equations that they produce to describe the shape of the survival curve are mathematically very complex as compared to the other models. Because of their complexity, these equations will not be presented in this work.

The lethal potentially lethal model or LPL model[44] is a model of radiation action which combines the ideas of lesion interaction and lesion repair process. The LPL model is based on the main assumption that two different types of lesion are produced by ionizing radiation: repairable (potentially lethal) lesions and non-repairable (lethal) lesions (see **Figure 3.9**).

Lethal lesions lead to death of the cell or its progeny and, thus, give rise to the linear component of cell killing. The potentially lethal lesions can interact with each other to form a lethal lesion (binary misrepair), can be "fixed" at some point in the cell cycle (fixation), or can be correctly repaired. It is believed that the binary misrepair is responsible for the quadratic component of cell killing in the LPL model.
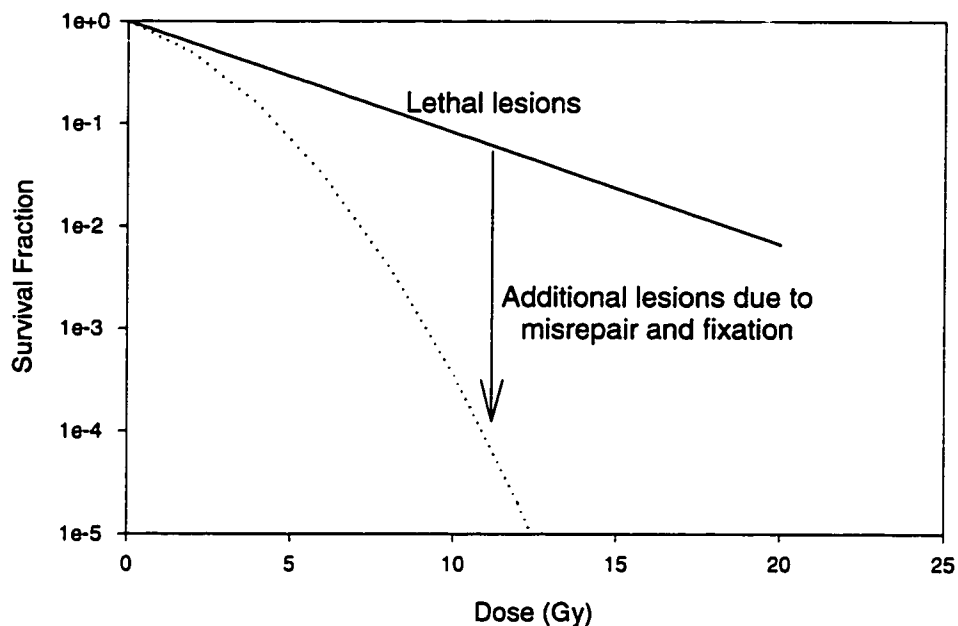
Figure 3.9: The lethal potentially lethal or LPL model.

Repair-saturation models propose that the shape of the survival curve depends only on a dose-dependent rate of repair.[45] The models assume that, in the absence of repair, (i.e. repair enzymes), all initial lesions, (i.e. lethal and potentially lethal lesions), lead to cell death and thus give rise to an exponential cell survival curve. In the presence of repair enzymes, however, the potentially lethal lesions are either repaired successfully or fixed at some point in the cell cycle. The repair of potentially lethal damage increases survival as shown in **Figure 3.10** but the amount of repair is dose dependent. At low doses, the repair enzymes are free to repair all the potentially lethal damage before fixation occurs. However, at higher doses, saturation of repair enzymes occurs. This saturation slows down the repair and as a result less damage can be repaired in the time available before fixation. The decrease in repair caused by saturation is believed to be responsible for the downward bending of the survival curve at higher doses.
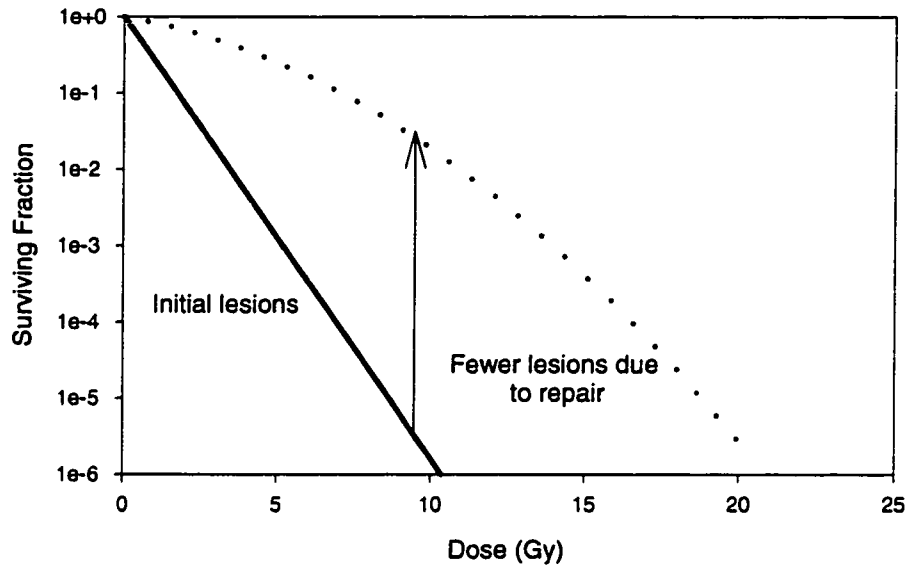
Figure 3.10: The repair-saturation model of radiation action.

3.3.4 Factors that Influence Cell Survival

3.3.4.1 Radiation Quality

Cell survival depends on the effective *LET* of the radiation beam used for treatment. As *LET* increases, both D_o and *n* decrease as shown in **Figure 3.11**. The decrease in D_o is attributed to the enhanced sensitivity of cells to high-*LET* radiation, while the decrease in the shoulder is attributed to a decrease in the capacity of the cells to recover from the sublethal radiation damage. As a result of the higher cell kill rate and lower repair of damage, high-*LET* radiation induces more biological damage than does low-*LET* radiation.
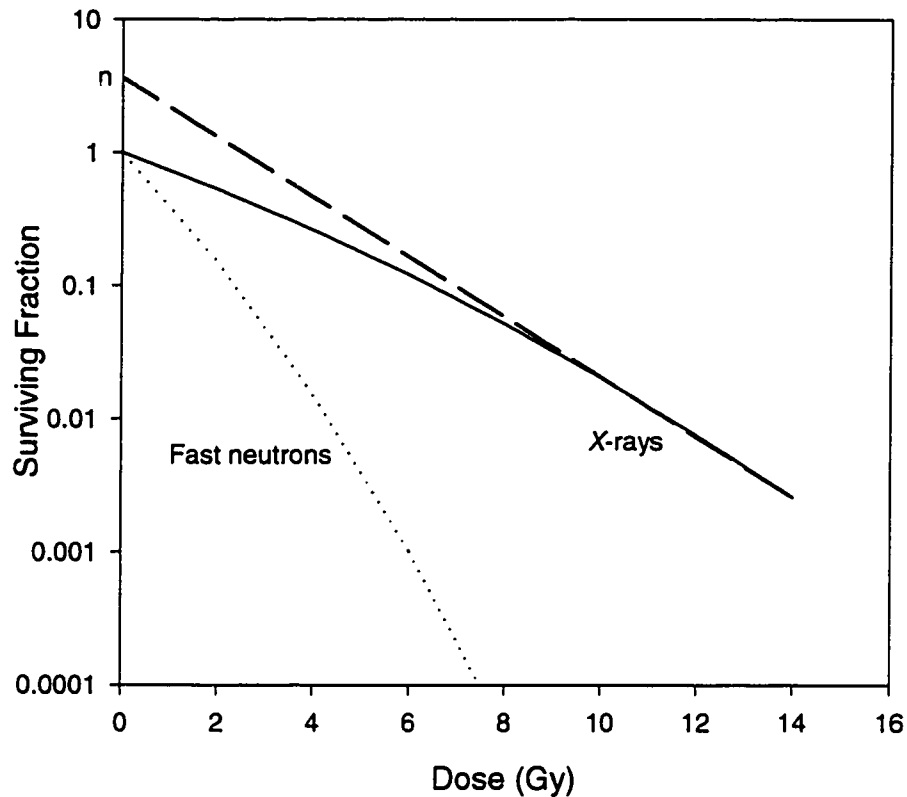
Figure 3.11: The effect of *LET* on the survival curve of mammalian cells.

3.3.4.2 Cell-cycle position

Experiments[46,47] have shown that radiosensitivity differs in different phases of the cell cycle as depicted in **Figure 3.12**. Differences in the pattern of sensitivity and resistance have been observed but, in general, many cell lines appear to have a resistant period in S phase and a sensitive period in G_2 phase.

These experiments also reveal that the radiosensitivity of asynchronous cell populations is dominated by the most resistant cells. Therefore, the survival curve of these heterogeneous populations is very similar to that of the most resistant component of the asynchronous population
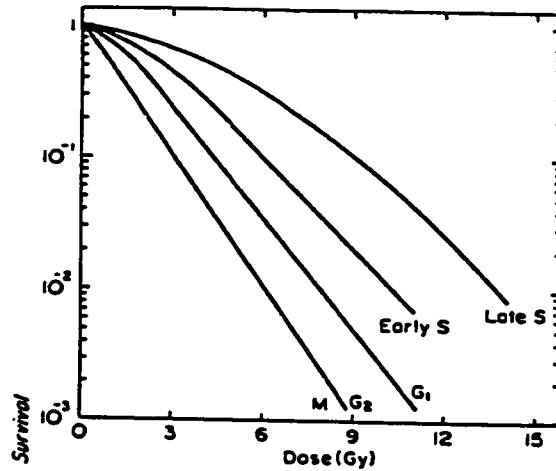
Figure 3.12: The effect of cell cycle position on the cellular radiosensitivity of Chinese hamster cells.[18]

3.3.4.3 Repair

Some of the radiation damage incurred in cells during irradiation can be repaired. Repair can be divided into potentially lethal damage repair (PLDR) and sublethal damage repair (SLDR). The effects on the of PLDR and SLDR on the survival curve are shown in **Figure 3.13**.
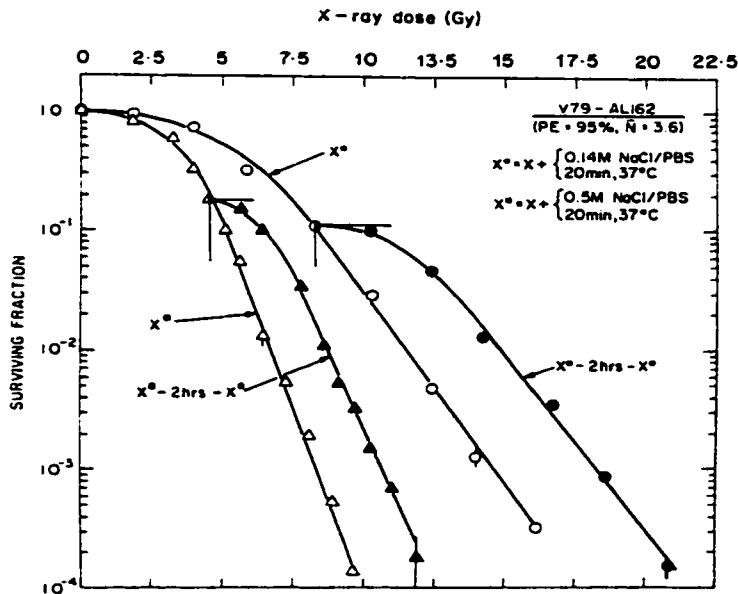
Figure 3.13: Single and fractionated dose-response curves of mammalian cells treated with isotonic or hypertonic saline. [48]

The increase in cell survival, i.e. the reappearance of the shoulder, observed when a dose of radiation is split into two fractions separated by a time interval is the result of sublethal damage repair. Many factors are involved in the repair of sublethal damage and they are summarized in **Figure 3.14**.
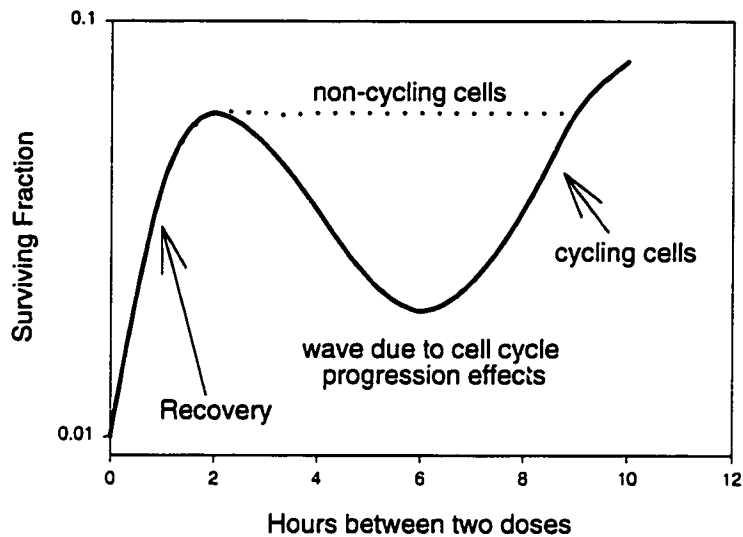
Figure 3.14: Typical time course of survival for non-cycling and cycling mammalian cells.

The initial rise results from sublethal damage repair in cells which survived the first dose. The decline and subsequent increase in survival observed in cycling cells results from the desynchronization and the progression of the cells through the phases of the cell cycle. The final increase in the curve occurs when the time interval between the two doses exceeds the cell cycle. The long time interval allows the cells to proliferate and double in number between dose fractions.

Potentially lethal damage repair occurs when cells are held under suboptimal growth conditions. The effects of potentially lethal damage repair on the survival curve is a decrease in the slope of the cell survival curve. Potentially lethal damage repair is believed to be the most important repair mechanism in relating the cell culture studies of human tumors to their clinical response.[49]

3.3.4.4 Re-oxygenation

Molecular oxygen is believed to be the most important modifier of the biologic effect of ionizing radiation. The degree of sensitization caused by the presence of oxygen is described by the oxygen enhancement ratio or OER. OER is the ratio of hypoxic to aerated doses required to give equivalent cell killing (see **Figure 3.15**). For most cells, the OER lies in the range from 2.5-3.5 for low-*LET* radiation and decreases to a value of unity for high-*LET* radiation. Until recently, it was believed that this fraction was independent of the survival level at which is was measured. However, recent studies suggest that the OER below 3 Gy has a slightly smaller value for low-*LET* radiation. The reason for this reduction is still unclear, but it is believed to be linked to the greater importance of single-hit killing in this region of the cell survival curve.[42]
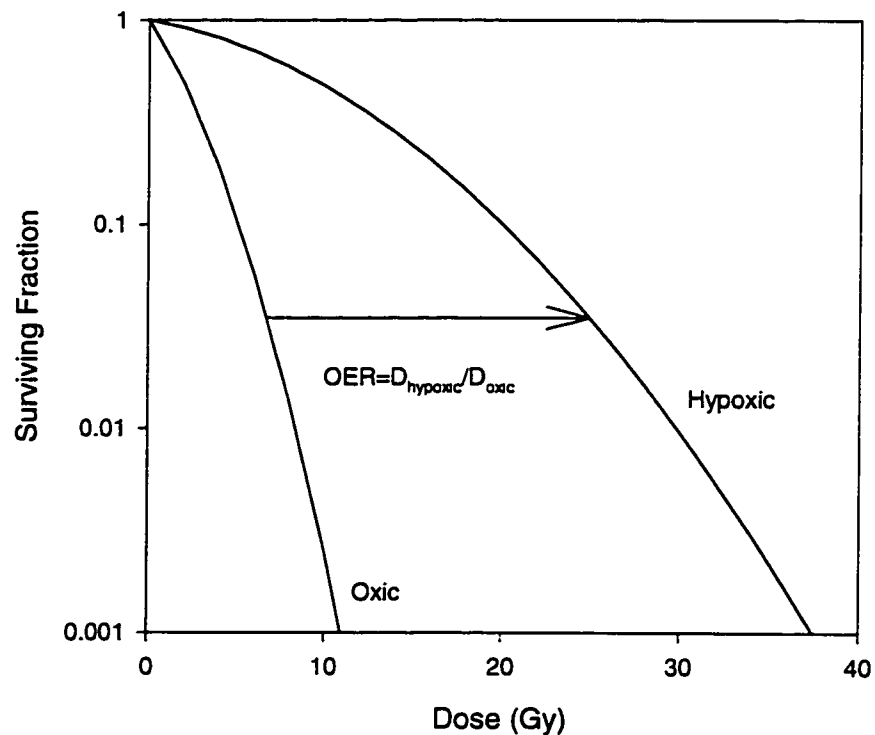
Figure 3.15: Typical survival curves for oxic and hypoxic cells treated with low-*LET* radiation.

For the oxygen effect to be observed, oxygen must be present either during irradiation or within a few milliseconds after the radiation exposure. The mechanism responsible for the enhancement is not fully understood but there is general agreement that oxygen acts at the level of the free radicals. It is believed that if oxygen is available. the damage produced in the DNA molecule by free radicals can be "fixed" or simply made permanent and irreparable. This is known as the *oxygen fixation hypothesis*.

Experiments on bacteria and mammalian cells suggest that only very small amounts (0 to 30 mm Hg) of oxygen are necessary to produce a dramatic increase in cell sensitivity[50]. Therefore, from a radiobiological point of view, most normal tissues can be considered well oxygenated, although it is now known that certain normal tissues, such as cartilage, skin and liver, are moderately hypoxic. Tumors, on the other hand, contain a significant proportion (10-20%) of hypoxic cells and are therefore more resistant to radiation.

Experiments on animals have shown that when tumors are irradiated with a single dose, most of the surviving tumor cells are mainly the original hypoxic cells, but that subsequently, the hypoxic fraction decreases and approaches its starting value. The phenomenon by which hypoxic cells become oxygenated following irradiation is termed reoxygenation. Reoxygenation cannot be measured in human tumors, but presumably it occurs in some tumors controlled by multifraction regimen.

3.4 Clinical Response

During external beam radiation therapy, both the tumor and normal surrounding tissues are irradiated. Since the main goal of radiotherapy is to control the tumor and minimize the damage to the healthy tissues, biophysical tools such as *NTCP* and *TCP* models, are needed to facilitate the evaluation of complex treatment plans and to develop an appropriate scoring function for plan optimization.

In order to use these quantitative models for optimization and evaluation purposes, the models must correctly describe the behavior of control and complication probabilities as a function of various parameters of the treatment plan, such as the following[51]:

1) physical: dose,

2) geometrical: volume and tissue architecture,

3) radiobiological: tissue sensitivity,

4) temporal: dose fractionation.

3.4.1 Tumor Response

3.4.1.1 Tumor Architecture

Tumors are composed of both neoplastic cells and normal tissue cells, such as blood cells and fibroblasts, which form the stroma. The neoplastic cells can be divided into four compartments based on their kinetic properties [52](see **Figure 3.16**).
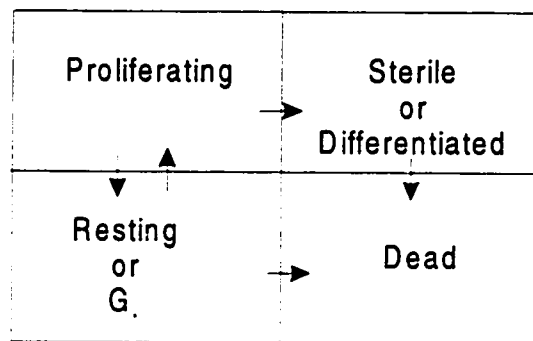
Figure 3.16: The four compartments of a tumor neoplastic cell population.

The most important compartments in radiotherapy are the proliferating and resting or G_o compartments. Cells in the proliferating compartment are the major contributor to growth of the tumor volume. Many of these cells have demonstrated the capacity to produce a large family of descendants within a test environment and are, therefore, known as clonogenic cells. G_o cells are resting cells that are capable of re-entering the cell cycle if needed and may, therefore, be clonogenic. Because of their clonogenic properties, cells from both these compartments need to be killed by the applied therapy. The movement of resting cells to the proliferating compartment is known as recruitment.

3.4.1.2 Tumor Control Models

Models of tumor control are, in general, based on the assumption that tumor recurrence represents the progeny of just one or several independent clonogenic cells

which survived the treatment. In other words, tumors regrow unless all clonogenic tumor cells are eradicated by irradiation.

Assuming, once again, that clonogenic cell kill is random and therefore obeys Poisson or binomial statistics, it is simple to derive the relationship between surviving fraction SF and tumor control probability TCP. It is:

$$TCP = (1 - SF(D))^k \qquad (3.12)$$

where k = number of clonogenic cells in the tumor,

and $SF(D)$ = the surviving fraction of clonogens after a dose D.

Other parameters such as fractionation, volume, tumor sensitivity can be incorporated in the above model but will be dealt with in the following chapter.

Under idealistic conditions, a sigmoid curve is expected if the dose of radiation is plotted against the likelihood of cure as predicted by Poisson statistics (see **Figure 3.17**).
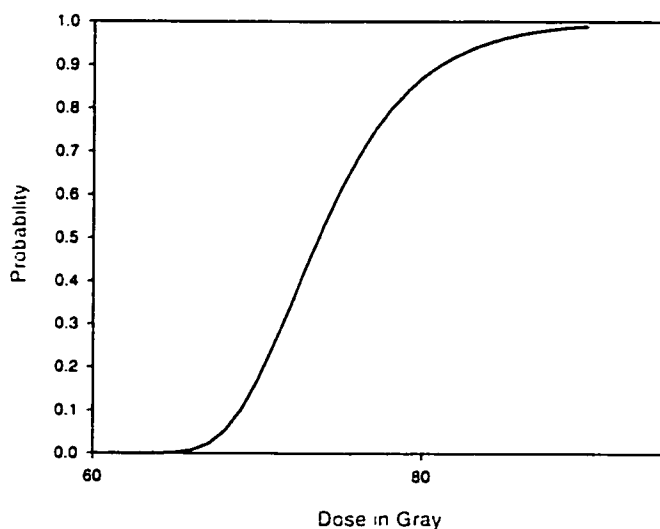
Figure 3.17: Typical tumor control probability curve for a melanoma tumor containing 10^8 clonogenic cells.

The shape and steepness of the sigmoid dose-response relation for tumors can be affected by many factors. For example, the heterogeneity between individual tumors tends to make the dose-cure relationship flatter than expected for a Poisson distribution.

53

3.4.2 Normal Tissue Response

3.4.2.1 Normal Tissue Architecture

As far as tumors are concerned, the surviving fraction of clonogenic cells determines the success or failure of a treatment regimen, but for normal tissues, however, it is not the whole story. The relationship between the survival of clonogenic cells and organ function depends on the structural organization of the tissue.[53]

For the purpose of modeling radiation response, a tissue is assumed to be composed of functional subunits or FSUs. These FSUs are either defined structurally as, for example, the nephrons in the kidney, or functionally (e.g. the volume or area that can be repopulated by one clonogen). The FSUs of a specific organ are also thought to contain a constant number of clonogens and to repopulate from one surviving clonogenic cell.

Three types of spatial arrangements of the FSUs in the tissue have been proposed:[54]

1) "Serial" or critical element (e.g. spinal cord, nerves):

> The integrity of each FSU is critical to organ function. Therefore damage to one results in a measurable probability of complication.

2) "Parallel" or integral response (e.g. liver, kidney, lung):

> A complication occurs only if a sufficient number of FSUs are destroyed.

3) Graded response (e.g. skin, mucosa):

> Radiation reaction occurs on a continuous scale.

Graded response tissues are different from "serial" and "parallel" architecture tissues in that they are fast renewing tissues. These fast renewing tissues can repopulate from outside (e.g. from adjacent FSUs). Thus, these FSUs are not independent from each other as is the case for "serial" and "parallel" architecture organs. This dependency has yet to be modeled, therefore *NTCP* models do not exist at the moment for such fast renewing tissues.

3.4.2.2 Normal Tissue Complication Models

If we assume that an FSU is capable of regenerating from one clonogenic cell, then the probability of killing one FSU is given by:

$$P_{FSU} = (1 - SF(D))^k \tag{3.13}$$

where k is the number of clonogenic cells per FSU, and $SF(D)$ is the surviving fraction after a dose D.

The probability of killing t of the N FSUs that compose the organ is well described by binomial statistics and is given by:

$$P_{tFSU} = \binom{N}{t} (P_{FSU})^t (1 - P_{FSU})^{N-t}. \tag{3.14}$$

For organs of "parallel" architecture, a complication is thought to occur when more than M FSUs are eradicated (i.e. $t = M+1$). Therefore, the probability of complication is simply:

$$NTCP_{Parallel} = \sum_{t=M+1}^{N} P_{tFSU} = \sum_{t=M+1}^{N} \binom{N}{t} P_{FSU}^t (1 - P_{FSU})^{N-t} \tag{3.15}$$

For organs of "serial" architecture, it is thought that damage to one FSU is enough to result in a measurable probability of complication. Therefore, $M=0$ and the normal tissue complication probability takes on the following form:

$$NTCP_{Serial} = \sum_{t=1}^{N} P_{tFSU} = 1 - (1 - P_{FSU})^N. \tag{3.16}$$

In the case where the organ survives if at least one FSU survives, as is the case for a tumor containing one clonogen per FSU, control occurs if $M=N-1$. Thus, the probability of tumor control is given by:

$$TCP = \sum_{t=N}^{N} P_{tFSU} = P_{tFSU} = P_{FSU}^N = (1 - SF(D))^{kN} \tag{3.17}$$

where k is the number of clonogenic cells per FSU, which is one for this special case, and N is the number of FSUs in the tumor or the number of clonogens.

As predicted by **equations (3.15)** and **(3.16)**, the probability of tissue complication increases according to binomial statistics with decreasing number of surviving functional sub-units. As for tumors, the shape of the organ-response curve is sigmoidal in nature

and its steepness varies with various factors, such as tissue heterogeneity, fractionation and tissue sensitivity.

4. EQUIVALENT UNIFORM DOSE MODELS

As previously stated in **Chapter 1**, the *EUD* concept proposed by Niemierko, assumes that any two dose distributions are equivalent if they cause the same radiobiological effect. Thus, for any non-uniform dose distribution delivered to a volume of interest, there exists a unique uniform dose distribution delivered in the same fashion, which causes the same radiobiological effect.

4.1 Niemierko's *EUD* Model for Tumors

Applying this concept to tumors, Niemierko was able to develop several *EUD* formulas for the planning target volume, which, during radiotherapy treatment, rarely receives a uniform dose distribution. All of these *EUD* formulas are based on the main assumption that the radiobiological effect, i.e. tumor control, is governed by the expected number of surviving clonogens within the planning target volume. Thus, for any non-uniform PTV dose distribution delivered according to a given fractionation scheme, there exists a unique uniform dose delivered in the same number of fractions, which results in the survival of the same number of clonogenic cells. This uniform dose is known as the Equivalent Uniform Dose or *EUD*.[55]

4.1.1 Basic *EUD* Model

In this section, Niemierko's basic *EUD* model, which stems from highly idealized assumptions, will be introduced. These assumptions will be examined and refined, and the formalism modified and extended accordingly.

Niemierko initially assumed that a planning target volume undergoing irradiation is ideally composed of a large number of identical independent clonogens. These clonogens are considered to be radiobiologically independent, in the sense that damage to any clonogen will have no effect upon its neighbors. This assumption is a weak one, as clonogenic cells do not grow autonomously after irradiation. Clonogenic cells exhibit a regenerative response in the form of accelerated repopulation after a lag period following injury (see **Figure 4.1**).[56] This accelerated repopulation suggests that clonogens are not radiobiologically independent and that a certain amount of interaction does indeed occur

between clonogens. This interaction could, theoretically, be modeled in terms of clonogen separation and density. For the purpose of this work clonogenic interaction will be assumed negligibie, hence clonogens will be treated as radiobiologically independent.
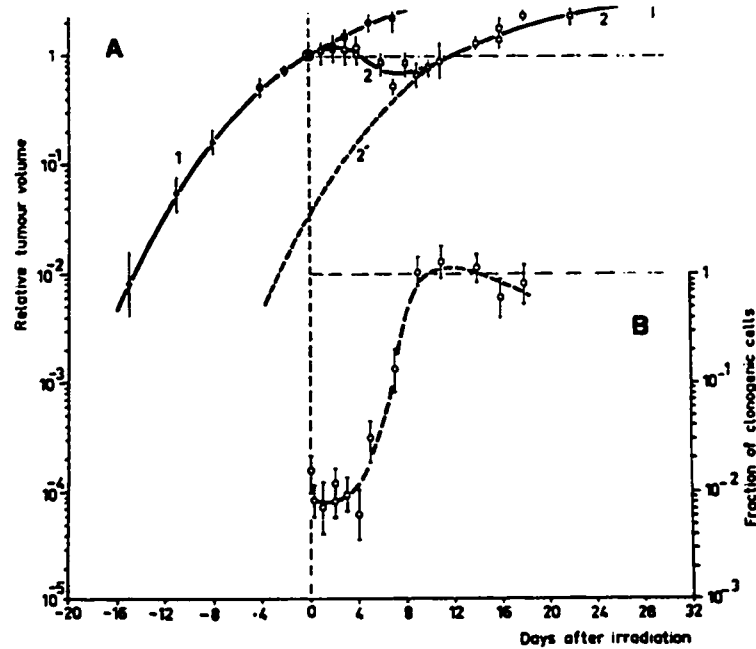
Figure 4.1: Illustration of accelerated repopulation.[57]

By further assuming that stochastic killing of the clonogens is well described by Poisson statistics, Niemierko was able to approximate the surviving fraction $SF(D)$ of cells irradiated to a dose D by an exponential function:[55]

$$SF(D) = \exp\left(-D\!\big/\!D_o\right)$$ (4.1)

where D_o is the mean lethal dose. Niemierko's use of the simple exponential model to describe the dose-response relationship of tumors, while somewhat crude, is mathematically simple. As mentioned in chapter 3, the empirical linear-quadratic model is currently the most popular dose-response model in radiation therapy as it fits adequately the clinical data. Niemierko does eventually make use of the LQ model, during his development of the EUD formula for fractionated therapy.

Since the radiosensitivity of clonogens is more commonly described in terms of the surviving fraction at the reference dose, D_{ref} of 2 Gy (SF_2), Niemierko redefined the surviving fraction in terms of SF_2 :[55]

$$SF(D) = (SF_2)^{D/D_{ref}}$$ (4.2)

where $SF_2 = \exp\left(-D_{ref}/D_o\right)$ and D_{ref}, which, for the purpose of this work, assumes the common value of 2 Gy, a well accepted daily dose fraction.

Because the dose throughout the planning tumor volume is never exactly uniform, one must calculate the overall survival fraction in order to obtain an equivalent uniform dose. The overall survival fraction can be calculated from either a dose-volume histogram or the dose calculation points. In his work, Niemierko employed dose-volume histograms to arrive at the overall survival fraction. However, if one wishes to obtain improved survival fraction results, dose calculation points should be used, as they are the primary dose data. DVHs are secondary as they are derived from the dose calculation points.

Another idealized assumption made by Niemierko, while developing his basic *EUD* formula, is that clonogenic cells are uniformly distributed across the planning target volume. Given this assumption, the overall survival fraction becomes the weighted average of all the survival fractions taken over all (n) near-homogeneous sub-volumes:[55]

$$SF(\{D_i\}) = \sum_{i=1}^{n} v_i \cdot SF(D_i)$$ (4.3)

where $SF(D_i)$ is the survival fraction at the ith voxel or sub-volume and v_i is the partial volume corresponding to dose D_i.

Since Niemierko assumed that there is a unique uniform dose that will give the same fraction of surviving clonogens in an idealized tumor volume as a given non-uniform dose distribution, the following equality can be used:

$$SF(EUD) = SF(\{D_i\}).$$ (4.4)

Thus,

$$(SF_2)^{EUD/D_{ref}} = \sum_{i=1}^{n} v_i \cdot (SF_2)^{D_i/D_{ref}} .$$ (4.5)

Solving the above equation yields the following Equivalent Uniform Dose formula for an idealized tumor volume:[55]

$$EUD = D_{ref} \ln\left[\sum_{i=1}^{n} v_i \cdot (SF_2)^{D_i/D_{ref}} \right] / \ln(SF_2).$$ (4.6)

4.1.2 Some Modifications of the Basic *EUD* Model

The preceding section outlined a mathematically simple version of the Equivalent Uniform Dose model which evolved from the dose-response characteristics of a hypothetical, idealized tumor. In this section, some modifications will be made, in order to refine the *EUD* model along the lines of more biologically realistic tumors.

4.1.2.1 Absolute Volume Effect

Since tumors are likely to vary in size, one may wish to relate the Equivalent Uniform Dose to the same absolute reference volume V_{ref}. Niemierko incorporated absolute volumes in his *EUD* model by assuming that the number of clonogenic cells within the tumor is proportional to the volume.[55] This is a very crude assumption as tumor growth is not always associated with clonogenic cell proliferation. However, for mathematical simplicity, Niemierko assumed that the number of clonogenic cells is linearly proportional to the planning target volume. The *EUD* formula in terms of V_{ref}, thus becomes:

$$EUD(V_{ref}) = D_{ref} \ln\left[\frac{1}{V_{ref}} \cdot \sum_{i=1}^{N} V_i \cdot (SF_2)^{D_i/D_{ref}} \right] / \ln(SF_2)$$ (4.7)

where V_{ref} is the average volume of tumors in a particular study and V_i is the absolute volume receiving dose D_i.

4.1.2.2 Non-Uniform Distribution of Clonogenic Cells

While initially only uniform clonogenic cell distribution was considered, the most general case would encompass the existence of non-uniform clonogen density. The

actual distribution of clonogens within a tumor is still unavailable at the present, but if this information were to become available, the spatial distribution of clonogenic cells could be easily incorporated in the model.

In the case of non-uniform clonogen distribution, the overall survival fraction becomes:

$$SF(\{D_i\}) = \frac{\left[\sum_{i=1}^{N} V_i \cdot \rho_i \cdot SF(D_i)\right]}{\sum_{i=1}^{N} V_i \cdot \rho_i} \tag{4.8}$$

where ρ_i and V_i are the local absolute densities of clonogens and volumes, respectively. Partial volumes could also have been used to calculate the overall survival fraction of non-uniform distribution of clonogens. Substituting **formula (4.8)** into **formula (4.5)** and then solving for EUD would yield the following formula:

$$EUD = D_{ref} \cdot \ln\left\{\frac{\left[\sum_{i=1}^{n} V_i \cdot \rho_i \cdot (SF_2)^{D_i/D_{ref}}\right]}{\sum_{i=1}^{n} V_i \cdot \rho_i}\right\} \Big/ \ln(SF_2). \tag{4.9}$$

4.1.2.3 Fractionation Effect

In order to develop a EUD model for fractionated therapy, Niemierko substituted the linear-quadratic model for the simple exponential, as the former, better fits the clinical data in the range of the daily dose fractions used in most current fractionated regimens.[55] Furthermore, the LQ model can be easily used, in practice, to compare different fractionation regimens.

In the linear-quadratic model, the survival probability SF, of a cell receiving a single dose, D, of radiation, has the form:

$$SF = \exp(-E) = \exp(-(\alpha \cdot D + \beta \cdot D^2)) \tag{4.10}$$

If, on the other hand, the dose is given in N_f well separated equal fractions of dose d and if repair of sublethal damage between fractions is allowed to take place, the exponent for the cell survival probability for this fractionated course of radiation becomes:

$$E = N_f\left(\alpha d + \beta d^2\right) \tag{4.11}$$

where N_f and d are the number and size of the dose fractions, and α and β are the linear and quadratic coefficients, respectively. The repair of sublethal damage is important, especially, in hyperfractionation radiotherapy (i.e. 2-3 fractions per day), as it ensures that the effects of the multiple doses are independent. Since tumors are typically considered fast-responding entities, sublethal damage repair more than likely occurs during the course of a multifraction regimen. If one could induce imcomplete repair of sublethal damage by significantly decreasing the interfraction time, better tumor control would be achieved as a result of a decrease in survival fraction (see **Figure 4.2**). However, this increase in tumor control would be matched by an increase in complication in acute reacting tissues such as skin and mucosa, as these normal tissues are also fast renewing.

Since the ratio (α / β) is the most accessible parameter in current literature, one may (following Niemierko) divide both sides of **equation (4.11)** by β, in order to bring α and β together as a ratio:

$$E\!\big/\!\beta = N_f\left(\alpha d\!\big/\!\beta + d^2\right) \tag{4.12}$$

or

$$E\!\big/\!\beta = D\left(\alpha\!\big/\!\beta + D\!\big/\!N_f\right) \tag{4.13}$$

where E / β is termed the total effect "TE", and has units of grays squared.

If one divides both sides of **equation (4.11)** by α, one gets the biological effective dose (BED):

$$BED = E\!\big/\!\alpha = D\left(1 + \frac{d}{\left(\alpha\!\big/\!\beta\right)}\right). \tag{4.14}$$

The biological effective dose is the dose which would produce the same effect if it could be delivered at extremely low dose rate. BED is frequently used in radiotherapy to compare different fractionation schedules.
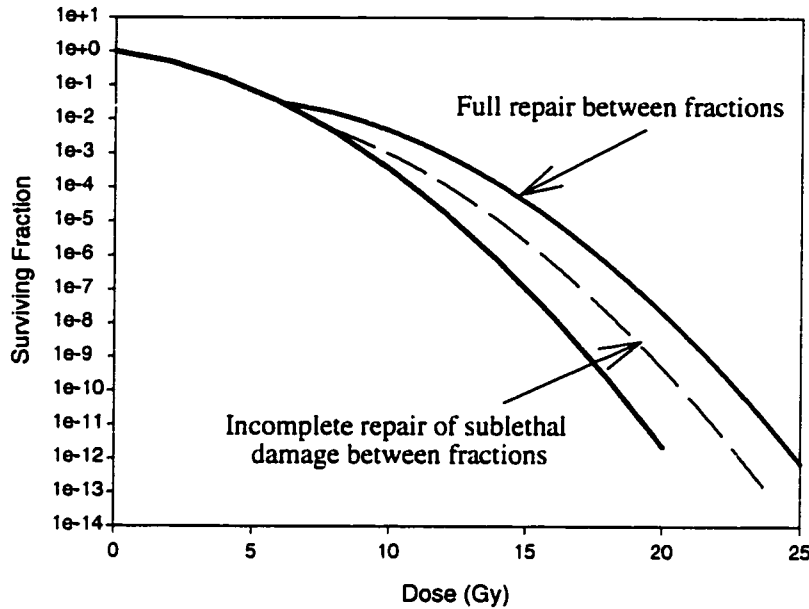
Figure 4.2: The effect of incomplete repair on the cell survival curve.

According to the linear-quadratic model, the surviving fraction can be calculated using SF_2 and (α / β) as follows:[55]

$$SF(D) = (SF_2)^{\frac{D}{D_{ref}} \cdot \frac{\alpha/\beta + D/N_f}{\alpha/\beta + D_{ref}}} .$$ (4.15)

Substituting **formula (4.15)** into the idealized **formula (4.4)** yields the following equation for the Equivalent Uniform Dose:[55]

$$EUD = \frac{N_f}{D_{ref}} \cdot \left[\left(\frac{-\alpha}{\beta} \right) + \sqrt{\left(\frac{\alpha}{\beta} \right)^2 + 4 \cdot \frac{D_{ref}}{N_f} \cdot \left(\frac{\alpha}{\beta} + D_{ref} \right) \cdot \frac{\ln A}{\ln(SF_2)}} \right]$$ (4.16)

where $A = \sum_{i=1}^{n} V_i \cdot \rho_i \cdot (SF_2)^{\frac{D_i}{D_{ref}} \cdot \frac{\alpha/\beta + D_i/N_f}{\alpha/\beta + D_{ref}}} \Big/ \sum_{i=1}^{n} V_i \cdot \rho_i$.

4.1.2.4 Proliferation Effect

Since tumors are fast growing structures, proliferation usually takes place during the course of fractionated radiotherapy. The linear-quadratic model can be extended to include the effect of proliferation. The correction added to the LQ model, by Niemierko,

in order to take proliferation into account, is based upon the assumption that the rate of cellular proliferation remains constant throughout the overall treatment time T. Adding a time factor to the LQ formula yields the following for the biological effect:[55]

$$E = N_f (\alpha \cdot d + \beta \cdot d^2) - \gamma \ T \qquad (4.17)$$

where γ is a constant related to the potential doubling time of the tumor, T_{pot}, by the expression $\gamma = \ln 2 / T_{pot}$, and T is the overall treatment time.

Since not all tumors initiate proliferation at the same time after injury, the overall time T can be replaced by $(T - T_k)$, where T_k is the time at which proliferation begins after the start of the treatment. We then have the biological effect E given by:[55]

$$E = N_f (\alpha \cdot d + \beta \cdot d^2) - \gamma \cdot (T - T_k). \qquad (4.18)$$

Assuming a constant rate of proliferation during the course of treatment, it can be shown that the surviving probability in terms of SF_2 and (α / β) for a dose D given in N_f fractions is:

$$SF(D) = 2^{[(T - T_k)/T_{pot}]} \cdot (SF_2)^{\frac{D}{D_{ref}} \left(\frac{\alpha/\beta + D/N_f}{\alpha/\beta + D_{ref}} \right)}. \qquad (4.19)$$

By substituting the above formula in the idealized **formula (4.4)**, it can be shown that the proliferation factor has no effect on the EUD, if the overall treatment time remains the same. This is to be expected as the proliferation factor depends only upon the overall treatment time and not upon the dose or the number of fractions.

4.1.2.5 Inter-Patient Heterogeneity

Since stochastic cell killing results in a Poisson distribution for surviving cell number, a steep dose-response curve is expected (see **Figure 4.3**) between 10% and 90%, for any one tumor or for a population of identical tumors.[58,59] However, clinical survival curves for human tumors are substantially shallower than expected from Poisson statistics (see **Figure 4.4**). A number of reports have indicated that inter-tumor variability of radiobiological parameters accounts for some of the shallowness observed in clinical survival.[60,61] Another factor that, on a much smaller scale, affects the steepness of the dose-response curve is the intra-tumor heterogeneity. In his present Equivalent Uniform

Dose model, Niemierko assumes that the radiobiological parameters are constants for individual tumors.[55] Thus, intra-tumor heterogeneity is assumed to be non-existent.
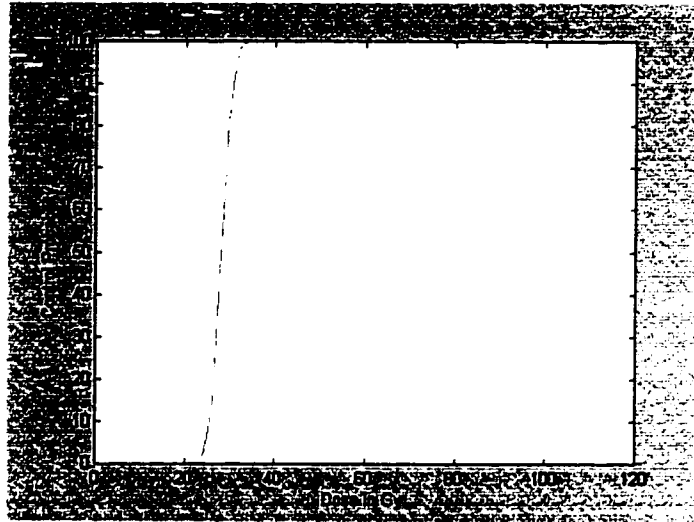
Figure 4.3: Expected dose-response curve for a single tumor or a population of identical tumors.
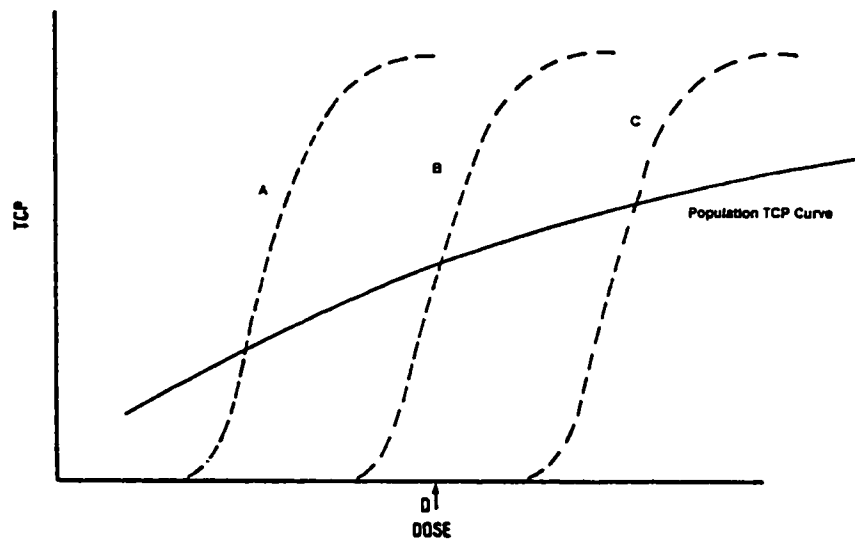
Figure 4.4: Distinction between heterogeneous population dose-response curve and the individual tumor dose-response curves labeled "A", "B", and "C".

Since the radiobiological parameters are unknown for an individual tumor in question, Niemierko uses the expected value of *EUD* taken over the heterogeneous population as the best estimate for the Equivalent Uniform Dose. In order to calculate the expected value of *EUD*, Niemierko further assumes that the clonogens radiosensitivity of

the heterogeneous population is characterized by the surviving fraction at 2 Gy, SF_2, and that SF_2 is $\ln(-\ln SF_2)$ distributed. The probability density function of SF_2 is Gaussian and is given by:[55]

$$\frac{1}{\sqrt{2\pi} \cdot \sigma_S} \cdot \exp\left[-\frac{(S - \overline{S})^2}{2\sigma_S^2}\right] \qquad (4.20)$$

where $S = \ln(-\ln SF_2)$,

$\overline{S} = \ln(-\ln \overline{SF_2})$,

and σ_S is the standard deviation of S about its mean value $\overline{S}$.

From the definition of the mathematical expectation of a random variable, it follows that for tumors with a distribution of S, the expected EUD takes the following form:

$$EUD = \frac{1}{\sqrt{2\pi} \cdot \sigma_S} \int_{-\infty}^{+\infty} \exp\left[-\frac{(S - \overline{S})^2}{2\sigma_S}\right] \cdot EUD(S)dS \qquad (4.21)$$

4.1.2.6 Intra-Tumor Heterogeneity

Even though tumors are considered single entities, they are not simple cell systems. On the contrary, tumors are extremely complex and heterogeneous. Not only are tumor cells dispersed throughout the phases of the cell cycle, but they are exposed to a variety of physiological conditions. As stated in chapter three, tumors can be divided into categories based upon the proliferative, clonogenic and oxygenated status of the tumor cells (see **Figure 3. 16**).

Since cellular radiosensitivity varies within the cell cycle and the amount of oxygen in the region, it is more than likely that clonogenic radiosensitivity is heterogeneous. The exact profile of clonogenic cell radiosensitivity is still unattainable but histological studies suggest that a mixture of hypoxic and oxic regions exist within a tumor, with the hypoxic cells being more radioresistant.[62] In terms of the LQ model, this would imply that tumors consist of clonogenic cells with varying α / β ratio; α / β being high for well-oxygenated cells and low for radioresistant clonogens.

If one assumes that the planning target volume is composed of a population (i.e. $N = N_1 + N_2$) of clonogenic cells with two distinct sensitivities: $\left(\frac{\alpha}{\beta}\right)_1$ for the oxic fraction and $\left(\frac{\alpha}{\beta}\right)_2$ for the hypoxic fraction, the survival fraction, given a total dose D, becomes:

$$SF(D) = \frac{\left(N_1 \exp\left[-D\left(\frac{\alpha_1}{\beta_1} + \frac{D}{N_f}\right)\right] + N_2 \exp\left[-D\left(\frac{\alpha_2}{\beta_2} + \frac{D}{N_f}\right)\right]\right)}{N}. \tag{4.22}$$

Plotting the survival fraction as a function of dose would yield a survival curve that is biphasic. An example of such a biphasic curve is shown in **Figure 4.5** for KHT mouse sarcoma cells irradiated under aerobic or hypoxic conditions. At low radiation doses, one can see that the dose-response is dominated by the aerobic cells as the cell survival curves are close to the oxic curve. At larger radiation doses, the presence of hypoxic clonogenic cells begins to influence the dose response and the survival curve eventually parallels the hypoxic curve.
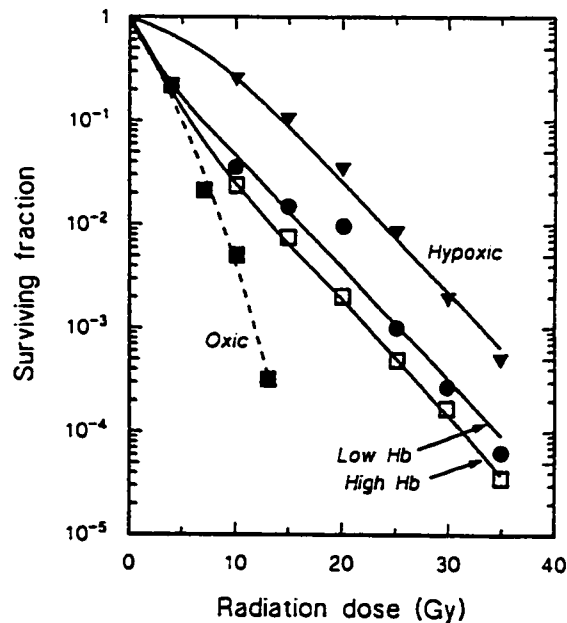
Figure 4.5: Cell survival curves for KHT mouse sarcoma cells irradiated under aerobic or hypoxic conditions.[63]

From the above figure, one can conclude that irradiation of a tumor will inevitably kill more well-oxygenated than hypoxic cells, thus increasing the hypoxic fraction immediately after irradiation. If reoxygenation is allowed to take place between fractions, tumor response will be dominated mainly by the well-oxygenated cell population as hypothetically shown in **Figure 4.6**.

If one assumes that the cellular radiosensitivity, α/β , is Gaussian distributed, the probability density function of α/β is given by:

$$\frac{1}{\sqrt{2\pi}\cdot\sigma_{\alpha/\beta}}\cdot\exp\left[-\frac{\left(\alpha/\beta - \overline{\alpha/\beta}\right)^2}{2\sigma_{\alpha/\beta}^2}\right]$$

(4.23)

and the expected survival fraction becomes:

$$SF(D)_{exp} = \frac{1}{\sqrt{2\pi}\cdot\sigma_{\alpha/\beta}}\int_{-\infty}^{\infty}\exp\left[-\frac{\left(\alpha/\beta - \overline{\alpha/\beta}\right)^2}{2\sigma_{\alpha/\beta}^2}\right]\cdot SF\left(D,\alpha/\beta\right)\cdot d\left(\alpha/\beta\right)$$

(4.24)

where $\sigma_{\alpha/\beta}$ is the standard deviation of α/β about its mean value $\overline{\alpha/\beta}$.

4.2 EUD Formulas for Normal Tissues

Even with all the advances made with 3D-CRT, it is still not feasible, during radiation therapy, to avoid normal structures. Unlike tumor dose distributions, which are more or less uniform, normal tissue dose distributions are far from it. The large dose inhomogeneities, associated with normal structure irradiation, make it difficult to adequately report these inhomogeneous dose distributions. As mentioned earlier in chapter one, this dose reporting problem leads to inaccurate collection of clinical data. Several recommendations have been made by ICRU to facilitate the task of dose reporting. However, as stated in chapter one, these recommendations have not yet been unanimously accepted.
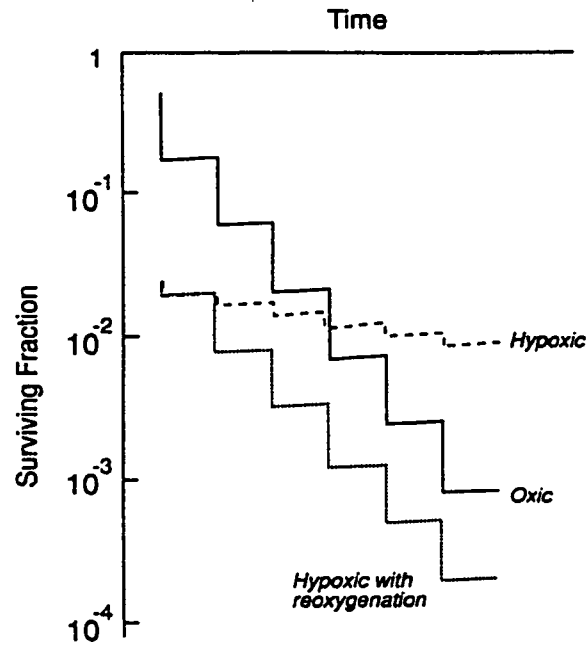
Figure 4.6: Survival curves for an hypothetical tumor containing 98% well-oxygenated cells and 2% hypoxic cells when given 6 fractions of radiotherapy.[64]

The concept of *EUD*, recently proposed by Niemierko is a potential solution to this problem. Unlike ICRU 50, which recommends reporting several doses, the *EUD* concept allows one to use a single number to describe the entire inhomogeneous dose distributions within a volume of interest. Because of its uniformity, the *EUD* also provides an additional tool to compare rival dose distributions for a volume of interest.

According to current literature, the concept of *EUD* has only been applied to tumors. Thus, it is the aim of this thesis to extend the *EUD* concept to normal structures, as they are never avoided during radiation treatment. In the following sections, the development of *EUD* formulas for normal structures are presented, starting with a brief description of the dose-response model of organs.

4.2.1 Dose-Response Model for Organs

For the purpose of modeling dose-response, a normal tissue is assumed to consist of a large number of independent functional sub-units. Each functional sub-unit is also assumed to be capable of regenerating from one clonogenic cell.

Thus, assuming independence of cell kill and the stochastic nature of dose deposition, the probability, P_{FSU}, of eradicating an FSU exposed to a uniform dose D is given by:

$$P_{FSU}(D) = (1 - SF(D))^k \qquad (4.25)$$

where $SF(D)$ is the surviving fraction of clonogenic cells irradiated to a uniform dose D or the probability of eradicating a clonogenic cell, and k is the number of clonogenic cells per FSU.

If one further assumes that the organ consists of N such identical FSUs, then the probability that t of the total N FSUs are killed as a result of the uniform dose distribution D can be expressed as follows:

$$P_t(D) = \binom{N}{t} \cdot P_{FSU}^t(D) \cdot [1 - P_{FSU}(D)]^{N-t} \qquad (4.26)$$

where $\binom{N}{t}$ is the binomial coefficient and $[1 - P_{FSU}(D)]$ is the probability that any given FSU survives a dose D.

Unlike tumors, which have no internal structure, normal organs differ markedly from one another in their architecture. Since these differences cause the normal structures to respond differently to radiation, one must take tissue architecture into account when modeling tissue response. In this work two idealized tissue architectures are considered: the serial and parallel architectures. These two architectures are characteristic of late-reacting normal tissues.

For serial architecture organs, such as the spinal cord and the bowels, a complication is assumed to occur if any one functional sub-unit is damaged. Thus, a serial organ survives only when all FSUs are spared. In this special case, the cumulative binomial probability for serial organ complication becomes:

$$NTCP_{ser}(D) = \sum_{t=1}^{N} \binom{N}{t} \cdot P_{FSU}^t(D) \cdot [1 - P_{FSU}(D)]^{N-t} . \qquad (4.27)$$

Note that the probability of serial organ complication must also be one minus the probability that each individual FSU survives:

$$NTCP_{ser}(D) = 1 - \prod_{i=1}^{N} [1 - P_{FSU}(D)] = 1 - [1 - P_{FSU}(D)]^N . \qquad (4.28)$$

From the above formula, one can conclude that the complication probability of serial organs is governed by the expected number of surviving FSUs. Therefore, for a volume of interest, one can assume that two different dose distributions are equivalent if the corresponding fraction of eradicated functional sub-units is identical:

$$P_{FSU}(EUD) = P_{FSU}(\{D_i\}) \tag{4.29}$$

For parallel architecture organs, such as kidneys and lungs, a complication is assumed to occur when more than M of the N FSUs are eradicated. That is, a parallel architecture organ has some functional reserve (M/N) of FSUs which is necessary for maintaining normal functionality.

The probability of complication for parallel organs can be expressed by the following cumulative binomial probability:

$$NTCP_{par}(D) = \sum_{t=M+1}^{N} \binom{N}{t} \cdot P_{FSU}^t(D) \cdot [1 - P_{FSU}(D)]^{N-t} = 1 - \sum_{t=0}^{M} P_t(D) \tag{4.30}$$

where $\sum_{t=0}^{M} P_t(D)$ is the probability of organ survival, i.e the probability, $P_{\leq M}(D)$, that M or less than M FSUs are eradicated, $P_{\leq M}(D)$.

Assuming that for a volume of interest two dose distributions are equivalent if they result in the same probability of organ survival, one can write the following equality:

$$P_{\leq M}(EUD) = P_{\leq M}(\{D_i\}) \tag{4.31}$$

One thing to bear in mind is that M varies depending on the given endpoint. For example, normal renal function can be sustained with approximately 30% to 50% of healthy nephrons while uremic death occurs when approximately 90% of the total number of nephrons are eradicated.[65]

4.2.2 *EUD* Formulas for Serial and Parallel Organs

In the following sections, the development of the *EUD* model for serial and parallel organs are presented, starting with the most basic of them all. As stated in the above section, the corresponding Equivalent Uniform Dose, for serial organs, is the dose which, when distributed uniformly across the volume of interest, will cause the same expected number of FSUs to survive as the given inhomogeneous dose distribution. For

parallel organs, the corresponding Equivalent Uniform Dose, is the dose which, when distributed uniformly across the volume of interest, will result in the same probability of survival.

4.2.2.1 Basic *EUD* Formula

If we assume that the FSUs are uniformly distributed across the volume of interest and that the clonogens within an FSU are identical and of constant number, the overall probability of eradicating an FSU is the weighted average of the probabilities taken over all n dose calculation points:

$$P_{FSU}(\{D_i\}) = \frac{1}{n} \sum_{i=1}^{n} [1 - SF(D_i)]^k \qquad (4.32)$$

where k is the number of clonogenic cells per FSU. Another idealized assumption made in the development of the basic *EUD* formula is that the FSUs within the sub-volume, V/n, are identical. It is more than likely that this is not the case, but for mathematical simplicity, this assumption will be considered acceptable.

4.2.2.1.1 Serial Architecture Organ

Since tissue complication for serial organs is governed by the expected number of surviving functional sub-units, one can determine the *EUD* for a specific volume of interest by assuming that two dose distributions are equivalent if they result in the same fraction of eradicated FSUs.

$$P_{FSU}(EUD) = P_{FSU}(\{D_i\}). \qquad (4.33)$$

Thus,

$$[1 - SF(EUD)]^k = \frac{1}{n} \sum_{i=1}^{n} [1 - SF(D_i)]^k \qquad (4.34)$$

and

$$SF(EUD) = 1 - \left[\frac{1}{n} \sum_{i=1}^{n} [1 - SF(D_i)]^k\right]^{1/k}. \qquad (4.35)$$

Assuming stochastic killing of the clonogens is well described by Poisson statistics and using the simple exponential model to describe the dose-response relationship, one obtains the following *EUD* formula for uniformly distributed FSUs:

$$EUD = -D_o \ln\left[1 - \left[\frac{1}{n}\sum_{i=1}^{n}[1 - SF(D_i)]^k\right]^{1/k}\right] \tag{4.36}$$

where $SF(D_i) = \exp\left(-\frac{D_i}{D_o}\right)$.

4.2.2.1.2 Parallel Architecture Organ

In order to evaluate the *EUD*, one must therefore calculate the probability of survival for the given non-uniform dose distribution, $P_{\leq M}(\{D_i\})$. If we assume that the FSUs are uniformly distributed across the parallel organ and if we consider the following non-uniform step dose distribution,

$N/2, D_1$	$N/2, D_2$
M_1	M_2

the probability of organ survival, $P_{\leq M}(\{D_1, D_2\})$ is the probability that the sum of the FSUs killed is equal or less than M, where $M = M_1 + M_2$. For simplicity, let $N = 4$ and $M = 2$. The probability of organ survival for such a case is:

$$P_{\leq 2}(\{D_1, D_2\}) = P_o(D_1) \cdot P_o(D_2) + P_o(D_1) \cdot P_1(D_2) + P_o(D_1) \cdot P_2(D_2)$$
$$+ P_1(D_1) \cdot P_o(D_2) + P_1(D_1) \cdot P_1(D_2) + P_2(D_1) \cdot P_o(D_2). \tag{4.37}$$

where $P_o(D_1)$ is the probability of eradicating zero FSUs in the first sub-volume or compartment, given a dose D_1, and is given by:

$$P_o(D_1) = \binom{N/2}{M_1} \cdot P_{FSU}^{M_1}(D_1) \cdot [1 - P_{FSU}(D_1)]^{N/2 - M_1}. \tag{4.38}$$

One can reduce the **formula (4.36)** as a double summation as follows:

$$P_{\leq 2}(\{D_1, D_2\}) = \sum_{j_1=0}^{2}\sum_{j_2=0}^{2-j_1} P_{j_1}(D_1) \cdot P_{j_2}(D_2). \tag{4.39}$$

Generalizing to the case in which the organ is divided into n equal sub-volumes, in which the dose D_i is constant within any sub-volume, the probability of organ survival becomes:

$$P_{\leq M}(\{D_1, D_2, ... D_n\}) = \sum_{j_1=0}^{M} \sum_{j_2=0}^{M-j_1} ... \sum_{j_n}^{M-j_1-...-j_n} P_{j_1}(D_1) \cdot P_{j_2}(D_2) \cdot ... P_{j_n}(D_n)$$
<div align="right">(4.40)</div>

where

$$P_{j_1}(D_1) = \binom{N/n}{j_1} \cdot P_{FSU}^{j_1}(D_1) \cdot [1 - P_{FSU}(D_1)]^{N/n-j_1}.$$

Since the assumption is made, for parallel organs, that any two given dose distributions are equivalent if they result in the same probability of survival, one can write the following:

$$P_{\leq M}(EUD) = P_{\leq M}(\{D_i\}).$$
<div align="right">(4.41)</div>

Thus,

$$\sum_{t=0}^{M} P_t(EUD) = \sum_{j_1=0}^{M} \sum_{j_2=0}^{M-j_1} ... \sum_{j_n}^{M-j_1-...-j_n} P_{j_1}(D_1) \cdot P_{j_2}(D_2) \cdot ... P_{j_n}(D_n).$$
<div align="right">(4.42)</div>

4.2.2.2 Absolute Volume Effect

Since the basic equivalent uniform dose formula for serial architecture organs is based upon the fraction of eradicated FSUs, one may wish to relate the equivalent uniform dose the same absolute reference volume V_{ref}. If one assumes that the number of FSUs within the serial organ is proportional to the volume, then one gets the following EUD formula for serial architecture organs:

$$EUD = -D_o \ln \left[1 - \left[\frac{1}{V_{ref}} \sum_{i=1}^{n} V_i \cdot [1 - SF(D_i)]^k \right]^{1/k} \right]$$
<div align="right">(4.43)</div>

where V_{ref} is the average volume of a specific serial organ (e.g. spinal cord) and V_i is the absolute volume receiving dose D_i. Since it is unlikely that the number of eradicated FSUs is linearly proportional to the volume, one should attempt to use the full definition of normal tissue complication to develop the EUD formula for serial organ.

4.2.2.3 Non-Uniform Distribution of Functional Sub-Units

It is more than likely that functional sub-units are not uniformly distributed within an organ. The actual distribution of FSUs within an organ is still unavailable at the

present, but if this information were to become available, the spatial distribution of FSUs could be incorporated in the model.

4.2.2.3.1 Serial Architecture Organ

In the case of non-uniform FSU distribution, the overall probability of killing an FSU or the fraction of eradicated FSUs for a given volume of interest becomes:

$$P_{FSU}(\{D_i\}) = \frac{\sum_{i=1}^{n} \rho_i \cdot V_i [1 - SF(D_i)]^k}{\sum_{i=1}^{n} \rho_i \cdot V_i} \tag{4.44}$$

where ρ_i is the local absolute density of functional sub-units and V_i is the absolute volume receiving a dose D_i. Since the organ is divided into n equal sub-volumes, $V_i = V / n$, the above formula reduces to:

$$P_{FSU}(\{D_i\}) = \frac{\sum_{i=1}^{n} \rho_i \cdot [1 - SF(D_i)]^k}{\sum_{i=1}^{n} \rho_i}. \tag{4.45}$$

Substituting **formula (4.45)** into the idealized **formula (4.33)**, one gets:

$$[1 - SF(EUD)]^k = \frac{\sum_{i=1}^{n} \rho_i \cdot [1 - SF(D_i)]^k}{\sum_{i=1}^{n} \rho_i} \tag{4.46}$$

Solving the above equation yields the following *EUD* formula:

$$EUD = -D_o \ln \left[1 - \left[\frac{\sum_{i=1}^{n} \rho_i \cdot [1 - SF(D_i)]^k}{\sum_{i=1}^{n} \rho_i} \right]^{\frac{1}{k}} \right]. \tag{4.47}$$

4.2.2.3.2 Parallel Architecture Organ

In the case of non-uniform FSU distribution, the number of FSUs per sub-volume, V / n, varies depending on the FSU density, ρ. Thus, the probability of organ survival becomes:

$$P_{SM}(\{D_1, D_2, ... D_n\}) = \sum_{j_1=0}^{M} \sum_{j_2=0}^{M-j_1} ... \sum_{j_n}^{M-j_1--j_n} P_{j_1}(D_1) \cdot P_{j_2}(D_2) \cdot ... P_{j_n}(D_n) \tag{4.48}$$

where

$$P_{j_1}(D_1) = \begin{pmatrix} \rho_1 \cdot V/n \\ j_1 \end{pmatrix} \cdot P_{FSU}^{j_1}(D_1) \cdot [1 - P_{FSU}(D_1)]^{\rho_1 V/n - j_1}.$$

Note that $\rho_1 \cdot V/n$ is the number of FSU in the first sub-volume irradiated to a dose D_1.

4.2.2.4 Fractionation Effect

Studies have shown, that when a fractionation scheme is changed in clinical practice, from many small doses to a few large doses, the treatment protocol involving a few large fractions always results in a lower survival fraction.[66] Since late responding tissues have a higher α/β ratio, the effects of fractionation will be more pronounced as shown in **Figures 4.7**. In order to take into account the effects of fractionation, one uses the linear-quadratic model.
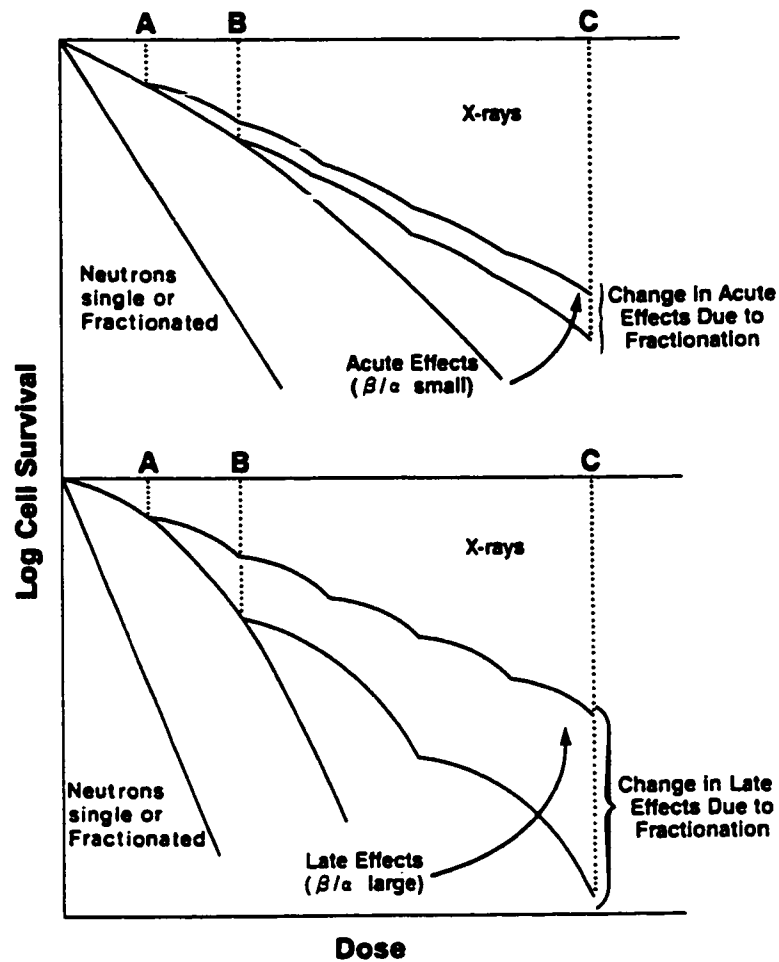
Figure 4.7: Change in late and early effects due to fractionation.[67]

According to the linear-quadratic model, the surviving fraction can be calculated in terms of the α / β ratio as follows:

$$SF(D) = \exp\left[-D \cdot \left(\frac{\alpha}{\beta} + \frac{D}{N_f}\right)\right] \qquad (4.49)$$

where D is the total dose and N_f is the number of fractions.

4.2.2.4.1 Serial Architecture Organ

Substituting **formula (4.49)** into the idealized serial organ **formula (4.33)**, one gets the following formula for EUD:

$$EUD = \frac{\left[-\alpha + SQRT\left\{ \alpha^2 - 4\beta \ln\left(1 - \left[\frac{\frac{V}{n}\sum_{i=1}^{n} \rho_i \cdot [1 - SF(D_i)]^k}{\sum_{i=1}^{n} \rho_i} \right]^{1/k} \right) \right\} \right]}{2\beta}$$

(4.50)

where $SF(D_i) = \exp\left[-D_i \cdot \left(\frac{\alpha}{\beta} + \frac{D_i}{N_f} \right) \right]$.

4.2.2.4.2 Parallel Architecture Organ

Substituting **formula (4.49)** into the parallel organ survival **formula (4.41)**, one gets the following:

$$P_{\leq M}(EUD) = \sum_{j_1=0}^{M} \sum_{j_2=0}^{M-j_1} \cdots \sum_{j_n}^{M-j_1-\cdots-j_n} P_{j_1}(D_1) \cdot P_{j_2}(D_2) \cdot \ldots P_{j_n}(D_n)$$

(4.51)

where

$$P_{j_1}(D_1) = \binom{N/n}{j_1} \cdot P_{FSU}^{j_1}(D_1) \cdot [1 - P_{FSU}(D_1)]^{N/n-j_1},$$

and

$$P_{FSU}(D_1) = \left[1 - \exp\left[-D_1 \cdot \left(\frac{\alpha}{\beta} + \frac{D_1}{N_f} \right) \right] \right]^k.$$

4.2.2.5 Proliferation Effect

Experimental laboratory data acquired from rodents shows that there is a clear distinction between tissues that are early responding , such as the skin, and those that are late responding, such as the spinal cord (see **Figure 4.8**).
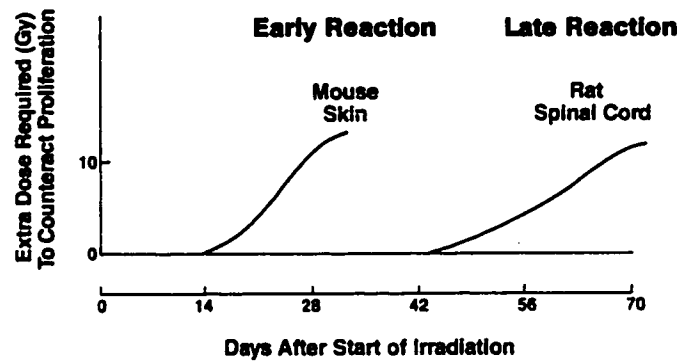
Figure 4.8: The extra dose required to compensate for proliferation in early- and late-responding rodent tissues as a function of time.[68]

It can be seen from **Figure 4.8**, that the extra dose required to counteract proliferation in late reacting mice tissues, does not increase until approximately 42 days, and then increases somewhat sigmoidally as a function of time.

If similar data were available for humans, the effects of proliferation would not be noticed until a much longer time because of the slower response of human tissues and longer cell cycle of the individual cells. One can conclude from this, that the time at which extra dose is needed to counteract proliferation in late responding human tissues, such as the spinal cord, is far beyond the overall time of any conventional radiotherapy extending to 6 or 8 weeks. Thus, one may assume, that the overall surviving fraction of late-responding tissues, for dose D given in N_f fractions over the time T is not affected by proliferation.

4.2.2.6 Partial Organ Irradiation

Partial organ irradiation is common in three-dimensional conformal radiation therapy as one tries to avoid as much as possible the critical structures. Since organs vary in their architecture, the volume effects should also vary as the two are linked together.

4.2.2.6.1 Serial Architecture Organ

Partial irradiation of serial organ can be incorporated in the basic *EUD* model. If one defines the *EUD* in terms of the fraction of eradicated FSUs, then one can easily

show that partial irradiation has no effect on the *EUD* as the absolute volume irradiated is not required to calculate the overall fraction of eradicated FSUs. However, if one wants to define the *EUD* in terms of the number of eradicated FSUs, then one must account for the absolute volume irradiated. In this particular case, **equation 4.43** should be used to determine the *EUD*.

4.2.2.6.2 Parallel Architecture Organ

Since it is assumed that a complication arises when more than M FSUs are eradicated, any treatment plan that irradiates less than M FSUs will cause no complication. Therefore, for any partial irradiation scheme, where

$$\left(\rho_1 + \rho_2 + \rho_3 + ... + \rho_n\right) \cdot \frac{V_{vol}}{n} \leq M, \quad P_{\leq M}(\{D_i\}) = 0 \text{ and } EUD = 0. \text{ For any other partial}$$

irradiation scheme, the probability of organ survival becomes:

$$P_{\leq M}(\{D_1, D_2, ... D_n\}) = \sum_{j_1=0}^{M} \sum_{j_2=0}^{M-j_1} ... \sum_{j_n}^{M-j_1-...-j_n} P_{j_1}(D_1) \cdot P_{j_2}(D_2) \cdot ... P_{j_n}(D_n)$$

where

$$P_{j_1}(D_1) = \begin{pmatrix} \rho_1 \cdot V_{vol} / n \\ j_1 \end{pmatrix} \cdot P_{FSU}^{j_1}(D_1) \cdot \left[1 - P_{FSU}(D_1)\right]^{\frac{\rho_1 \cdot V_{vol}}{n} - j_1}.$$

4.2.2.7 Intra-Patient Heterogeneity

Formulas (4.32-4.51) assume perfect homogeneity of the irradiated tissues, that is, no variation of the radiobiological parameters of the model ($\alpha, \beta,$ and k). However, it is more than likely that cells, within the same organ, differ in radiosensitivity and that not every FSU contains exactly k clonogens. If one assumes no correlation between $\alpha, \beta,$ and k and a normal (or log-normal in the case of k) distribution of the parameters, one can take the expected value of *EUD* as the best estimate for the Equivalent Uniform Dose, for an individual. Thus,

$$EUD_{ind} = \int G_{ind} \cdot EUD \cdot d(\alpha) d(\beta) d(\log(k)) \tag{4.52}$$

80

where $G_{ind} = \dfrac{1}{\left(\sqrt{2\pi}\right)^3 \sigma_{ind}} \times \exp\left[-\left(\dfrac{(\alpha-\bar{\sigma})^2}{2\sigma_\alpha^2}\right)-\left(\dfrac{(\beta-\bar{\beta})^2}{2\sigma_\beta^2}\right)-\left(\dfrac{\left(\log(k)-\overline{\log(k)}\right)^2}{2\sigma_{\log(k)}^2}\right)\right]$,

and

$\sigma_{ind} = \sigma_\alpha \cdot \sigma_\beta \cdot \sigma_{\log(k)}$.

4.2.2.8 Inter-Patient Heterogeneity

Since it is more than likely that the flattening of the dose-response is due to inter-patient heterogeneity, one must take it into account when modeling the observed response curve of a population. If it is assumed, once again, that the radiobiological parameters in the model ($\bar{\alpha}, \bar{\beta}, \overline{\log(k)}, \bar{M},$ and $\bar{N}$) are not correlated and normally or (log-normally) distributed, one can take the expected value of *EUD* taken over the heterogeneous population as the best estimate for the Equivalent Uniform Dose. Thus,

$$EUD_{pop} = \int G_{pop} \cdot EUD_{ind} \cdot d(\bar{\alpha})d(\bar{\beta})d(\overline{\log(k)})d(\bar{M})d(\bar{N}) \tag{4.53}$$

where

$$G_{pop} = \dfrac{1}{\left(\sqrt{2\pi}\right)^5 \sigma_{pop}} \times$$

$$\exp\left[-\left(\dfrac{(\bar{\alpha}-\bar{\bar{\sigma}})^2}{2\sigma_{\bar{\alpha}}^2}\right)-\left(\dfrac{(\bar{\beta}-\bar{\bar{\beta}})^2}{2\sigma_{\bar{\beta}}^2}\right)-\left(\dfrac{\left(\overline{\log(k)}-\overline{\overline{\log(k)}}\right)^2}{2\sigma_{\overline{\log(k)}}^2}\right)-\left(\dfrac{(\bar{M}-\bar{\bar{M}})^2}{2\sigma_{\bar{M}}^2}\right)-\left(\dfrac{(\bar{N}-\bar{\bar{N}})^2}{2\sigma_{\bar{N}}^2}\right)\right],$$

and

$$\sigma_{pop} = \sigma_{\bar{\alpha}} \cdot \sigma_{\bar{\beta}} \cdot \sigma_{\overline{\log(k)}} \cdot \sigma_{\bar{M}} \cdot \sigma_{\bar{N}}.$$

The model expressed in **formula (4.53)** is an 8-dimensional integral and thus, would be very time-consuming to evaluate. In order to facilitate computation, one can simplify the integral by assuming that the heterogeneity of all parameters can be expressed by only a few parameters. This simplification serves as a reasonable first approximation as many of these parameters are not yet available. If one assumes, for example, that the heterogeneity is characterized by the parameter M and $\log(k)$, **formula (4.53)** can be simplified to the following two-dimensional integral:

$$EUD_{pop} = \int G_{pop} \cdot EUD_{ind} \cdot d\left(\overline{\log(k)}\right) d\left(\overline{M}\right)$$

(4.53)

where

$$G_{pop} = \frac{1}{\left(\sqrt{2\pi}\right)\sigma_{\overline{M}}} \times \exp\left[-\frac{\left(\overline{M} - \overline{\overline{M}}\right)^2}{2\sigma_{\overline{M}}^2}\right],$$

and

$$G_{ind} = \frac{1}{\left(\sqrt{2\pi}\right)\sigma_{\overline{\log(k)}}} \times \exp\left[-\frac{\left(\overline{\log(k)} - \overline{\overline{\log(k)}}\right)^2}{2\sigma_{\overline{\log(k)}}^2}\right].$$

Note that for the serial organs, where there can be no variation of M, a parameter other than M must be used as the integrated variable in the simplified model.

5. PRACTICAL APPLICATIONS OF THE IDEALIZED *EUD* FORMULAS

5.1 Introduction

In the preceding chapter, several *EUD* formulas were developed for the planning target volume and for serial and parallel architecture organs, ranging from simple to complex. As stated earlier, these *EUD* formulas provide potential planning tools that can summarize, with a single number, any dose distribution, thus simplifying and improving dose reporting methods.

In order to test the validity and understand the behavior of these idealized *EUD* formulas, simple dose distributions were initially generated and their equivalent uniform dose (*EUD*) evaluated. Following these initial tests, several practical treatment plans were designed on both a 2.5-dimensional and 3-dimensional radiation treatment planning system. Their corresponding dose distributions were then evaluated using the appropriate *EUD* formulas. The constructed treatment plans used in this portion of the investigation covered three distinct cancer sites (i.e. prostate, lung and ethmoid sinus) and therefore allowed a number of critical serial and parallel architecture structures to be evaluated.

The results obtained from these various evaluations are presented and discussed in this chapter, starting with the results from the preliminary tests. Also included in this chapter are a brief description of the two radiation treatment planning systems, the basic/idealized *EUD* formulas and the *EUD* parameters used to perform these evaluations and a discussion of the *EUD* uncertainties.

5.1.1 2.5-Dimensional Radiation Therapy Planning

All 2.5-D treatment planning processes are extensions of 2-D radiation therapy planning methods, which assume that a patient consists of a single transverse plane which contains the radiation beams central axes.[69] The major difference between the two processes is that the 2.5-D treatment planning method, unlike the 2-D radiation therapy planning process, acquires additional patient information from one or more planes

parallel to the initial transverse plane in order to account for the critical structures that lie outside the central plane.

In a 2.5-D radiotherapy planning system dose distributions are calculated in both the initial central axes plane and additional parallel planes. Furthermore, dose distributions are displayed as isodose distributions within the plane of interest. Radiation doses in both processes are calculated using a 2-D algorithm with the assumption that the radiation dose lies in the plane of calculation, thus beam divergence is assumed to occur only in that single plane. Since the radiation doses are calculated to a grid of points in the calculation plane, dose-volume histograms can be constructed and used to display the plan information.

During the first part of the practical tests, a 2.5-D radiotherapy planning system was used to construct treatment plans for several patients suffering from either prostate cancer or cancer of the ethmoid sinuses. For each of these patients, a single transverse CT slice delineating the major critical structures and planning target volume was chosen as the plane of interest and dose distributions were calculated using a 2-D algorithm. Dose-volume histograms were then generated by allocating a thickness, typical of the dose grid width, to the plane of interest.

5.1.2 3-Dimensional Radiation Treatment Planning

3-D radiation treatment planning considers the delivery of tumoricidal doses in volumes of tissues rather than in individual planes.[70] Patient information is acquired in the form of several closely spaced transverse computed tomography or CT images to give a volumetric representation of the patient anatomy. Radiation doses are calculated in a 3-D dose matrix and the dose algorithm accounts for beam divergence in all directions. Since a large amount of information is available in 3-D radiation therapy, dose-volume histograms are often used to summarize and display the plan information.

For the final set of simulations, a 3-D radiotherapy planning system was used to construct plans for patients with prostate and lung cancers and also several different plans for a single patient with prostate cancer. Dose distributions were calculated using a 3-D dose algorithm and dose-volume histograms were subsequently generated using a 1 Gy dose bin width.

5.2 *EUD* Assumptions, Formulas and Parameters

This section gives a brief description of all the idealized *EUD* formulas used throughout the preliminary and practical tests and their underlying assumptions. Most of the radiobiological parameters involved in these idealized *EUD* formulas were arbitrarily defined as the majority of them are not yet clinically well established.

5.2.1 PTV *EUD*

For mathematical simplicity, it was assumed that the planning target volume consists of a large number of uniformly distributed independent clonogenic cells, with identical radiobiological sensitivity, D_0. Furthermore, it was assumed that the planning target volume consists only of the gross tumor volume. When the dose at each point within the volume of interest was available, the following idealized formula was used to evaluate the equivalent uniform dose:

$$EUD = -D_o \cdot \ln\left(\sum_{i=1}^{n} \frac{1}{n} \cdot \exp\left(-D_i \middle/ D_o\right)\right) \tag{5.1}$$

where n is the total number of dose points within the tumor volume. However, when dose-volume histograms were the main source of information, the equivalent uniform dose of the tumor was determined with the following idealized *EUD* formula:

$$EUD = -D_o \cdot \ln\left(\sum_{i=1}^{n} v_i \cdot \exp\left(-D_i \middle/ D_o\right)\right) \tag{5.2}$$

where v_i is the partial volume and n is the number of partial volumes in the tumor volume.

The mean lethal dose, D_0, for the practical tests and the last section of the preliminary tests was derived from the prescribed dose by assuming that tumor control was achieved when the survival fraction reached 10^{-5}. Thus,

$$D_o = \frac{D \cdot \log(\exp(1))}{5} \tag{5.3}$$

where D is the prescribed dose to the tumor. For the first preliminary test, the mean lethal dose was assumed to be 2 Gy for all structures of interest.

5.2.2 Serial Architecture Organ *EUD*

For the following tests, serial architecture organs were assumed to consist of a large number of independent functional sub-units, each capable of regenerating from one clonogenic cell. Furthermore, it was assumed that these FSUs were uniformly distributed throughout the serial organ and that each clonogenic cell was identical. For simplicity, the mean lethal dose for any serial architecture organ enclosed within the irradiated volume was assumed to be equivalent to the mean lethal dose of the tumor volume. Finally, the number of clonogenic cells or clonogens per functional sub-unit, k, was kept for the most part constant (i.e. 100 clonogens/FSU) to facilitate comparison of results and simplify the *EUD* computation. In the first initial test, the number of clonogens per FSU was however assumed to be 10^5 to give the *EUD* results a more realistic meaning. The idealized formula use to determine the serial organ *EUD* depended on treatment planning system used to generate the dose distributions. When the dose at each point within the volume of interest was available, the following formula was used to evaluate the idealized equivalent uniform dose:

$$EUD = -D_o \cdot \ln\left(1 - \left[\sum_{i=1}^{n} \frac{1}{n} \cdot \left(1 - \exp\left(-D_i / D_o\right)\right)^k\right]^{1/k}\right) \qquad (5.4)$$

where k is the number of clonogenic cells per functional sub unit or FSU. However, when dose-volume histograms were the main source of information, the equivalent uniform dose of the serial organ was determined with the following idealized *EUD* formula:

$$EUD = -D_o \cdot \ln\left(1 - \left[\sum_{i=1}^{n} v_i \cdot \left(1 - \exp\left(-D_i / D_o\right)\right)^k\right]^{1/k}\right). \qquad (5.5)$$

5.2.3 Parallel Architecture Organ *EUD*

For parallel structures, the following formula was used to calculate the probability of organ survival:

$$P_{\leq M}(\{D_1, D_2, .. D_n\}) = \sum_{j_1=0}^{M} \sum_{j_2=0}^{M-j_1} ... \sum_{j_n}^{M-j_1-...j_n} P_{j_1}(D_1) \cdot P_{j_2}(D_2) \cdot ... P_{j_n}(D_n) \qquad (5.6)$$

where

$$P_{j_1}(D_1) = \binom{N/n}{j_1} \cdot P_{FSU}^{j_1}(D_1) \cdot \left[1 - P_{FSU}(D_1)\right]^{N/n - j_1} \text{ for } n \text{ dose distribution points, and}$$

$$P_{j_1}(D_1) = \binom{N \cdot v_1}{j_1} \cdot P_{FSU}^{j_1}(D_1) \cdot \left[1 - P_{FSU}(D_1)\right]^{N \cdot v_1 - j_1} \text{ for dose-volume histograms.}$$

In both situations, M is the number of FSUs that ensures organ survival, and N is the total number of FSUs within the organ of interest. To decrease the computational load during the practical tests, new differential dose-volume histograms were constructed for parallel architecture organs, with dose bin widths of 10 Gy.

Once the probability of organ survival was computed, an attempt was first made to solve for the equivalent uniform dose by approximating the *EUD* cumulative binomial distribution by a normal distribution. However, in many instances the probability of organ survival was smaller than 0.5, thus rendering the use of the above approximation impossible. The equivalent uniform dose for parallel organ architecture was finally solved by relating the *EUD* cumulative binomial distribution to a Fisher-distribution or F-distribution. An F-distribution with m and n degrees of freedom is a continuous probability distribution with the following probability density function:

$$f_p(x;m,n) = \frac{\Gamma\left(\frac{m+n}{2}\right)}{\Gamma\left(\frac{m}{2}\right) \cdot \Gamma\left(\frac{n}{2}\right)} \cdot \frac{m^{\frac{m}{2}} \cdot n^{\frac{n}{2}} \cdot p^{(\frac{m}{2}-1)}}{(n + mp)^{(m+n)/2}} \qquad (5.7)$$

where

$$p = \frac{m}{m + n \cdot F},$$

Γ is the incomplete beta function and p is the probability of eradicating a functional sub-unit given an equivalent uniform dose, *EUD*.

The mean lethal dose, D_o, for parallel organs was, once again, assumed to be equal to the mean lethal dose for the tumor. Except for the first initial test, each FSU was deemed to contain 100 clonogenic cells. For the first preliminary test, an FSU was

assumed to contain 10^5 clonogens. The rest of the radiobiological parameters characterizing the parallel organs were also chosen to minimize the computational load. The total number of functional sub-units, N, never exceeded 200 and the functional reserve, $(1- M / N)$, was kept, for the most part, at approximately 80% unless stated.

5.2.4 *EUD* Uncertainties

Since the equivalent uniform dose is derived from both patient data and several radiobiological parameters, all subject to some uncertainties, an error analysis is warranted. Furthermore, it is important to understand how these uncertainties propagate through the calculation and lead to an uncertainty $\delta(EUD)$ in the final idealized *EUD*. In this section, the limit error formulas necessary to evaluate the *EUD* uncertainty for all possible structures are presented, starting with the *EUD* limit error formula for the planning target volume. For mathematical simplicity, the uncertainties of several of the radiobiological parameters and patient data were assumed negligible. The rest of the uncertainties were roughly estimated. All error limit formulas presented in this section were derived for treatment plans that employed the primary dose data (i.e. dose calculation points) to arrive at the equivalent uniform dose.

5.2.4.1 PTV

The equivalent uniform dose limit error for tumor volumes was derived from **equation (5.1)** and is given by:

$$\delta(EUD) = |EUD| \cdot \left[\frac{\delta(D_o)}{|D_o|} + \frac{\sum_{i=1}^{n}\left[\left|\exp\left(-D_i/D_o\right)\right| \cdot \left[\frac{\delta(D_i)}{|D_o|} + \frac{|D_i| \cdot \delta(D_o)}{|D_o^2|}\right]\right]}{\sum_{i=1}^{n}\left|\exp\left(-D_i/D_o\right)\right| \cdot \left|\ln\left[\frac{1}{n} \cdot \sum_{i=1}^{n}\exp\left(-D_i/D_o\right)\right]\right|} \right] \tag{5.8}$$

where n is the number of calculation dose points inside the tumor volume, $\delta(D_i)$ is the uncertainty in the absorbed dose at the ith calculation point and $\delta(D_o)$ is the uncertainty in the mean lethal dose. The uncertainty in the mean lethal dose in the following investigations was assumed to be small (i.e .1% of D_o) even though the mean lethal dose was arbitrarily defined. For mathematical simplicity, the overall uncertainty in the

absorbed dose was defined as a constant value of 0.5 Gy. Clinically, the overall uncertainty is a combination of random and systematic uncertainties and is usually less than 5%. When dose-volume histograms were used to calculate the *EUD*, the uncertainty in the partial volume, v_i, was assumed negligible and the uncertainty in the dose was kept at 0.5 Gy regardless of the dose bin widths.

5.2.4.2 Serial Architecture Organ

The *EUD* error for any serial architecture organ containing n calculation dose points can be calculated as follows:

$$\partial(EUD) = |EUD| \cdot \left[\frac{\delta(D_o)}{|D_o|} + \frac{\sum_{i=1}^{n} \left| \frac{1}{n} \cdot \left(1 - SF(D_i)\right)^k \right| \cdot \left(\frac{\delta(D_i)}{|D_i|} + \frac{|D_i| \delta(D_o)}{|D_o^2|} \right)}{\left| \sum_{i=1}^{n} \frac{1}{n} \cdot \left(1 - SF(D_i)\right)^k \right| \cdot \left| \ln \left[1 - \left[\frac{1}{n} \sum_{i=1}^{n} \left(1 - SF(D_i)\right)^k \right]^{1/k} \right] \right|} \right] \tag{5.9}$$

where k is the number of clonogenic cells per functional sub-unit and $SF(D_i)$ is the fraction of surviving clonogenic cells at the *ith* absorbed dose. The uncertainty in the clonogenic density was assumed negligible in our evaluations of both serial and parallel architecture organs.

5.2.4.3 Parallel Architecture Organ

Because of the complexity of the parallel architecture organ *EUD* formula, the *EUD* uncertainty was presumed to be the largest deviation from the best *EUD* estimate. To determine the maximum and minimum *EUD*s, the F-distribution was used to compute an *EUD* for both extreme probabilities of organ survival. The uncertainty in the parallel architecture organ survival probability is given by:

$$\delta\left(P_{\leq M}(\{D_1, D_2, \ldots D_n\})\right) = \sum_{j_1=0}^{M} \sum_{j_2=0}^{M-j_1} \ldots \sum_{j_n}^{M-j_1-\ldots j_n} \delta\left(P_{j_1}(D_1)\right) \cdot \delta\left(P_{j_2}(D_2)\right) \ldots \delta\left(P_{j_n}(D_n)\right) \tag{5.10}$$

where

$$\delta\left(P_{j_1}(D_1)\right) = P_{j_1}(D_1) \cdot \left(\frac{j_1 \cdot \delta\left(P_{FSU}(D_1)\right)}{P_{FSU}(D_1)} + \frac{(N_1 - j_1) \cdot \delta\left(1 - P_{FSU}(D_1)\right)}{1 - P_{FSU}(D_1)} \right),$$

$$\frac{\delta\left(P_{FSU}\left(D_{1}\right)\right)}{P_{FSU}\left(D_{1}\right)} = \frac{\delta\left(1 - P_{FSU}\left(D_{1}\right)\right)}{1 - P_{FSU}\left(D_{1}\right)},$$

and

$$\delta\left(P_{FSU}\left(D_{1}\right)\right) = k \cdot \left[1 - \exp\left(-D/D_{o}\right)\right]^{k-1} \cdot \exp\left(-D/D_{o}\right) \cdot \left(\frac{\delta(D_{1})}{D_{o}} + \frac{\delta(D_{o})}{D_{o}^{2}}\right).$$

For mathematical simplicity, the uncertainties in the total number of FSUs and in the functional reserve were assumed to be negligible.

5.3 Simple Preliminary Tests

The main purpose of these preliminary tests was to study the behavior of the various idealized *EUD* models. In order to accomplish this task, 2 sets of dose volume histograms were analyzed. The first set of DVHs was carefully constructed to study the effects of the maximum dose on the equivalent uniform dose; the second, to study the effects of changing various radiobiological parameters on the idealized *EUD*.

5.3.1 Maximum Dose Effect on the EUD

5.3.1.1 Sample DVHs

The effects of the maximum dose on the idealized equivalent uniform dose was studied by constructing several simple dose volume histograms with various dose maxima for equal relative volume as shown in **Figure 5.1**. These dose maxima were carefully selected by generating a curve of radiobiological effect under consideration versus dose for each structure of interest, and then determining the range of doses that encompassed all three curves.
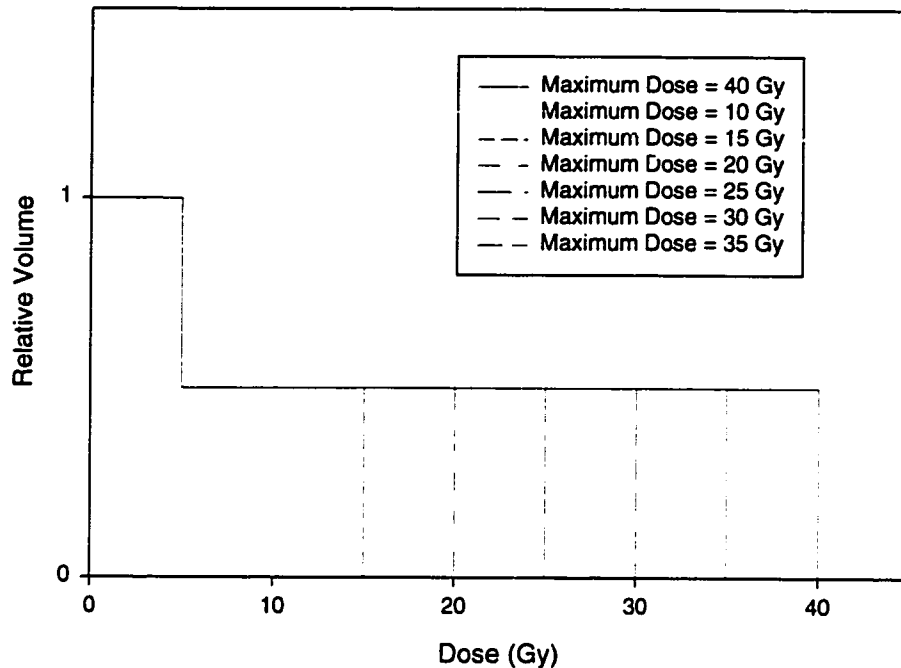
Figure 5.1: Typical dose-volume histograms to evaluate the effect of the maximum dose on the equivalent uniform dose.

5.3.1.2 Results

The idealized equivalent uniform doses for each structure of interest, are presented in **Table 5.1**. For the parallel architecture organ, it was assumed that the total number of functional sub-units within the organ was equal to sixty and that a complication arose when more than 10%, 30% or 70% of these FSUs were eradicated. The mean lethal dose, D_o, was assumed to be 2 Gy for all structures and for both serial and parallel organs, each FSU was assumed to contain 10^5 clonogens. Since the idealized *EUD* formulas for serial organs and tumors are independent of the number of FSUs within the structure (i.e. for tumors, each FSU contains one clonogen), the number of FSUs within the serial organ and the number of clonogens within the tumor remained undefined for this test.

MAXIMUM DOSE	EUD (Gy) FOR STRUCTURE OF INTEREST				
	TUMOR VOLUME	SERIAL ARCHITECTURE	PARALLEL ARCHITECTURE 10%	PARALLEL ARCHITECTURE 30%	PARALLEL ARCHITECTURE 70%
10.0	6.2	10.0	0	0	0
15.0	6.4	15.0	0	0	0
20.0	6.4	19.7	0	0	0
25.0	6.4	22.9	23.3	23.0	0
30.0	6.4	23.7	26.0	25.2	0
35.0	6.4	23.8	28.4	27.0	0
40.0	6.4	23.8	30.7	28.5	0

Table 5.1: The effect of the maximum dose on the equivalent uniform dose.

5.3.1.3 Discussion

For simplicity, all the idealized *EUD* results are displayed to one decimal place as the error analysis performed for all structures indicates that the uncertainties in the *EUDs* were less than one percent. To fully understand the behavior of the idealized *EUD* formulas, one must refer to radiobiological effect versus dose curves for these particular structures (see **Figure 5.2**). The results for the tumor volume, presented in the above table, show *EUD* values that are close to the minimum dose. They also show that the *EUD* values slowly increase and level off at a value of 6.4 Gy. The leveling off of the tumor *EUD* with dose occurs because the fraction of eradicated clonogens $(1-SF(D))$ peaks, for this particular case, at a prescribed dose of about 12 Gy. Any additional dose to the tumor past 12 Gy does not affect this radiobiological effect, and subsequently, no change occurs in the *EUD* past this dose. This latter behavior is also seen for the serial organ, but it occurs at a much higher dose. Since the fraction of eradicated FSUs, for this specific serial organ, reaches 100% at around 34 Gy, any increase in dose past 34 Gy does not affect the probability of killing an FSU and thus the *EUD* remains the same (23.8 Gy) after this dose. The results for the serial organ also show that while the probability of killing an FSU is zero, the *EUD* is equivalent to the maximum dose. Between the two limit
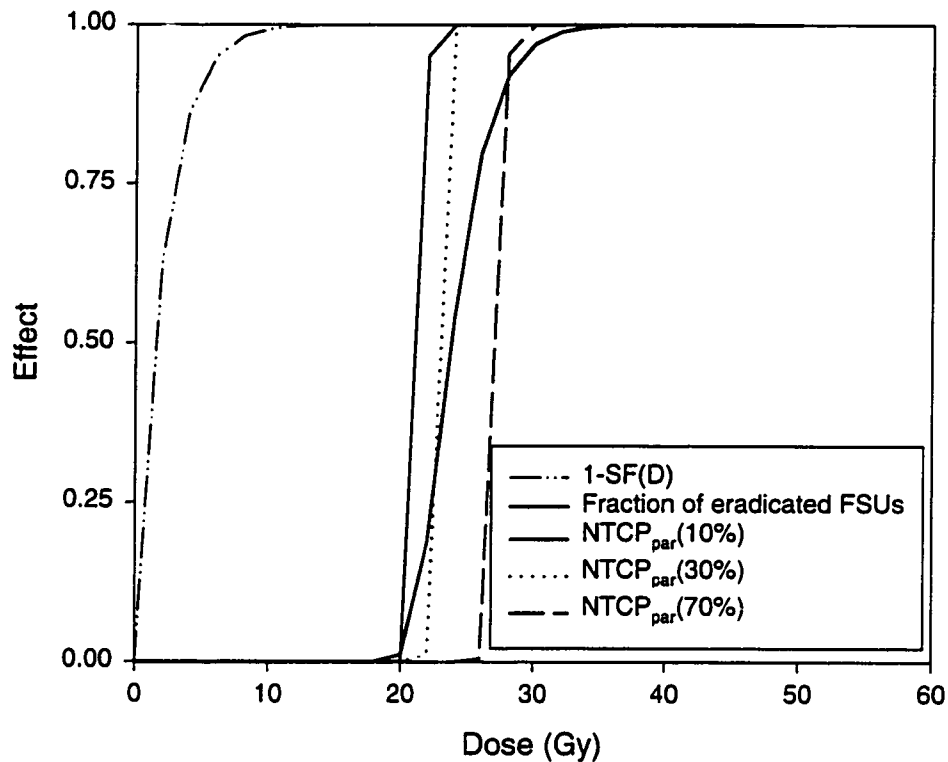
Figure 5.2: Curves of radiobiological effect versus dose for the structures of interest.

values (0 and 1), the *EUD* increases as a function of maximum dose. The *EUD* results for the parallel organ illustrate a volume effect as expected. For all three defined functional reserves, the *EUD* is zero for each dose-volume histogram with a maximum dose equal or less than 20 Gy. This is expected as the probability of killing an FSU is approximately zero below a dose of 20 Gy (see **Figure 5.2**). Since the probability of killing an FSU starts to increase at around 20 Gy and reaches a maximum of one at about 34 Gy, the probability of killing more than *M* FSUs begins to increase with dose after 20 Gy. This trend can be seen in the results by an increase in *EUD* as a function of maximum dose for the parallel architecture organ with a functional reserve of either 90% or 70%, respectively. For the case of the parallel organ with a small functional reserve (i.e 30%), the *EUD* is zero for each dose-volume histogram because the probability of

93

killing an FSU in the volume receiving 5 Gy is zero. Since no more than 30 FSUs can be killed in this particular scenario, the probability of killing more than 70% (i.e. $M = 42$) of the FSUs is zero and so is the *EUD*.

5.3.2 Effects of Parameters on the *EUD*

In this section, the values of the radiobiological parameters were varied to investigate how the equivalent uniform dose for each structure of interest varied as a function of these parameters. A simple 2 step dose-volume histogram (**Figure 5.3**) was constructed to study the effects of these radiobiological parameters on the *EUD*.
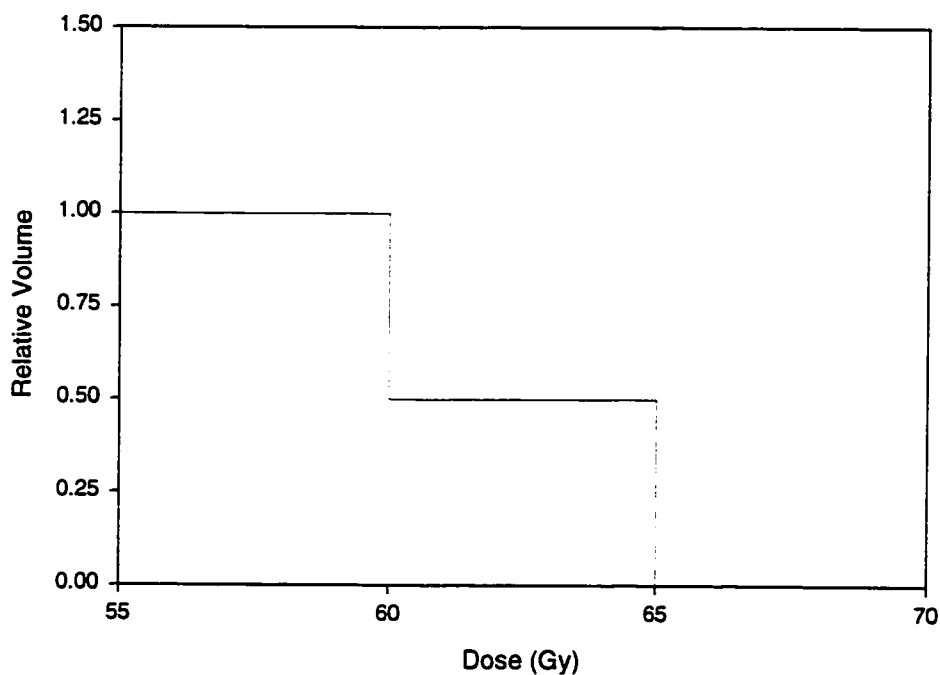

Figure 5.3: The 2 step dose-volume histogram used to study the various effects of the radiobiological parameters on the *EUD*.

5.3.2.1 D_o- Mean Lethal Dose

In order to study the effect of the mean lethal dose on the equivalent uniform dose, the mean lethal dose was varied from a value of 2.5 Gy to 10.0 Gy in increments of 2.5 Gy. The starting mean lethal dose for this study was 2.5 Gy. For both serial and parallel architecture organs, the clonogenic density was kept at 100 clonogens per FSU and the

total number of FSU in each parallel organ was assumed to be 30. Furthermore, the functional reserve for the parallel architecture organ was set to 50%. The resulting equivalent uniform doses for the tumor volume and both serial and parallel architecture organs are presented in the following table (**Table 5.2**).

D_o	EUD (Gy) FOR STRUCTURE OF INTEREST		
	PTV	Serial Architecture	Parallel Architecture
2.5	61.4	61.4	-
5.0	61.9	61.9	62.2
7.5	62.1	62.1	62.3
10.0	62.2	62.2	62.4

Table 5.2: The effect of an increase in the mean lethal dose on the equivalent uniform dose for each structure of interest.

The results of the study show that the equivalent uniform dose increases as the mean lethal dose increases for all structures of interest. Note that the *EUD* for parallel architecture organs with a mean lethal dose of 2.5 Gy is unavailable because the *EUD* solving technique used wasn't precise enough. However we can estimate, from the above results, that the *EUD* value lies between 61.4 Gy and 62.2 Gy.

5.3.2.2 k - Clonogenic Density

The effect of the clonogenic density on the *EUD* was studied for both serial and parallel architecture organs. No effect could be observed for the tumor volume as it was assumed that the clonogenic density was uniform and that the tumoricidal idealized *EUD* depended only on the surviving fraction of clonogens. The effect of a clonogenic density increase was studied by incrementing the clonogenic density by a factor of 10, starting at a minimum of 1 clonogen per FSU to a maximum of 10,000 clonogens per FSU. For parallel architecture organs the total number of FSU was set to 30 and the mean lethal dose was assumed to be (6.983±0.007) Gy for both structures. Furthermore, a complication was assumed to arise if more than 50% of the total number of FSUs were

eradicated. The resulting equivalent uniform doses for both serial and parallel architecture organs are presented in **Table 5.3**.

	EUD (GY) FOR STRUCTURE OF INTEREST	
Clonogenic Density - k	Serial Architecture	Parallel Architecture
1	62.1	62.3
10	62.1	62.3
100	62.1	62.3
1,000	62.1	62.3
10,000	62.6	62.4

Table 5.3: The effect of a clonogenic density increase on the *EUD* for serial and parallel architecture organs.

The *EUD*s resulting from an increase in clonogenic density indicate that both parallel and serial architecture organs are largely unaffected by an increase in clonogenic density from 1clonogen/FSU to 1,000 clonogens/FSU. However, the last *EUD* results of **Table 5.3** reveal an increase in the *EUD* for both serial and parallel architecture organs as a function of clonogenic density.

5.3.2.3 N - Total Number of FSUs

Due to the assumptions underlying the simplest serial *EUD* model, the serial architecture organ idealized *EUD* was established to be independent of the total number of functional sub-units. Therefore, the effect of increasing the total number of functional sub-units on the idealized *EUD* was only investigated for parallel architecture organs. For the purpose of this study, the total number of FSU was increased by a value of 10, starting at a minimum of 10 and ending at a maximum of 100. Furthermore, the mean lethal dose was kept at (6.983 ± 0.007) Gy and a complication was assumed to arise if more than 75% of the total number of FSU were eradicated by the treatment. The resulting EUDs are displayed in the following table (**Table 5.4**).

Total Number of FSUs (N)	Parallel Architecture *EUD*
10	62.4
20	62.4
30	62.4
40	62.4
50	62.4
60	62.4
70	62.4
80	62.4
90	62.4
100	62.4

Table 5.4: The effect of the total number of FSUs on the *EUD* for parallel architecture organs.

The *EUD* results presented in the above table show that *EUD* is unaffected by the total number of FSUs for a specific complication.

5.3.2.4 Functional Reserve

The effect of the functional reserve $(1-M/N)$ on the idealized equivalent uniform dose for a parallel architecture organ was studied in this section by increasing M by a factor of 10, starting at a minimum value of 10 and terminating at a maximum value of 50. The total number of FSU for this study was set to 60 and the mean lethal dose was assumed to be (6.983 ± 0.007) Gy. Furthermore, the clonogenic density was set to a value of 100 clonogens per FSU for mathematical simplicity. The results of this study are displayed in **Table 5.5**.

(*M*)	Parallel Architecture *EUD*
10	62.4
20	62.4
30	62.3
40	62.2
50	62.1

Table 5.5: Equivalent uniform dose as a function of *M* for parallel architecture organs.

The above *EUD* results indicate that as the functional reserve (1-*M/N*) decreases the *EUD* decreases as expected. Thus, the results confirm the need for higher uniform doses to achieve the same level of complication in parallel architecture organs which require smaller functional reserves to perform adequately.

5.3.3 Effects of Organ Architecture on the *EUD*

It is sometimes quite difficult to determine whether an organ (e.g. heart) is of parallel or serial architecture. In many clinical situations, an organ is classified as a mixed organ, having a parallel architecture component and a serial architecture component. In order to understand the behavior of such a complex architecture, one must first of all understand the behavior of both underlying architectures on the equivalent uniform dose. In this section, the effect of the critical organ architecture on the *EUD* was studied using the 3 dose-volume histograms for the heart used in the following lung cancer study (**Figure 5.26**). The radiobiological parameters defined in **section 5.4.3** were applied to both architectures and the *EUD* results are presented in the following table (**Table 5.6**).

DVH #	EUD (Gy) for Heart Architecture Type	
	Serial	Parallel
1	30.6	34.3
2	30.0	29.2
3	30.6	0.0

Table 5.6: The effects of the organ architecture on the equivalent uniform dose.

The *EUD* results presented in the above table suggest that the corresponding heart *EUD* does indeed depend upon the tissue architecture. This dependence upon the tissue architecture is quite obvious for DVH#3 as the *EUD* for this DVH is zero when one makes the assumption that the heart is a parallel organ. Thus, if one assumes that the heart is a parallel architecture organ, no heart complication would result in this particular patient.

5.4 Results and Discussion of Practical Tests

The dose-volume histograms used, in the preliminary tests, to summarize the dose distributions within the volumes of interest were simple step functions. In real clinical situations, the dose-volume histograms exhibit greater complexity. To study the effects of these dose-volume histograms on the equivalent uniform dose, several practical plans were designed on both a 2.5-D and 3-D radiation therapy treatment planning system. The latter practical plans were then evaluated using the proper idealized *EUD* model and the results were subsequently analyzed. The following is a brief description and discussion of these practical plans, their dose-volume histograms and their resulting equivalent uniform doses.

5.4.1 Prostate Cancer

Figure 5.4 delineates five major structures pertinent to the treatment of patients with prostate cancer. For the purpose of this work, it was postulated that both the bladder and femoral heads were parallel architecture organs and that a complication arose when 20% of their total functional sub-units were eradicated. It was also hypothesized that all

clonogenic cells within the critical structures were as radiobiologically sensitive as those of the tumor and that the functional sub-units were uniformly distributed within the structures of interest. Finally, a mean lethal dose, $D_o = (6.775\pm0.007)$ Gy was assumed since a dose of (78.0 ± 0.5) Gy was prescribed to the tumor. Each functional sub-unit was assumed to contain 100 clonogenic cells.
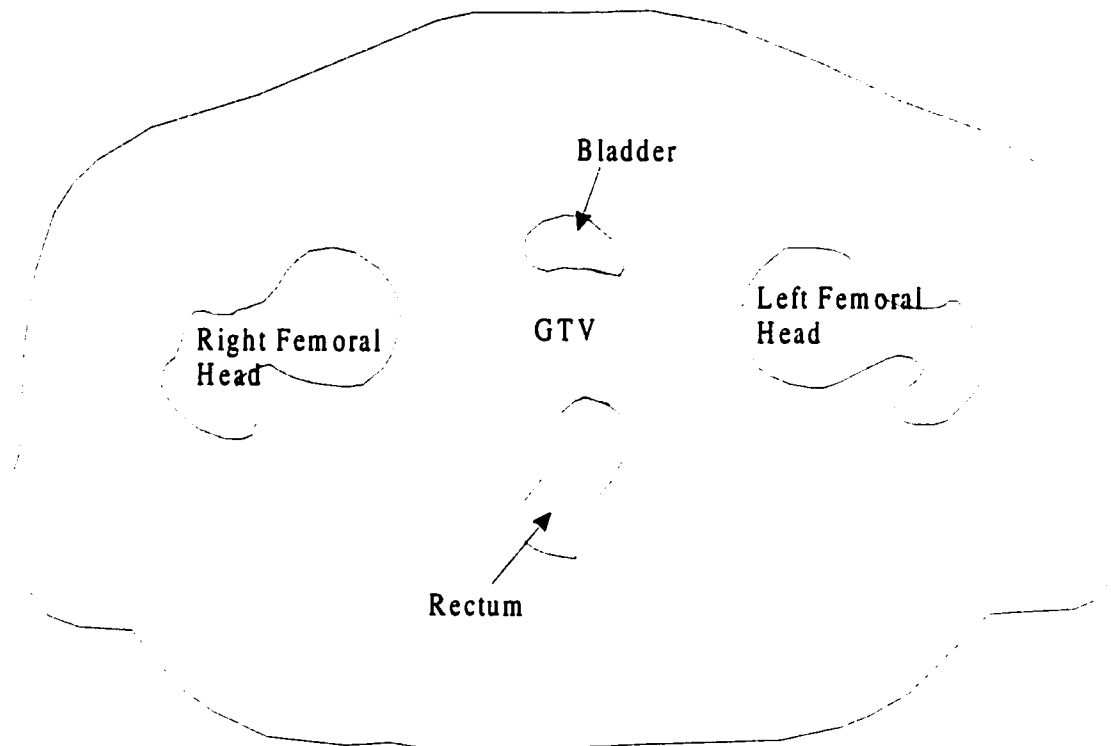

Figure 5.4: A typical cross-sectional CT view delineating five major structures involved in treating a patient with prostate cancer.

Two different cases of prostate cancer were studied in this work. In the first case, several treatment plans for a single patient were designed using a 2.5-D treatment planning system. Dose-volume histograms were then generated for these plans by assuming a CT slice thickness of 0.525 cm. In the second case, treatment plans for three different patients were generated using a 3-D radiotherapy planning system.

5.4.1.1 Case 1

In the following figures (i.e. **Figures 5.5-5.9**), the dose-volume histograms for each structure of interest with their corresponding *EUD*s are presented, starting with those

of the tumor volume. Each dose-volume histogram corresponds to a particular beam arrangement.

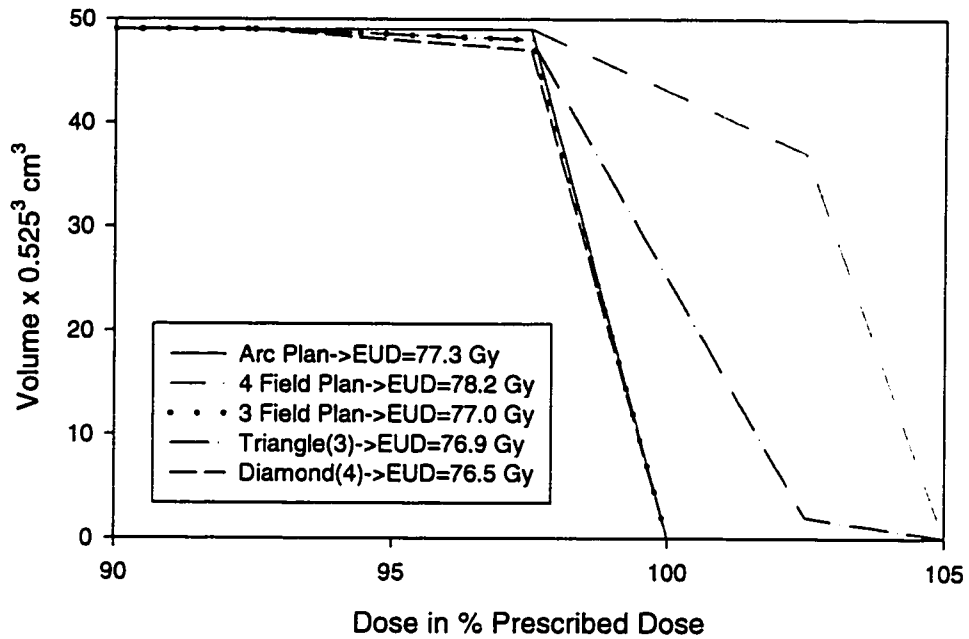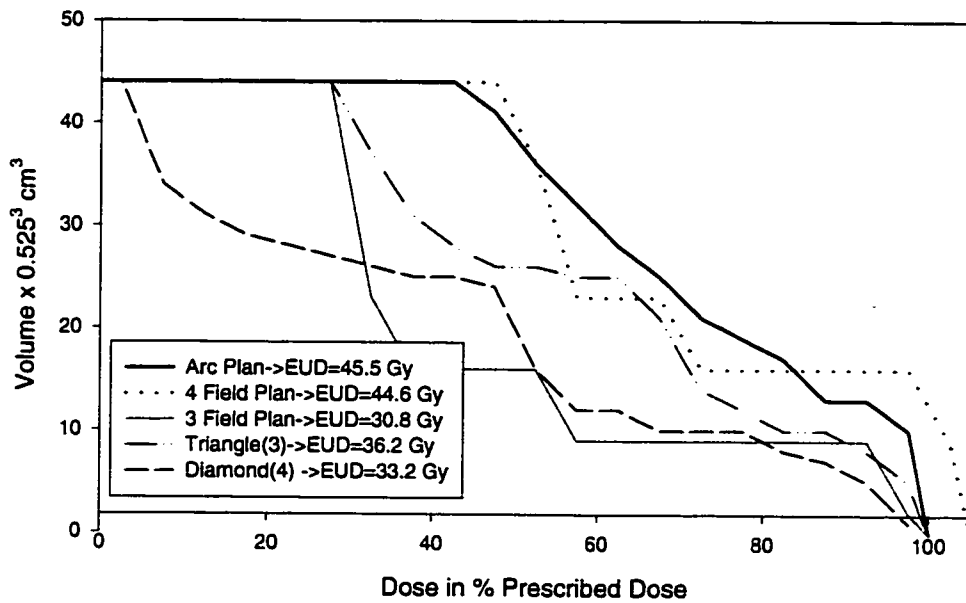**Figure 5.5**: Cumulative dose-volume histograms for the planning target volume.

Figure 5.6: Cumulative dose-volume histograms for the rectum.
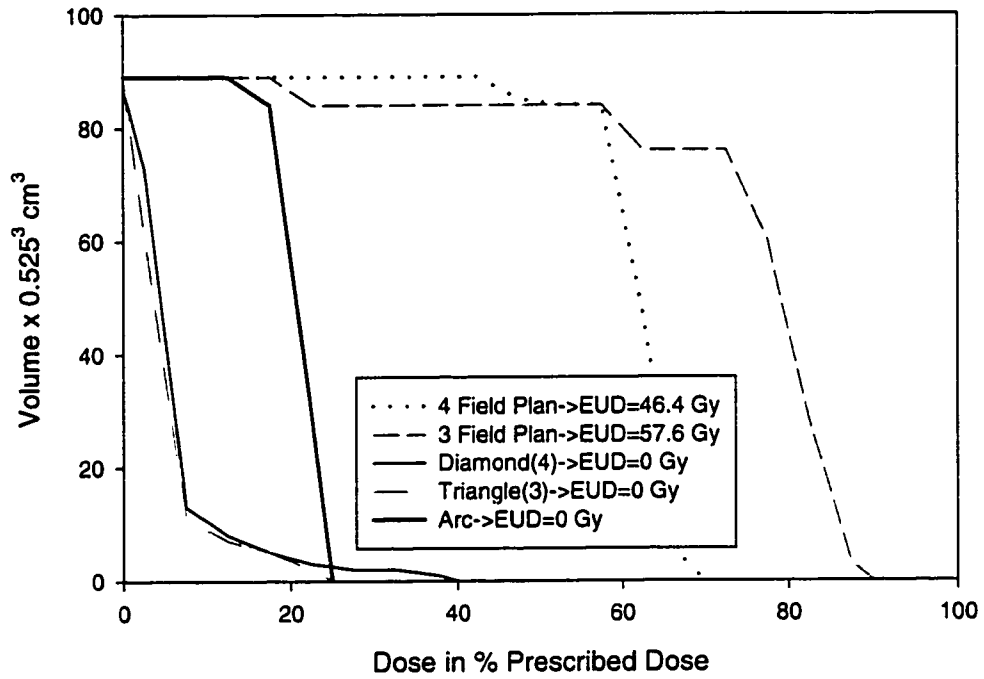
Figure 5.7: Cumulative dose-volume histograms for the left femoral head.
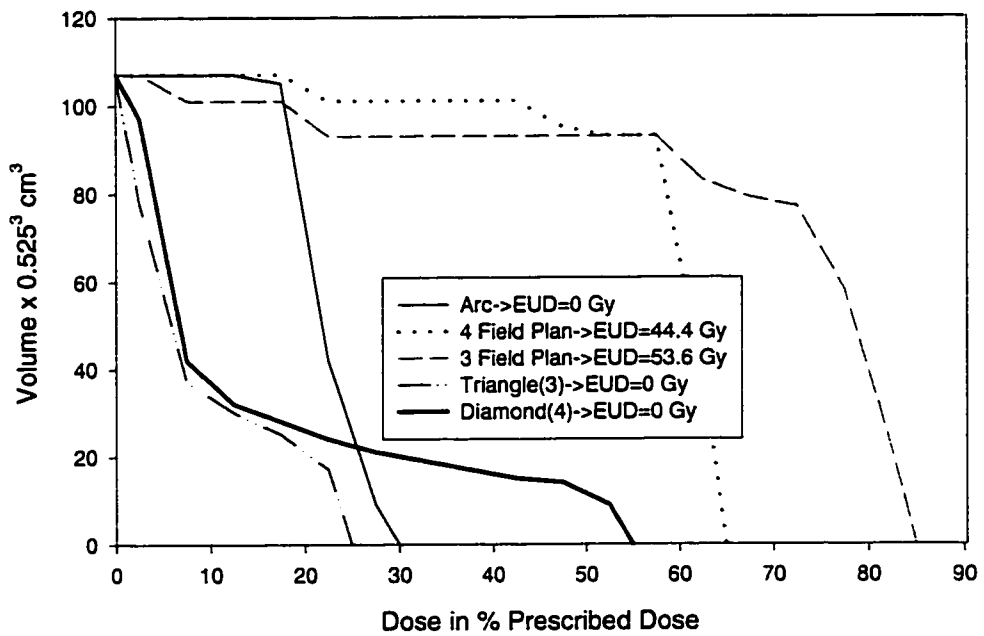

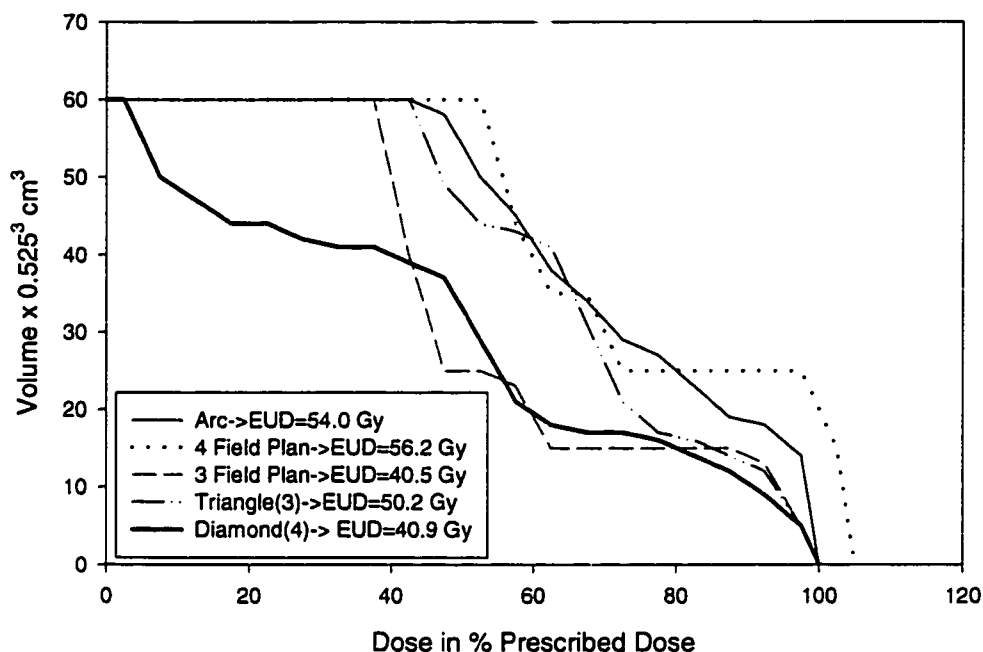**Figure 5.8**: Cumulative dose-volume histograms for the right femoral head.

Figure 5.9: Cumulative dose-volume histograms for the bladder.

A summary of the resulting equivalent uniform doses for each beam arrangement is presented in **Table 5.7**. In order to minimize the computational load, differential dose-volume histograms with a dose bin width of 10 Gy were used to calculate the *EUD* for parallel architecture organs.

VOLUME OF INTEREST	*EUD* (Gy) FOR VOLUME OF INTEREST				
	ARC	**3 FIELD**	**4 FIELD**	**TRIANGLE**	**DIAMOND**
TUMOR VOLUME	77.3	77.0	78.2	76.9	76.5
RECTUM	45.5	30.8	44.6	36.2	33.2
LEFT FEMUR	0	57.6	46.4	0	0
RIGHT FEMUR	0	53.6	44.4	0	0
BLADDER	54.0	40.5	56.2	50.2	40.9

Table 5.7: *EUD* summary of several treatment plans for a patient with prostate cancer.

The calculated *EUD*s presented in the above table show that the treatment plan with the traditional 4-field beam arrangement has the highest tumor equivalent uniform dose and is thus the best beam configuration to maximize the tumor control. The results also indicate that no complication (i.e. *EUD*=0 Gy) will arise in the left and right femoral heads of this prostate cancer patient if the triangle or diamond beam arrangement or arc therapy is employed. Finally, the results show that some beam arrangements are better than others to avoid certain specific critical structures but that there is no unique beam arrangement that will simultaneously maximize tumor control and minimize all individual normal tissue complications.

5.4.1.2 Case 2

In the following figures (i.e. **Figures 5.10-5.14**), the dose-volume histograms for each structure of interest and their corresponding *EUD*s are presented, starting with those of the tumor volume. Each dose-volume histogram corresponds to a particular patient treatment plan generated by a 3-D radiotherapy planning system.
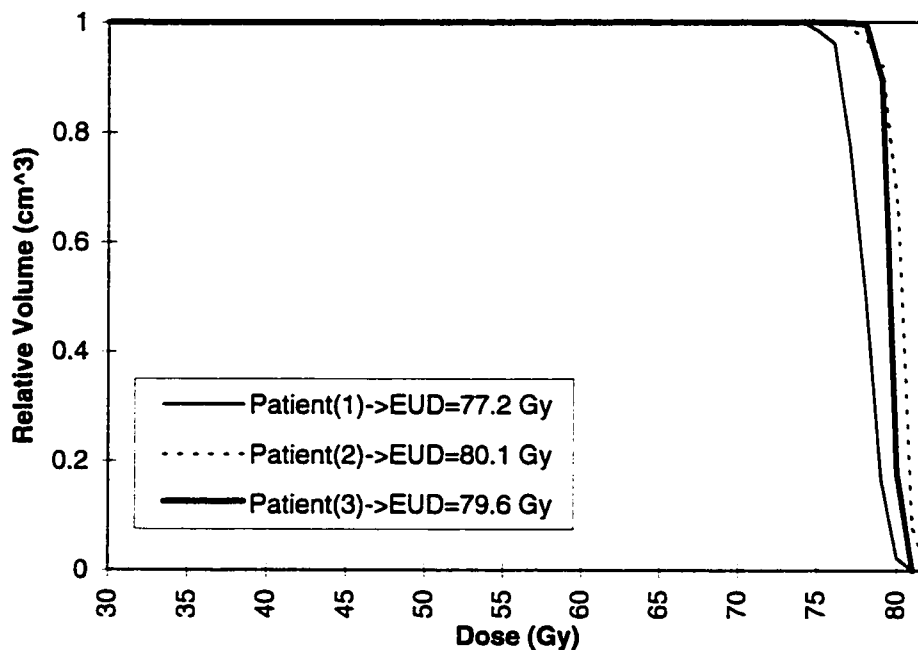

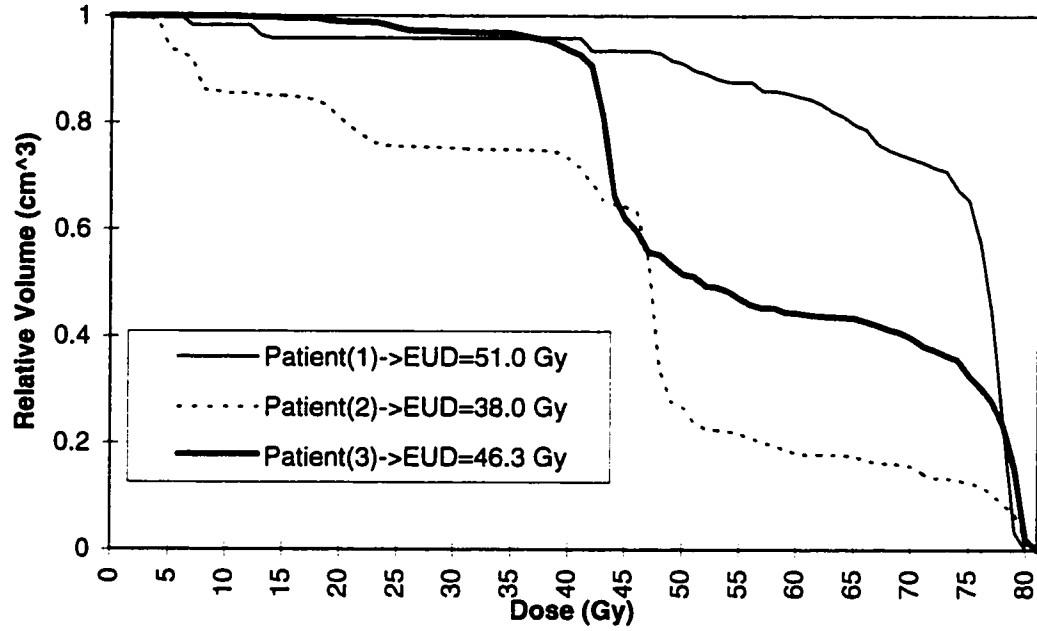**Figure 5.10**: Cumulative dose-volume histograms for the planning target volume.

Figure 5.11: Cumulative dose-volume histograms for the rectum.
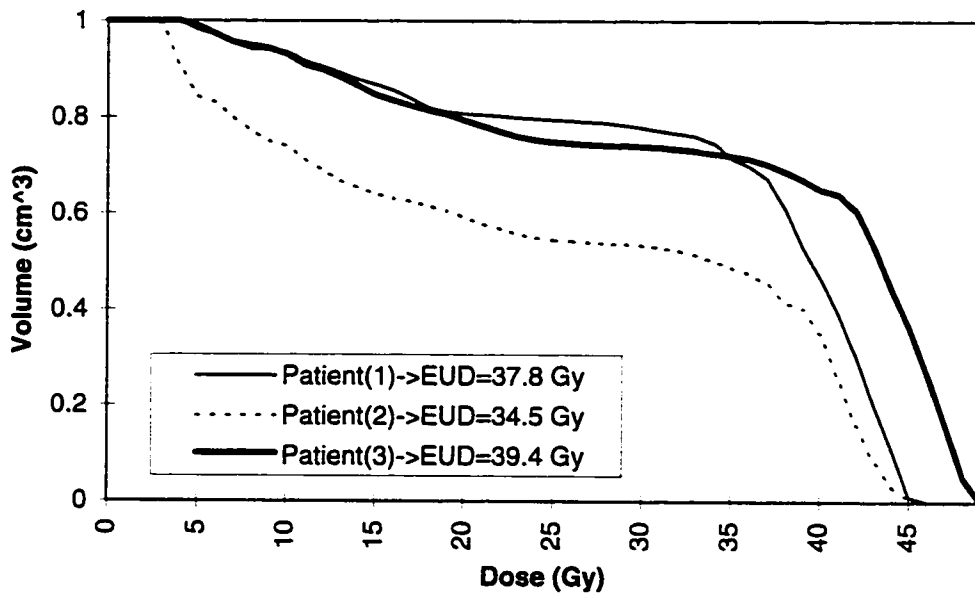
Figure 5.12: Cumulative dose-volume histograms for the left femoral head.
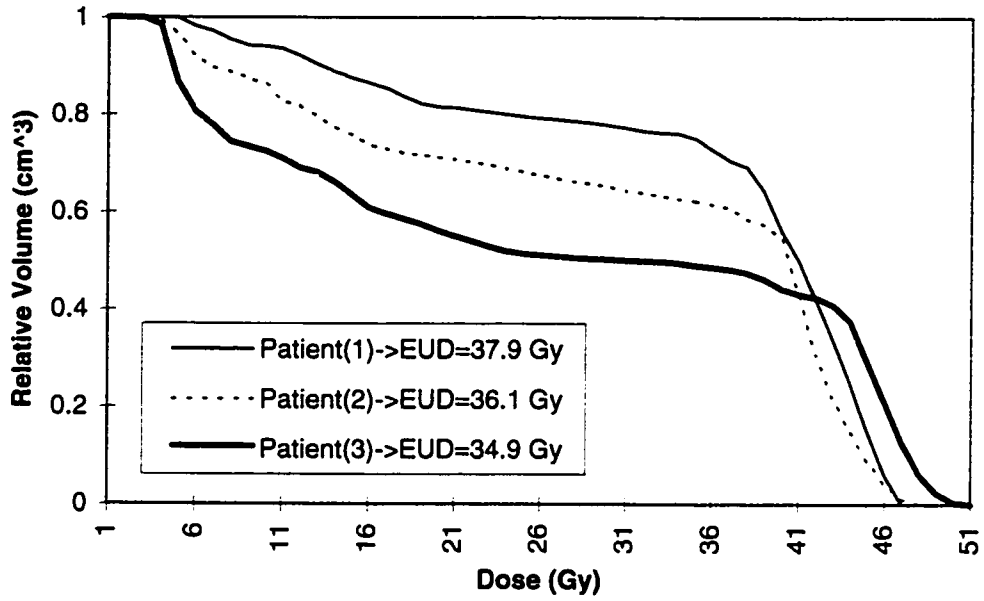
Figure 5.13: Cumulative dose-volume histograms for the right femoral head.
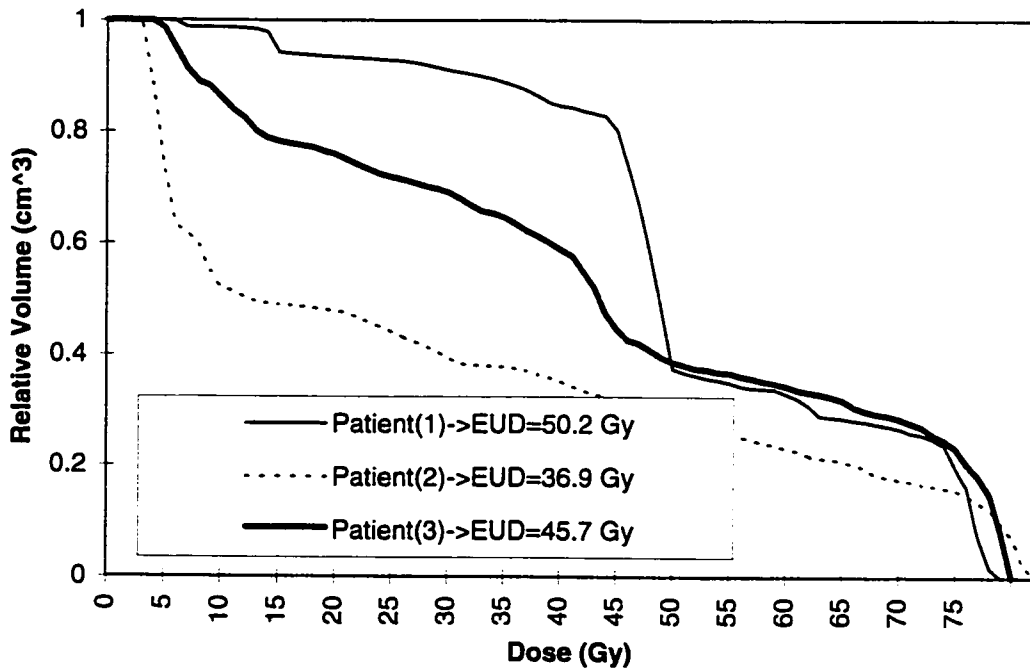

Figure 5.14: Cumulative dose-volume histograms for the bladder.

The equivalent uniform doses calculated for all three patients are presented in **Table 5.8**. In order to evaluate the *EUD* for parallel architecture organs, intermediate

differential dose-volume histograms with a 10 Gy dose bin width were again derived from the above dose-volume histograms.

VOLUME OF INTEREST	EUD (Gy) for Volume of Interest		
	1	2	3
TUMOR VOLUME	77.8	80.1	79.5
LEFT FEMURAL HEAD	37.8	34.5	39.4
RIGHT FEMURAL HEAD	37.9	36.1	34.9
BLADDER	50.1	36.9	45.7
RECTUM	51.0	38.0	46.3

Table 5.8: *EUD* results for each individual prostate cancer patient treated with a 3-D radiation therapy treatment planning system.

The results from the above table show that the treatment plan for the second patient has the highest tumoricidal *EUD*. The results also indicate that all irradiated critical structures in patient#2, with the exception of the right femoral head, have the lowest *EUD*s. Finally, all critical structures in patient#1, except for the left femoral head, have the highest *EUD*s.

5.4.2 Cancer of the Ethmoid Sinuses

Figure 5.15 delineates the six major structures of interest in patients with cancer of the ethmoid sinuses. For the purpose of this work, it was assumed that all critical structures were serial architecture organs. Furthermore, it was again postulated that all clonogenic cells within the critical structures were as sensitive as the tumor of interest and that each functional sub-unit contained 100 clonogenic cells. The functional sub-units were also presumed to be uniformly distributed within the structure of interest. Finally, it was assumed that the mean lethal dose, $D_o = (5.212\pm0.005)$ Gy since a dose of (60.0 ± 0.5) Gy was prescribed to the tumor.
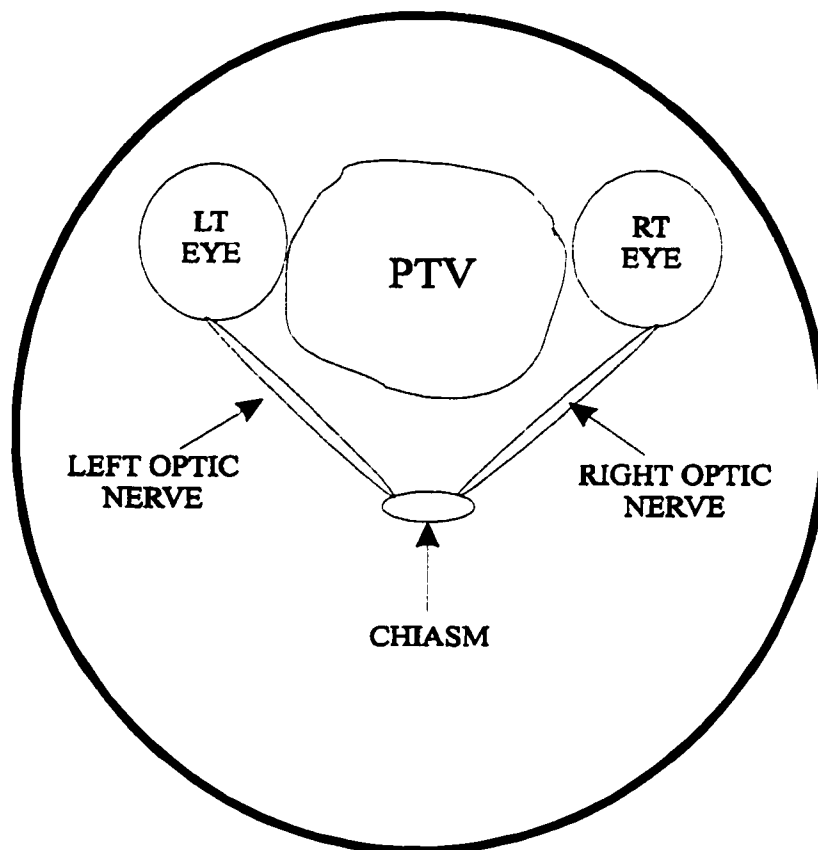
Figure 5.15: Schematic of major structures affected during irradiation of the ethmoid sinuses.

In the single case of cancer of the ethmoid sinuses analyzed in this work, several treatment plans for a single patient were designed using a 2.5-D treatment planning system. Dose-volume histograms were then generated for these plans by assuming a CT slice thickness of 0.5 cm. The following figures (i.e. **Figures 5.16-5.21**), display the dose-volume histograms for each structure of interest and their corresponding *EUD*s, starting with those of the tumor volume. Each dose-volume histogram corresponds to a particular beam arrangement. The *EUD* results are also summarized in **Table 5.9**.
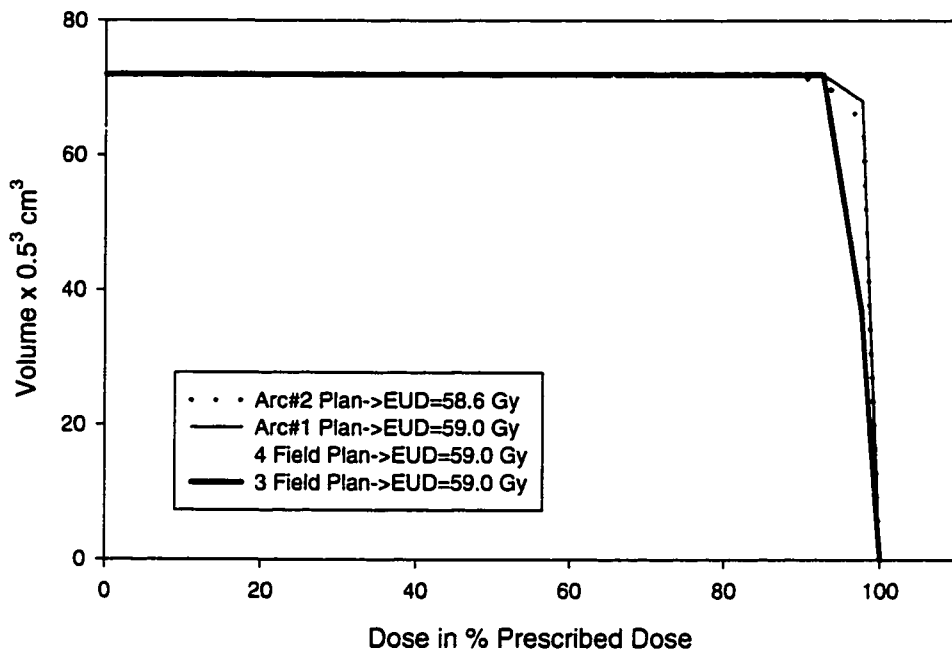
Figure 5.16: Cumulative dose-volume histograms for the tumor volume.
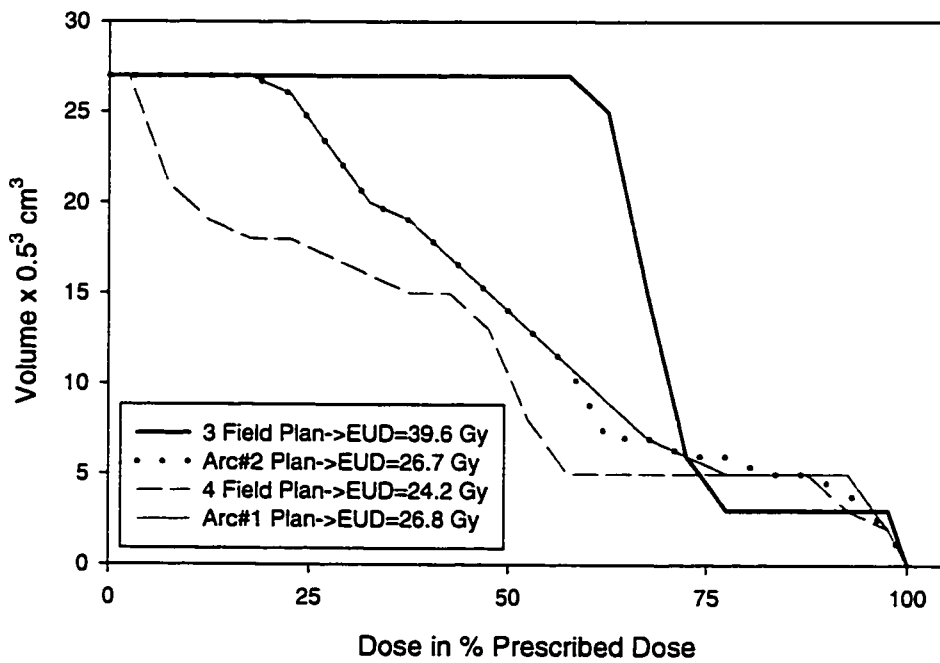

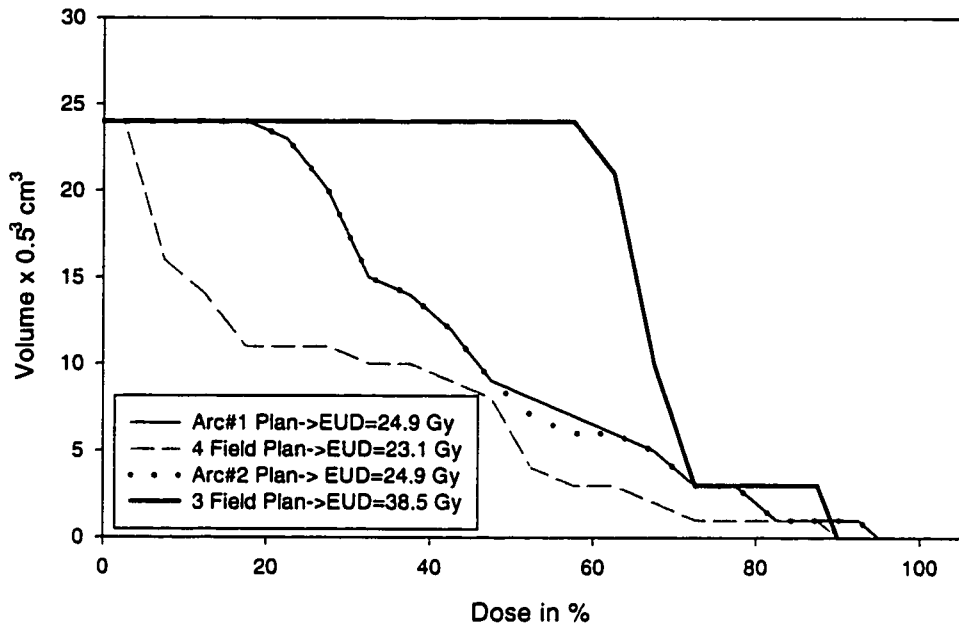**Figure 5.17**: Cumulative dose-volume histograms for the right eye.

Figure 5.18: Cumulative dose-volume histograms for the left eye.
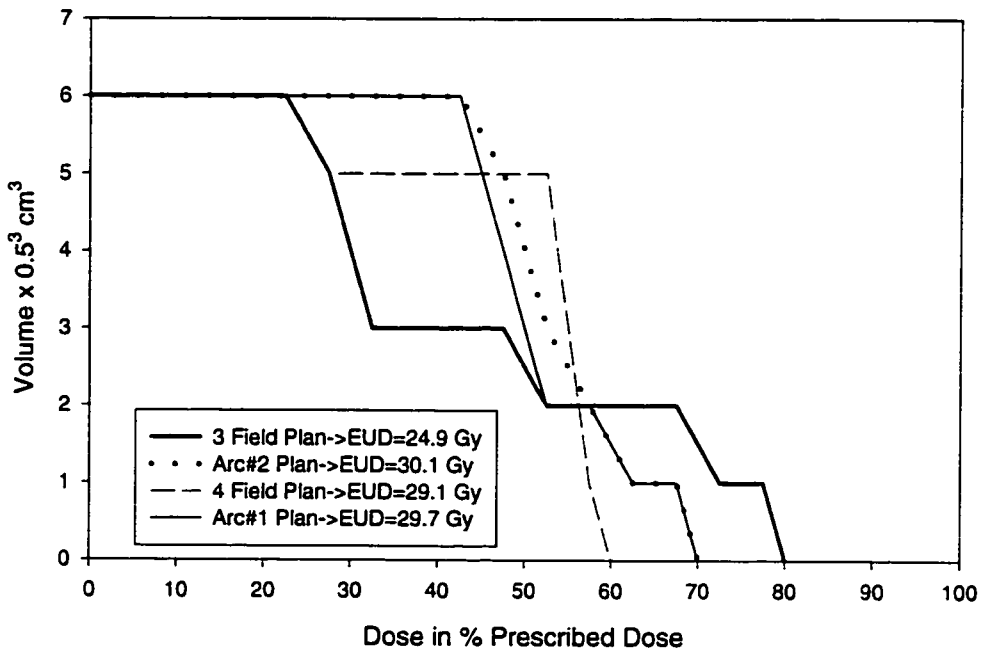

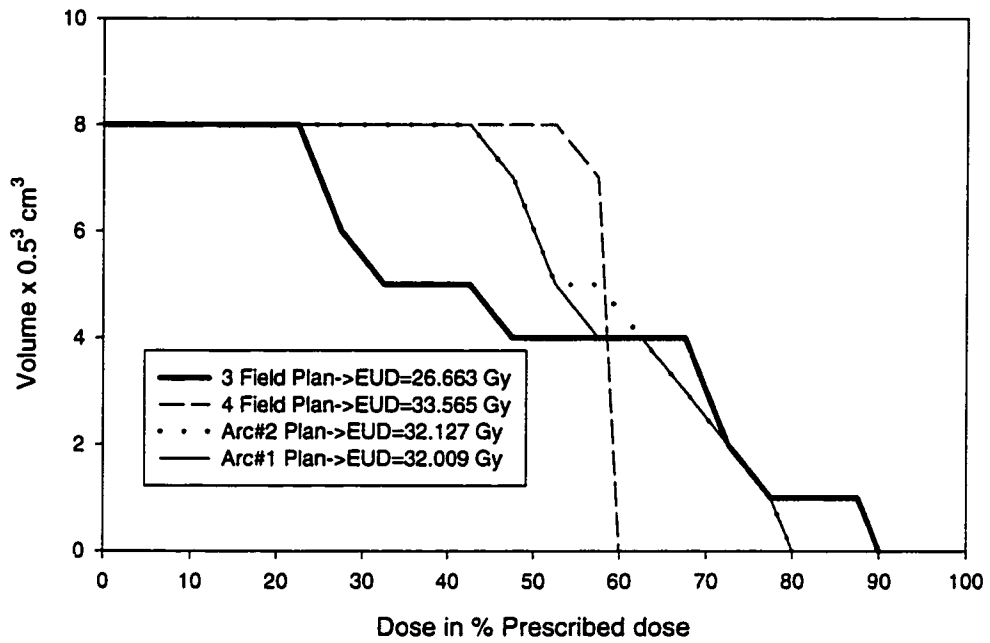**Figure 5.19**: Cumulative dose-volume histograms for the right optical nerve.

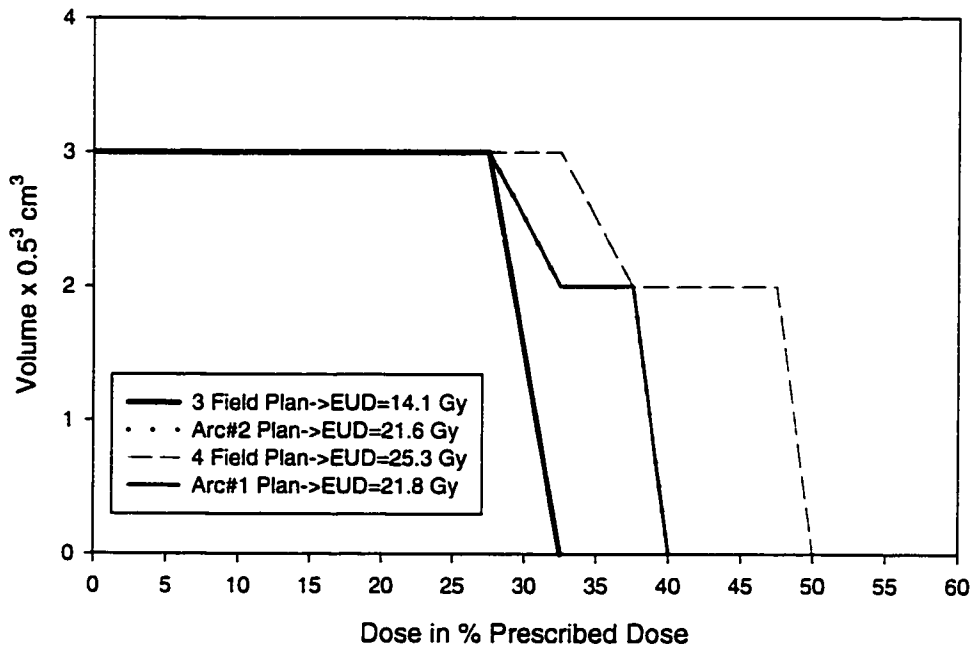**Figure 5.20:** Cumulative dose-volume histograms for the left optical nerve.

Figure 5.21: Cumulative dose-volume histograms for the chiasm of a patient with cancer of the ethmoid sinuses.

VOLUME OF INTEREST	EUD (Gy) for Volume of Interest			
	ARC#1	ARC#2	3 FIELD	4 FIELD
TUMOR VOLUME	59.0	58.6	59.0	59.0
RIGHT EYE	26.8	26.7	39.6	24.9
LEFT EYE	24.9	24.9	38.5	23.1
RIGHT OPTICAL NERVE	29.7	30.1	24.9	29.1
LEFT OPTICAL NERVE	32.0	32.1	26.7	33.6
CHIASM	21.8	21.6	14.1	25.4

Table 5.9: *EUD* results of several treatment beam arrangements for a patient with cancer of the ethmoid sinuses.

The preceding dose-volume histograms and their corresponding equivalent uniform doses show that most of the beam arrangements have identical resulting tumoricidal *EUD*s. They also show that regardless of the beam arrangement, the chiasm is the critical structure with the lowest *EUD*. This is to be expected as the beam arrangement were chosen to try and spare the chiasm as much as possible. Finally, the results indicate that the 3-field beam arrangement has the highest probability of causing complication to both eyes. However, the same beam arrangement has the lowest *EUD*s for the chiasm and both optical nerves.

5.4.3 Lung Cancer

Figures 5.22-5.24 delineates seven major structures of interest in treating lung cancer patients. For the purpose of this work, it was assumed that the heart, liver and both lungs were parallel architecture organs and that a complication arose when 20% of their total functional sub-units were eradicated. It was also hypothesized that all clonogenic cells within the critical structures were as radiobiologically sensitive as the tumor of interest and that functional sub-units were uniformly distributed. Finally, it was assumed that the mean lethal dose, D_o = (6.983±0.007) Gy since a dose of (80.0±0.5) Gy was prescribed to the tumor and that each functional sub-unit contained exactly 100 clonogenic cells.
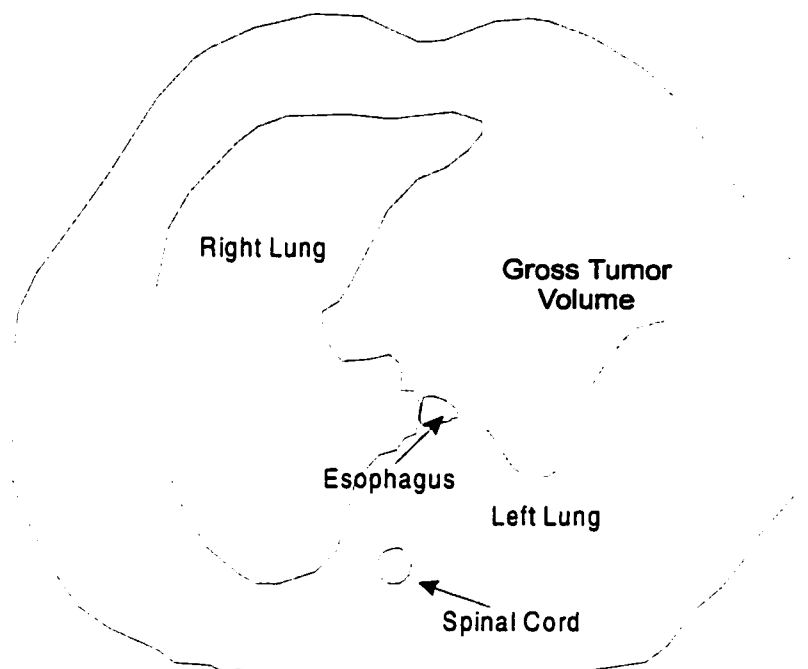
Figure 5.22: Central axis CT slice showing a portion of the major structures irradiated during lung cancer radiotherapy.
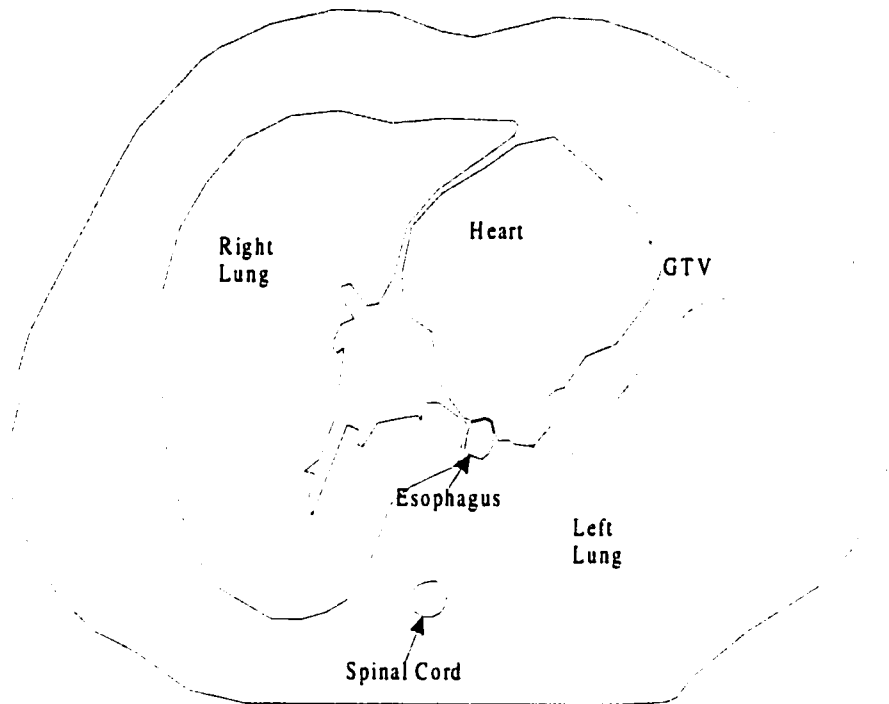
Figure 5.23: A superior CT slice showing some of the major structures irradiated during lung cancer radiotherapy. The CT slice is situated 5 cm above the central axis.
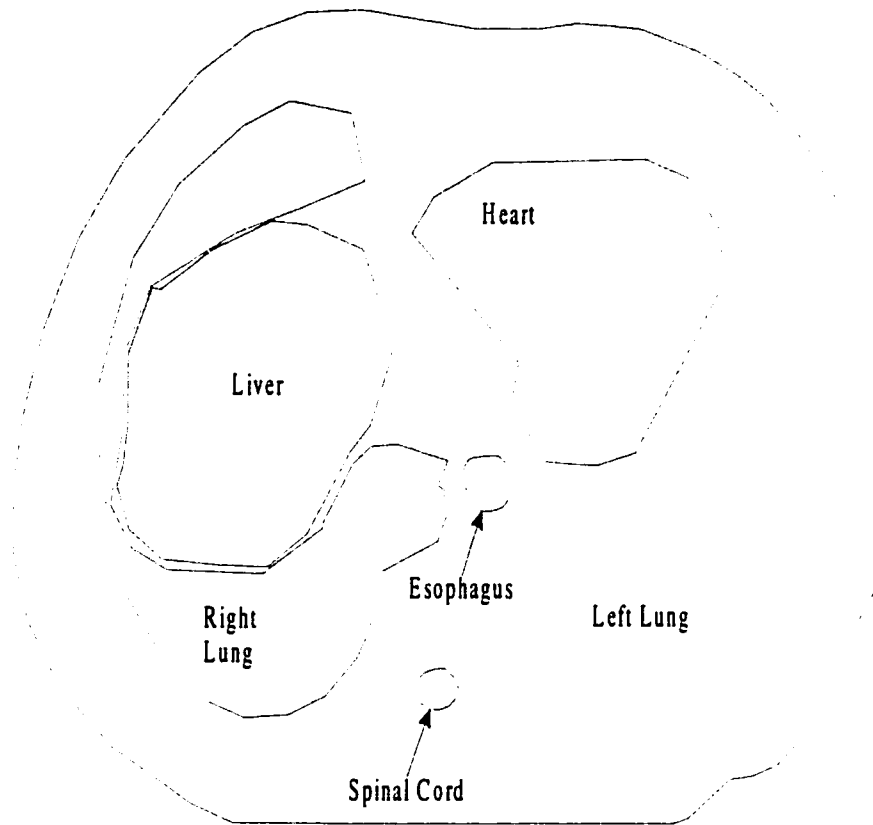
Figure 5.24: 5 cm inferior CT slice showing some of the major structures irradiated during lung cancer radiotherapy.

In the single case of lung cancer analyzed in this *EUD* evaluation, treatment plans for three individual patients were designed using a 3-D treatment planning system. These treatment plans are presented in the form of dose-volume histograms in the following figures (i.e. **Figures 5.25-5.31**). The calculated *EUD*s are included in these figures and summarized in **Table 5.10**.
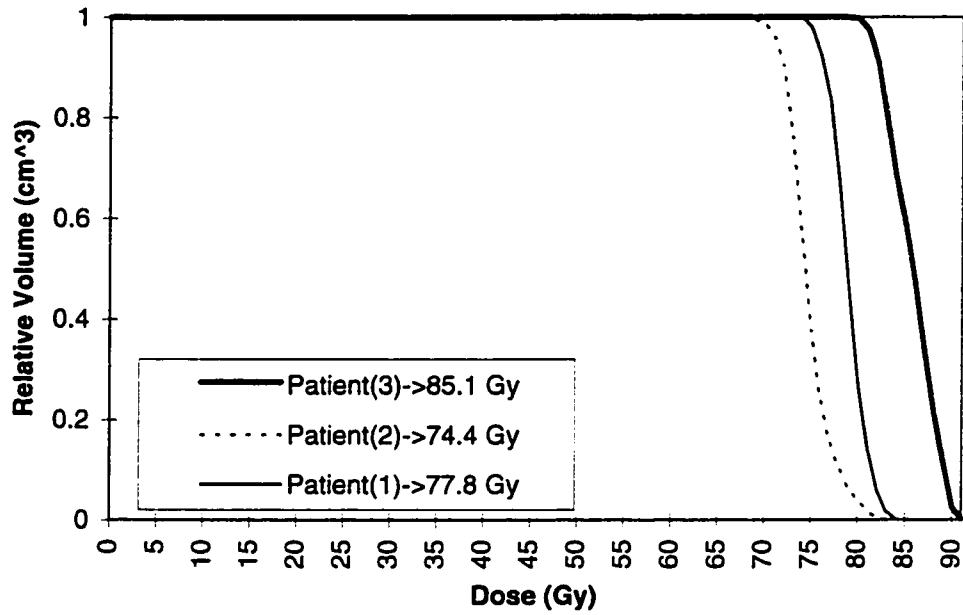
Figure 5.25: Cumulative dose volume histogram for the planning target volume of three individual patients irradiated with a prescribed dose of (80.0±0.5) Gy.
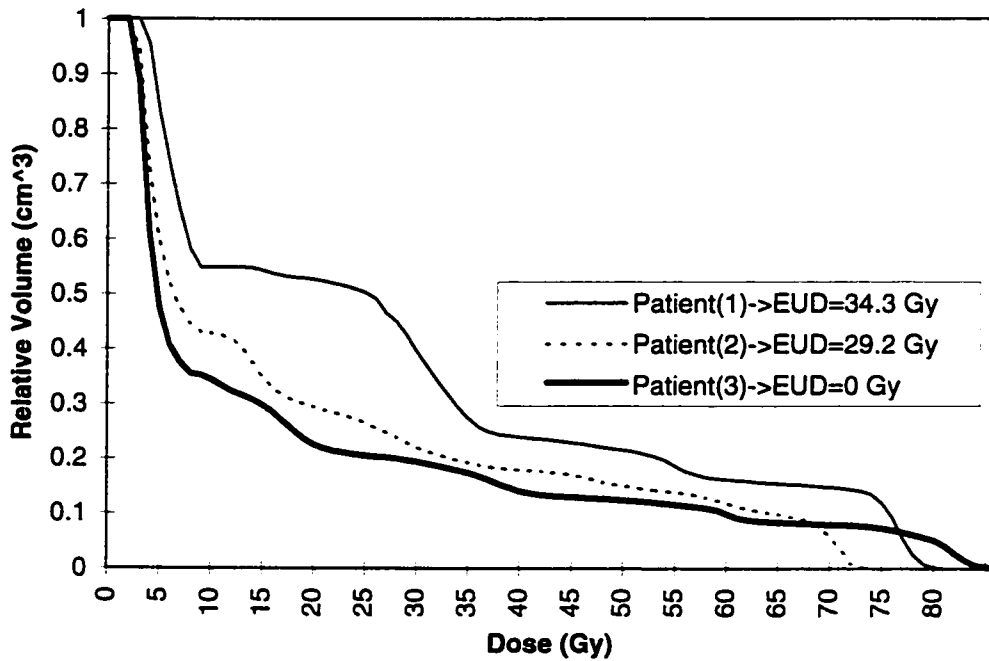
Figure 5.26: Cumulative dose-volume histograms for the heart.
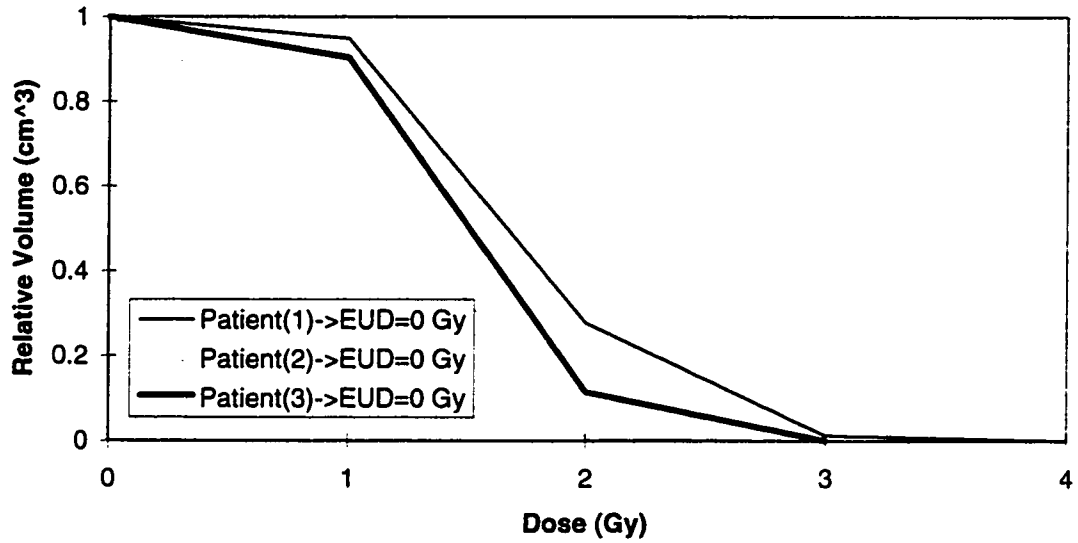
Figure 5.27: Cumulative dose-volume histograms for the liver.
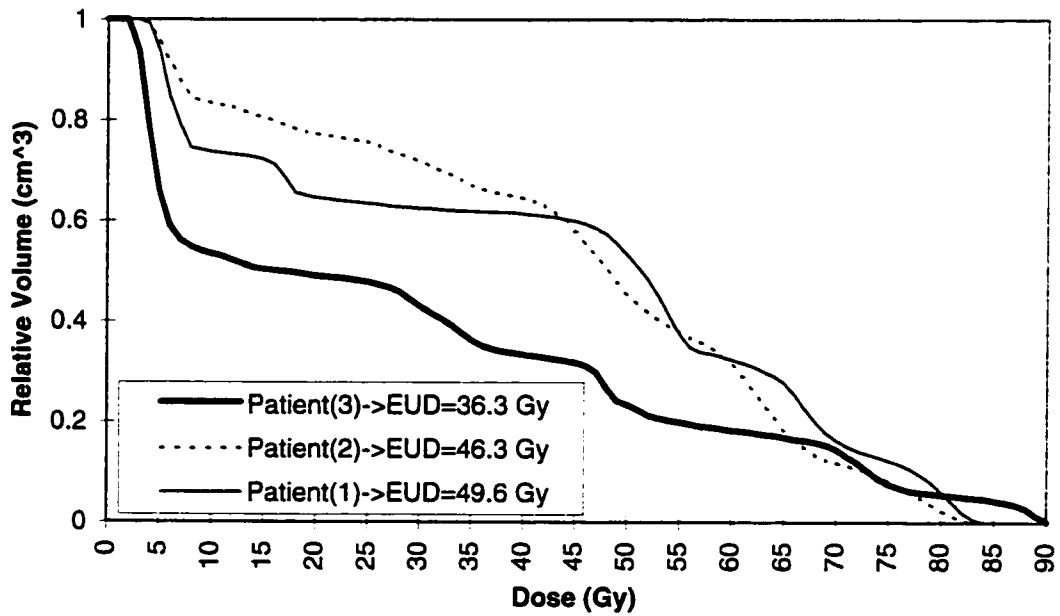
Figure 5.28: Cumulative dose-volume histogram of the remaining left lung for 3 patients with lung cancer treated with a 3-D radiotherapy treatment planning system.
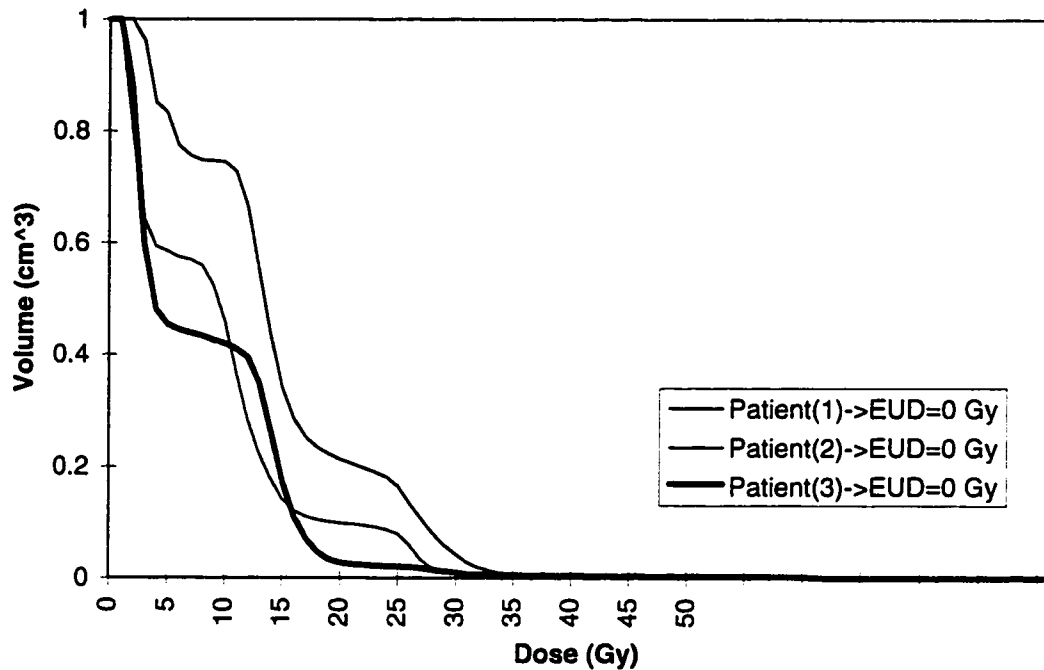
Figure 5.29: Cumulative dose-volume histograms of the right lung for 3 patients with lung cancer.
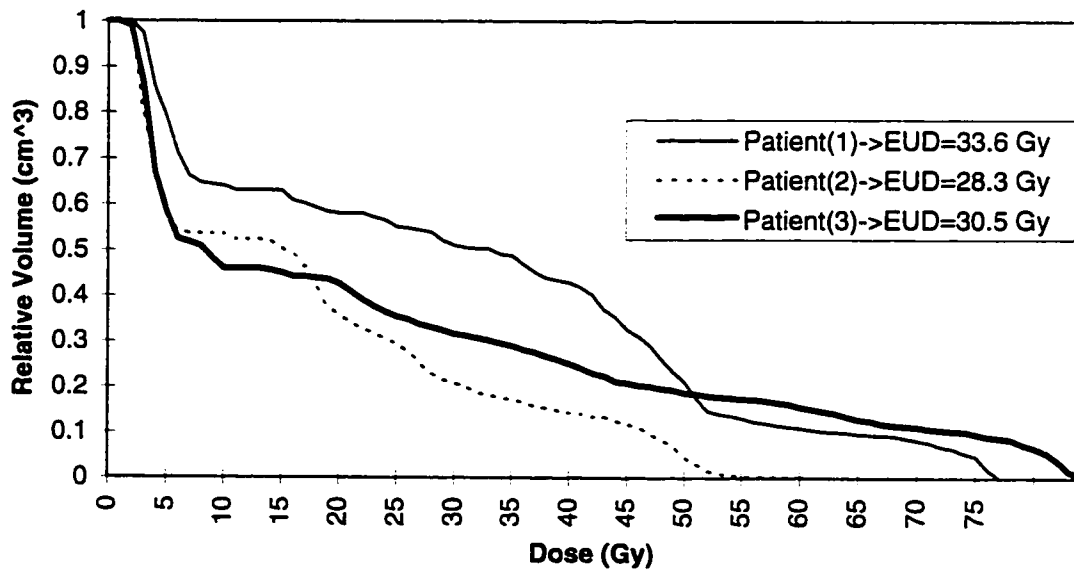
Figure 5.30: Cumulative dose-volume histograms for the esophagus treated with a 3-D radiation therapy planning system.
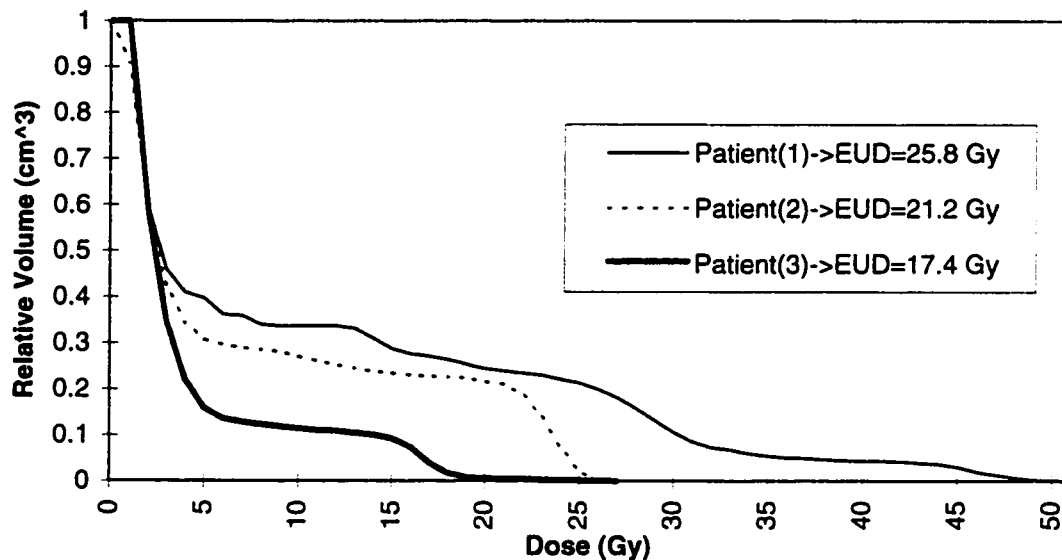
Figure 5.31: Cumulative dose-volume histograms for the spinal cord.

VOLUME OF INTEREST	EUD (Gy) for Volume of Interest		
	1	**2**	**3**
TUMOR VOLUME	77.8	74.3	85.1
LEFT LUNG	49.6	46.3	36.3
RIGHT LUNG	0.0	0.0	0.0
LIVER	0.0	0.0	0.0
HEART	34.3	29.2	0.0
ESOPHAGUS	33.6	28.3	30.5
SPINAL CORD	25.8	21.2	17.4

Table 5.10: *EUD* results for three lung cancer patients treated with a 3-dimensional radiotherapy planning system.

The *EUD* results along with their corresponding dose-volume histograms indicate that all 3 patients risk little liver and right lung complications. The results also show large *EUD* fluctuations from the prescribed dose for the tumor volume. Furthermore, the results reveal that patient#3 has the lowest probabilities of spinal cord and left lung complications and little risk of heart complication. Finally, the results indicate that the

spinal cord is the critical structure with lowest *EUD*, in accordance with the design of these treatment plans.

6. SUMMARY

A method of radiobiologically summarizing dose distributions with a single number, known as the equivalent uniform dose (*EUD*), has been examined and extended to dose distributions in normal tissue.

The equivalent uniform dose models for normal tissues are based upon the assumption that any two dose distributions are equivalent if they cause the same radiobiological effect. Unlike tumors, normal organs or tissues differ markedly from one another in their architecture and therefore respond differently to radiation. In this work, two fundamental tissue architectures were considered: the serial and the parallel architecture. For a serial architecture organ, complications are assumed to arise if any one functional sub-unit is eradicated. For a parallel architecture organ, complications are deemed to occur when more than M of the N functional sub-units are damaged. That is, a parallel architecture organ has a functional reserve ($1-M/N$) of functional sub-units which is necessary for maintaining normal functionality.

Using the above biological definition of normal tissue complication, several equivalent uniform dose formulas were developed for parallel architecture organs, ranging from simple to complex. For serial architecture organs, the equivalent uniform dose formulas were developed by assuming that normal tissue complication was governed by the expected number of eradicated functional sub unit. The simple normal tissue *EUD* formulas, developed in this work, stem from highly idealized assumptions, such as uniform distribution of FSUs and uniform clonogenic cell radiosensitivity, while the more complex normal tissue *EUD* models were developed based upon more realistic assumptions, such as a Gaussian distribution of cellular radiosensitivity.

The simplest idealized normal tissue and tumor *EUD* models were applied to a variety of dose distributions in order to illustrate their potential as dose summarizing tools. In addition to portraying their potential as dose summarizing tools, the idealized equivalent uniform dose formulas tested in this work shed light on some dose distribution endpoint(s) that influence tumor control and normal tissue complications.

The *EUD* results obtained in the preliminary tests reveal how important it is to know the underlying radiobiological parameters of a given structure. Since any variation in these parameters modifies the radiobiological effect, it is important to appropriately define these parameters in order to improve the clinical significance of the *EUD*. The equivalent uniform doses obtained from the preliminary tests reaffirm the importance of the minimum absorbed dose to the planning target volume in relation to tumor control. The equivalent uniform doses calculated for the serial architecture organs show that the *EUD* depends upon the radiobiological parameters that define the probability of eradicating a functional sub unit. When the probability of killing an FSU is at its minimum, the *EUD* corresponds to the maximum dose delivered to the structure. However, when the probability of eradicating a functional sub unit is at its maximum, an increase in dose will not change the *EUD*. Between these two limit values, *EUD* increases as a function of dose. The equivalent uniform doses resulting from the preliminary dose-volume histograms for parallel architecture organs support the belief that parallel architecture organs exhibit a larger volume effect than do serial architecture organs. The *EUD* results obtained for the parallel architecture organs also reflect the need for higher uniform doses to cause complications in parallel architecture organs which require smaller functional reserves to maintain functionality. Finally, the results for the parallel organs suggest that as the fractional reserve of these structures is increased, their response to radiation approaches the serial architecture organs response, as expected.

The application of the developed idealized *EUD* models to clinical distributions demonstrates how non-uniform dose distributions can be summarized with a single number, thus eliminating the need to report several doses in the documentation of treatment plans. Future clinical implementation of this *EUD* reporting method will allow radiotherapy centers to generate better *NTCP* and *TCP* curves and render the application of these biological indices more significant. However, before implementing the *EUD* models, both individual patient and population averaged radiological parameters must be accurately determined as the clinical significance of the *EUD* results greatly depends upon these parameters. Finally, a more appropriate radiobiological effect (i.e *NTCP*

definition) should be contemplated to develop the serial architecture organ *EUD* formulas as the definition used in this work does not account correctly for the absolute volume effect.

[1] Alberta Cancer Board Publication. (1996). A Snapshot of Cancer in Alberta. Division of Epidemiology, Prevention and Screening.

[2] ICRU Report no. 50. (1993). Prescribing, Recording, and Reporting Photon Beam Therapy. Bethasda MD, Maryland: International Commission on Radiation Units and Measurements.

[3] Niemierko A. (1996). Treatment Evaluation. In: Mackie TR, Palta JR., eds. Teletherapy: Present and Future. Proceedings of the 1996 Summer School. Madison, Wisconsin: Advanced Medical Publishing; 175-189.

[4] Steel GG. (1997). Growth kinetics of tumours. Oxford: Clarendon Press; 268-308.

[5] Trott KR. (1989). Relation between cell survival and gross endpoints of tumour response and tissue failure. In: Steel GG, Adams GB, Horwich A., eds. The biological basis of radiotherapy. 2nd Edition. New York: Elsevier Science Publishers B. V. ; 65-76.

[6] Lyman JT. (1985). Complication probabilities as assessed from dose-volume histograms. *Radiation Research*, **104**: S13-S19.

[7] Lyman JT, Wolbarst AB. (1987). Optimization of radiation therapy: 3. A method for assessing complication probabilities from dose-volume histograms. *International Journal of Radiation Oncology, Biology and Physics*, **13**: 103-109.

[8] Withers HR, Taylor JMG, Maciejewski B. (1988). Treatment volume and tissue tolerance. *International Journal of Radiation Oncology, Biology and Physics*, **14:** 751-759.

[9] Wolbarst AB, Chin LM, Svensson GK. (1982). Optimization of radiation therapy: integral-response of a model biological system. *International Journal of Radiation Oncology, Biology and Physics*, **8:** 1761-1769.

[10] Burman C & al. (1991). Fitting normal tissue tolerance data to an analytic function. *International Journal of Radiation Oncology, Biology and Physics*, **21:** 123-135.

[11] Lyman JT, Wolbarst AB. (1987). Optimization of radiation therapy: 3. A method for assessing complication probabilities from dose-volume histograms. *International Journal of Radiation Oncology, Biology and Physics*, **13:** 103-109.

[12] Kutcher CJ, Burman C. (1989). Calculation of complication probability factors for non-uniform normal tissue irradiation: the effective volume method. *International Journal of Radiation Oncology, Biology and Physics*, **16:** 1623-1630.

[13] Mohan R, Steven AL, Pizzuto D, Wu Q. (1998). Three-dimensional conformal radiotherapy. In: Khan FM, Potish RA., eds. Treatment Planning in Radiation Oncology. Baltimore, Maryland: Williams and Wilkins; 147-186.

[14] Dutriex A. (1987). Prescription, Precision and Decision in Treatment Planning. *International Journal of Radiation Oncology, Biology and Physics*, **13:** 1291.

[15] Hendrickson F. (1988). Dose Prescription Dilemma. Editorial. *International Journal of Radiation Oncology, Biology and Physics*, **14:** 595.

[16] Purdy JA. (1995). Volume and dose specification for three-dimensional conformal radiation therapy. In: Purdy JA, Emani B., eds. Proceedings of an International Symposium. Madison, Wisconsin: Medical Physics Publishing; 11-14.

[17] Langer M, Morrill SS, Lane, R. (1998). A test of the claim that plan rankings are determined by relative complication and tumor-control probabilities. *International Journal of Radiation Oncology, Biology and Physics*, **41:** 451-457.

[18] Niemierko A. (1997). Reporting and analyzing dose distributions: A concept of equivalent uniform dose. *Medical Physics*, **24:** 103-110.

[19] Boag JW. (1975). 12th Failla Memorial Lecture. The time scale in radiobiology. In: Nygaard O, Alder HI, Sinclair WK., eds. Radiation Research. New York: Academic Press; 9-29.

[20] Attix FH. (1986). Introduction to radiobiological physics and radiation dosimetry. New York: A Wiley-Interscience Publication; 124-125.

[21] Attix FH. (1986). Introduction to radiobiological physics and radiation dosimetry. New York: A Wiley-Interscience Publication; 138-146.

[22] Attix FH. (1986). Introduction to radiobiological physics and radiation dosimetry. New York: A Wiley-Interscience Publication; 131-138.

[23] Johns HE, Cunningham JR. (1983). The physics of radiology. 4th Edition. Springfield, Illinois: Charles C Thomas; 155-158.

[24] Hall EJ. (1994). Radiobiology for the radiologist. 4th Edition, Philadelphia: J. B. Lippincott Company; 8-10.

25 Attix FH. (1986). Introduction to radiobiological physics and radiation dosimetry. New York: A Wiley-Interscience Publication; 20-36.

26 Hall EJ. (1994). Radiobiology for the radiologist. 4th Edition, Philadelphia: J. B. Lippincott Company; 156-157.

27 Hall EJ. (1994). Radiobiology for the radiologist. 4th Edition, Philadelphia: J. B. Lippincott Company; 153-164.

28 Paic G. (1988). Effect of ionizing radiation on chemical compounds and biological tissues. In: Paic G., ed. Ionizing radiation: Protection and dosimetry. Boca Raton, Florida: CRC Press; 15-25.

29 Hill RP. (1992). Cellular basis of radiotherapy. In: Hill RP, Tannock IF, eds. The basic science of oncology. 2nd Edition. Permagon Press; 259-275.

30 Paic G. (1988). Effect of Ionizing Radiation on Chemical Compounds and Biological Tissues. In: Paic G, ed. Ionizing Radiation: Protection and Dosimetry. Boca Raton, Florida: CRC Press; 28-39.

31 McMillan TJ, Steel GG. (1993). Molecular aspects of radiation biology. In: Steel GG, ed. Basic clinical radiobiology for radiation oncologists. New York: Edward Arnold Publishers; 211-224.

32 Korner IJ, Geunter K, Malz W. (1978). Kinetics of single-strand break rejoining X-ray and neutron-irradiated Chinese Hamster cells. Studies in Biophysics, 70: 175-182.

[33] Bryant PE, Blöcher D. (1980). Measurement of the kinetics of DNA double-strand break repair in Ehrlich ascites tumour cells using the unwinding method. *International Journal of Radiation Biology*, **38:** 335-347.

[34] Hall EJ. (1994). Radiobiology for the radiologist. 4th Edition. Philadelphia: J.B. Lippincott Company; 107-132.

[35] Radford IR. (1985). The level of induced DNA double-strand breakage correlates with cell killing after X-irradiation. *International Journal of Radiation Biology*, **48:** 45-54.

[36] Frankenber D, Frankenber-Schager M, Blöcher D, Harbich R. (1981). Evidence for DNA double strand breaks as the critical lesions in yeast cells irradiated with sparsely or densely ionizing radiation under oxic or anoxic conditions. *Radiation Research*, **88:** 524-532.

[37] Powell S, McMillan TJ. (1990). DNA damage and repair following treatment with ionizing radiation. *Radiotherapy and Oncology*, **19:** 95-108.

[38] Joshi GP, Nelson WJ, Revell SH, Shaw CA. (1982). X-ray induced chromosome damage in live mammalian cells, and improved measurements of its effects on their colony-forming ability. *International Journal of Radiation Biology and Related Studies in Physics, Chemistry and Medicine*, **41(2):** 161-181.

[39] Carrano AV. (1973). Chromosone aberrations and radiation-induced cell death. II. Predicted and observed cell survival. *Mutation Research*, **17:** 355-356.

[40] Conforth MN, Bedford JS. (1987). A quantitative comparison of potentially lethal damage repair and the rejoining of interphase chromosone breaks in low passage normal human fibroblasts. *Radiation Research*, **111:** 385-405.

[41] Buick RN, Tannock IF. (1992). Properties of malignant cells. In: Hill RP, Tannock IF, eds. The basic science of oncology. 2nd Edition. Permagon Press; 139-153.

[42] Steel GG. (1989). Survival of clonogenic cells: cell-survival curves. In: Steel GG, Adams GE, Horwich A., eds. The biological basis of radiotherapy. 2nd Edition. New York: Elsevier Science Publishers B. V; 45-63.

[43] Bristow RG, Hardy PA, Hill RP. (1990). Comparison between in vitro radiosensitivity and in vivo radioresponse of murine tumor cell lines: 1, Parameters of in vitro radiosensitivity and endogenous cellular glutathione levels. *International Journal of Radiation Oncology, Biology and Physics*, **18:** 133-145.

[44] Curtis SB. (1986). Lethal and potentially lethal lesions induced by radiation: a unified repair model. *Radiation Research*, **106:** 252-270.

[45] Joiner MC. (1993). Models of radiation cell killing. In: Steel GG, ed. Basic clinical radiobiology for radiation oncologists. New York: Edward Arnold Publishers; 40-46.

[46] Sinclair WK. (1968). X-ray responses in mammalian cells in vitro. *Radiation Research*, **33:** 620-643.

[47] Terasima T, Tolmach LJ. (1961). Changes in the X-ray sensitivity of HeLa cells during the division cycle. *Nature*, **190:** 1210-1211.

[48] Utsumi H, Elkind MM. (1979). Potentially lethal damage versus sublethal damage: independent repair processes in actively growing Chinese hamster cells. *Radiation Research*, **77**: 346-360.

[49] Hellman S. (1997). Principles of cancer management: Radiation therapy. In: DeVita VT, Hellman S, Rosenberg SA., eds. <u>Cancer: Principles and practice of oncology</u>. 5th Edition. Philadelphia: Lippincott-Raven Publishers; 307-330.

[50] Hall EJ. (1994). <u>Radiobiology for the radiologist</u>. 4th Edition. Philadelphia: J.B. Lippincott Company; 133-153.

[51] Niemierko A, Goitein M. (1992). Modeling tissue response to radiation: the critical volume model. *International Journal of Radiation Oncology, Biology and Physics*, **25**: 135-145.

[52] Begg AC. (1993). Cell proliferation in tumours. In: Steel GG., ed. <u>Basic Clinical Radiobiology</u>. New York: Edward Arnold Publishers; 14-22.

[53] Hall EJ. (1994). <u>Radiobiology for the radiologist</u>. 4th Edition. Philadelphia: J.B. Lippincott Company; 45-74.

[54] Withers HR, Taylor JMG, Maciejewski B. (1988). Treatment volume and tissue tolerance. *International Journal of Radiation Oncology, Biology and Physics*, **14**: 751-759.

[55] Niemierko A. (1997). Reporting and analyzing dose distributions: A concept of equivalent uniform dose. *Medical Physics*, **24**: 103-110.

[56] Maciejewski B, Withers HR, Taylor JM, Hliniak A. (1989). Dose fractionation and regeneration in radiotherapy for cancer of the oral cavity and oropharynx: tumor

dose-response and repopulation. *British Journal of Radiological Oncology, Biology and Physics*. **16:** 831-843.

[57] Hermens AF, Barendsen GW. (1969). Changes of cell proliferation characteristics in a rat rhabdom before and after x-irradiation. *European Journal of Cancer*, **5:** 173-189.

[58] Fisher JJ, Moulder JE. (1975). The steepness of the dose-response curve in radiation therapy. Theoretical considerations and experimental results. *Radiology*. **117:** 179-184.

[59] Withers HR, Peters LJ. (1980). Basic principles of radiotherapy. In: Fletcher GH., ed. Textbook of radiotherapy, 3rd Edition. Philadelphia: Lea and Febiger; 138-142.

[60] Deacon J, Peckman MJ, Steel GG. (1984). The radioresponsiveness of human tumours and the initial slope of the cell survival curve. [Review] *Radiotherapy and Oncology*, **2:** 317-323.

[61] Okunieff P, Morgan D, Niemierko A, Suit HD. (1995). Radiation dose-response of human tumours. *International Journal of Radiation Oncology, Biology and Physics*, **32:** 1227-1237.

[62] Thomlinson RH, Gray LH. (1955). The histological structure of some human lung cancers and the possible implications for radiotherapy. *British Journal of Cancer*, **9:** 539-549.

[63] Hill RP, & al. (1991). The effect of anaemia on the fraction of hypoxic cells in an experimental tumour. *British Journal of Radiology*, **44:** 299-304.

[64] Hall EJ. (1988). Radiobiology for the radiologist. 3rd Edition. Philadelphia: J. B. Lippincott Company; 133-152.

[65] Fine LG. (1991). How little kidney tissue is enough? [editorial; comment]. *New England Journal of Medicine*, 325(15): 1097-1099.

[66] Hall EJ. (1994). Radiobiology for the radiologist. 4th Edition. Philadelphia: J. B. Lippincott Company; 211-229.

[67] Withers HR, Thames HD, Peters LJ. (1982). Differences in the fractionation response of acute and late responding tissues. In: Karcher KH, Kogelnik HD, Reinartz G., eds. Progress in Radio-Oncology II, New York: Raven Press; 287-296.

[68] Fowler JF. (1983). La Ronde- radiation sciences and medical radiology. *Radiotherapy Oncology*, 1: 1-22.

[69] Starkshall,G. (1996). 2-D versus 3-D Radiotherapy Treatment Planning. In: Palta J, Mackie TR., eds. Teletherapy: Present and Future. Advanced Medical Publishing; 18-19.

[70] Starkshall,G. (1996). 2-D versus 3-D Radiotherapy Treatment Planning. In: Palta J, Mackie TR., eds. Teletherapy: Present and Future. Advanced Medical Publishing; 19-20.